Realization of Active and Passive Optical Components and their Applications Using Multilayered Polymer/Inorganic Thin Films

THESIS SUBMITTED TO

UNIVERSITY OF CALICUT

In Partial Fulfillment

For the Award of the Degree of

Doctor of Philosophy in Physics

under the Faculty of Science

by

Mrs. LISHA C. L.

Under the guidance of

Dr. PRADEESH K.

Research Department of Physics
Government Victoria College, Palakkad

November 2022

Realization of active and passive optical components and their applications using multilayered polymer/inorganic thin films

Ph.D. Thesis in Physics

Author:

Lisha C. L.

Department of Physics

Govt. Victoria College, Palakkad

(Affiliated to the University of Calicut)

Kerala, India-678001

Email: lishacl9@gmail.com

Under the guidance of :

Dr. Pradeesh K.

Assistant Professor

Department of Physics

Govt. Victoria College, Palakkad

Email: pradeeshk@gvc.ac.in

&

Co-guidance of:

Dr. V. Geetha

Research Co-Guide

Department of Physics

Govt. Victoria College, Palakkad

Email: geethavishnu22@yahoo.com

DEPARTMENT OF PHYSICS
GOVERNMENT VICTORIA COLLEGE, PALAKKAD
Kerala, India, PIN 678001
Affiliated to the University of Calicut
NAAC Accreditation - A Grade
NIRF Rank – 85
Email: physics@gvc.ac.in | Web: www.gvc.ac.in/physics

CERTIFICATE

This is to certify that the thesis entitled **"REALIZATION OF ACTIVE AND PASSIVE OPTICAL COMPONENTS AND THEIR APPLICATIONS USING MULTILAYERED POLYMER/INORGANIC THIN FILMS"** being submitted herewith to the University of Calicut for the award of the degree of Doctor of Philosophy in Physics, is a bona fide record of the original research work completed by Mrs. Lisha C. L., under my supervision and guidance at Dept. of Physics, Govt. Victoria College Palakkad under the University of Calicut and to the best of my knowledge and belief that this work has not been included in any other thesis submitted previously for the award of any degree.

Dr. Pradeesh K
Research Guide
Assistant Professor
Dept. of Physics
Govt. Victoria College
Palakkad

Place: Palakkad
Date:

DEPARTMENT OF PHYSICS
GOVERNMENT VICTORIA COLLEGE, PALAKKAD
Kerala, India, PIN 678001
Affiliated to the University of Calicut
NAAC Accreditation - A Grade
NIRF Rank – 85
Email: physics@gvc.ac.in | Web: www.gvc.ac.in/physics

CERTIFICATE

This is to certify that the thesis entitled **"REALIZATION OF ACTIVE AND PASSIVE OPTICAL COMPONENTS AND THEIR APPLICATIONS USING MULTILAYERED POLYMER/INORGANIC THIN FILMS"** being submitted herewith to the University of Calicut for the award of the degree of Doctor of Philosophy in Physics, is a bona fide record of the original research work completed by Mrs. Lisha C. L., under my co-guidance at Dept. of Physics, Govt. Victoria College Palakkad under the University of Calicut and to the best of my knowledge and belief that this work has not been included in any other thesis submitted previously for the award of any degree.

Dr. V. Geetha
Research Co-Guide
Dept. of Physics
Govt. Victoria College
Palakkad

Place: Palakkad
Date:

DEPARTMENT OF PHYSICS
GOVERNMENT VICTORIA COLLEGE, PALAKKAD
Kerala, India, PIN 678001
Affiliated to the University of Calicut
NAAC Accreditation - A Grade
NIRF Rank – 85
Email: physics@gvc.ac.in | Web: www.gvc.ac.in/physics

CERTIFICATE

This is to certify that the corrections recommended by both the adjudicators have been made in the thesis entitled "REALIZATION OF ACTIVE AND PASSIVE OPTICAL COMPONENTS AND THEIR APPLICATIONS USING MULTILAYERED POLYMER/INORGANIC THIN FILMS", submitted by Ms. Lisha C. L. and that the contents in the thesis and the soft copy are one and the same

Dr. Pradeesh K
Research Guide
Assistant Professor
Dept. of Physics
Govt. Victoria College
Palakkad

Place: Palakkad
Date:

DECLARATION

I do hereby declare that the research work presented in the thesis "**REALIZATION OF ACTIVE AND PASSIVE OPTICAL COMPONENTS AND THEIR APPLICATIONS USING MULTILAYERED POLYMER/INORGANIC THIN FILMS** " is original and has been carried out by me under the supervision of **Dr. Pradeesh K.**, Department of Physics, Government Victoria College, Palakkad (Affiliated to University of Calicut). I further declare that to the best of my knowledge the thesis does not contain any part of any work that has been submitted for the award of any degree or diploma or similar title either in this university or in any other university without proper citation**.**

Date: **Lisha C. L.**

Place:

ACKNOWLEDGEMENTS

It would not have been possible to write this Ph.D. thesis without the help and support of the kind people around me, to only some of whom it is possible to give particular mention here. It is great privilege to express my profound gratitude and heartfelt thanks to my research supervisor **Dr. Pradeesh K.**, Department of Physics, Govt. Victoria College, Palakkad for his illuminating guidance, stimulating discussions and constant encouragement given to me during the entire tenure of my research work. I am fortunate to be his research student who has supported me throughout my research work with his patience and knowledge whilst allowing me the room to work in my own way.

I express my heartfelt thanks to Dr. Ambily Krishnan, HOD of Physics, GVC, Palakkad for the timely and valuable solutions to the problems that I have faced at different stages of the work. I thank Dr. Geetha V., my co-Guide and Prof. O. K. Ramesan former HOD of Physics, Govt. Victoria College Palakkad for the timely supportive suggestions of this work. I also thank present and Former Principal of Govt. Victoria College Palakkad, present and Former Principal of SNGS College Pattambi and present and Former Principal of GPTC, Shoranur. I also express my gratitude to Dr. Binitha N. N., Professor, University of Calicut and Resmi K. R., Part Time Research Scholar, Department of Physics, Govt. Victoria College Palakkad.

I owe my sincere thanks to Department of Physics and Department of Chemistry of SNGS college, Pattambi and all the faculty members and Research scholars of Govt. Victoria College Palakkad. Also, I express my special thanks to STIC, Cochin University, IISc. Bangalore and St. Thomas College, Thrissur for providing me the experimental facilities.

I also thank my husband Mr. Sasikumar C. R., my son Mr. Niranjan A. S., my father Mr. C. C. Lohithakshan, my mother Mrs. Sarada M.M. and my sister Mrs. Linsha C. L. for their kind patience, unconditional love and support during all these days. Without their support, I do not think I could overcome the difficulties during these years. I also gladly express my sincere thanks, to all those loving personalities who have directly or indirectly helped me in some way or other during the course of this work. And foremost, to the Almighty God, for the never-ending support and mercy and giving me the strength to overcome all the difficulties that I have faced in this research work.

CONTENTS

Page No.

PREFACE

Now a days, multilayer thin films are common elements of many opto-electronic and photonic devices and the industrial development of these materials has led to the realization of active and passive optical elements and commonly found in all kinds of optical characterization setups. The optical thin films have numerous applications in many fields of science and technology. For the design of multilayer thin films, a variety of methods have been explored. The most adaptable method is numerical simulation. Optical surfaces having any desired reflectance and transmittance can be achieved by means of thin film coatings. Active and passive optical components have their role and importance in opto-electronic and photonic devices. In our thesis, the active optical components we had used are quantum dots and fluorescein materials and the passive optical components are the multilayer thin films. Multilayer thin films, with layer thicknesses on the nanoscale, have a unique geometry that results in a wide range of novel features and behavior not seen in the bulk.

The multi layered thin film coatings can be conveniently used to realise various optical filters like anti-reflection coatings, highly reflecting mirrors, high pass filters, comb filters etc. Distributed Bragg reflectors are one of the most prominent optical materials used in optoelectronics. Due to its unique features and cost-effective fabrication methods, such as the sol-gel method, they have gained a lot of attention in opto-electronic and photonic devices. These highly reflective dielectric mirrors are employed in waveguides, laser resonators, optical filters and sensors, together with other applications. The present thesis entitled "**Realization of active and passive optical components and their applications using multilayered polymer/inorganic thin films**" reports the fabrication method of these featured DBRs and incorporate their uses into photonic and optoelectronic applications.

On incorporating these multilayers with an emitting material or quantum dots, forming a cavity like structure, have a wide range of applications. Among the quantum dots, Carbon Quantum Dots (CQDs) are rising stars due to their low cost, strong fluorescence, nontoxicity, adjustable luminescence range, excellent light stability, non-blinking property and good solubility etc. In our research work, we had developed highly stable, optically transparent and variable refractive index polymer-inorganic nano composite by solution chemistry method and fabricated DBR using this polymer. Highly luminescent carbon quantum dots from glucose were prepared by microwave assisted hydrothermal method. We have observed the plasmon coupled fluorescence tuning in metal dielectric multi layered structures by reverse Kretschman configuration and studied the influence of PMMA on SPCE tuning. Surface plasmon resonance is a promising technique and now a days, surface plasmon resonance and surface plasmon coupled emission are widely used in the field of biosciences and material sciences. The study of the light matter interaction or energy transfer mechanism by incorporating carbon quantum dots or emitting materials with multilayers have wide range of opto-

electronic and bio-photonic applications. So, we had adopted simple, low cost and green assisted method for the preparation of all the sample and these works will create wide possibilities in the fabrication of opto-electronic and photonic devices. Hence it is believed that the results of this study have practical importance owing to their numerous applications.

All the results obtained from these studies are documented under eight chapters of the thesis. The last chapter of the thesis is the recommendations for the future work. References closely related to the present work have been compiled to the extent possible and given at the end of the thesis. Some of the results reported in this thesis have been presented in National and International seminars/conferences and also published in international journals.

LIST OF FIGURES

LIST OF TABLES

List of Publications

1. **Lisha C. Lohithakshan,** Geetha V. and Kannan P., 2020, Single polymer-variable index for the design and fabrication of variable stop band distributed Bragg reflectors, *Optical Materials, 110*, p.110509. (Impact factor 3.754)
2. **Lisha C. Lohithakshan**, Pattarathil M.S., Geetha V. and Kannan P., 2020 July., Photoluminescent Glucose Derived Carbon Quantum Dots for Photonic and Optoelectronic Applications., In *Optical Devices and Materials for Solar Energy and Solid-state Lighting* (pp. JTu4C-12). Optical Society of America (Conference Proceedings)
3. **Lisha C. Lohithakshan**, and Kannan P., 2022, Realisation of optical filters using multi-layered thin film coatings by transfer matrix model simulations, Materials Today Proceedings. (Impact factor 1.46)
4. Plasmon coupled fluorescence tuning-steering duality in metal dielectric multilayered structures. (To be communicated…)

Conference Presentations

1) *"Photoluminescent Glucose Derived Carbon Quantum Dots for Photonic and Optoelectronic Applications"* International conference on OSA Advanced Photonic Congress 2020.

2)*"Design and optimization of distributed Bragg reflectors using transfer matrix model simulations"* International conference on Recent Trends in Photonics (NPS2021)

3*)"Quantum dots and its photonic and biomedical applications"* National symposium on Advanced materials.

4)"Realisation of optical filters using multi-layered thin film coatings by transfer matrix model simulations" International conference on Recent advances in engineering materials (ICRAEM 2022)

Chapter -1

Introduction

Introduction

Most of the materials science research and its technological developmental studies were progressed by carrying out the basic studies of the materials in their thin film form. Thin film technology was known for several decades. Later it was identified that the thin film characteristics differ abruptly from its bulk counterpart. Some of the optical properties like reflection, transmission and absorption of optical materials could be altered by varying the thickness, refractive index and the crystalline nature of the materials in thin film form. Further interesting properties were observed on stacking multiple layers of thin films with each layer having optical constants different from other layers. Here we have explored various multilayer designs using numerical simulations and its possible practical applications in the field of optics and photonics by fabricating multilayers using cost effective and ecofriendly materials and methods. Multilayered thin films can either be a part of or in full integrated to an optical device. Further potential of these multilayers in an optical device as a passive component and as an active component were explored in this work. This chapter gives an introduction, theoretical background, motivation of the work, various multilayer designs and its possible application designs.

1.1. Bulk vs Low Dimensional Structures

Tracing the origins of many of the most beautiful phenomena in the universe is a very interesting study. Many of these beautiful phenomena are different from each point of view. Nanomaterial properties are completely different from bulk material properties. These low-dimensional materials are of valuable because they connect the bulk materials and the molecular domains. The optical properties of crystalline and non-crystalline media are dramatically altered by reducing the characteristic size of materials, which also makes it possible to create materials with novel and distinctive qualities. The changes in optical characteristics of materials caused by decreasing their characteristic size are caused by the photon/light confinement effect. A material is said to be in a confined structure when its electrical or optical characteristics change noticeably as a result of confinement in at least one dimension (1D). (Scher et al., 2016) So, the two-dimensional (2D) materials, such as quantum wells (Q-wells), are confined to one dimension; (Barbagiovanni et al., 2014) one-dimensional (1D) materials, such as quantum wires (Q-wires) are confined to two dimensions; (Edvinsson,

2018) and zero-dimensional (0D) materials, such as quantum dots, are confined to all three dimensions. (Edvinsson, 2018)

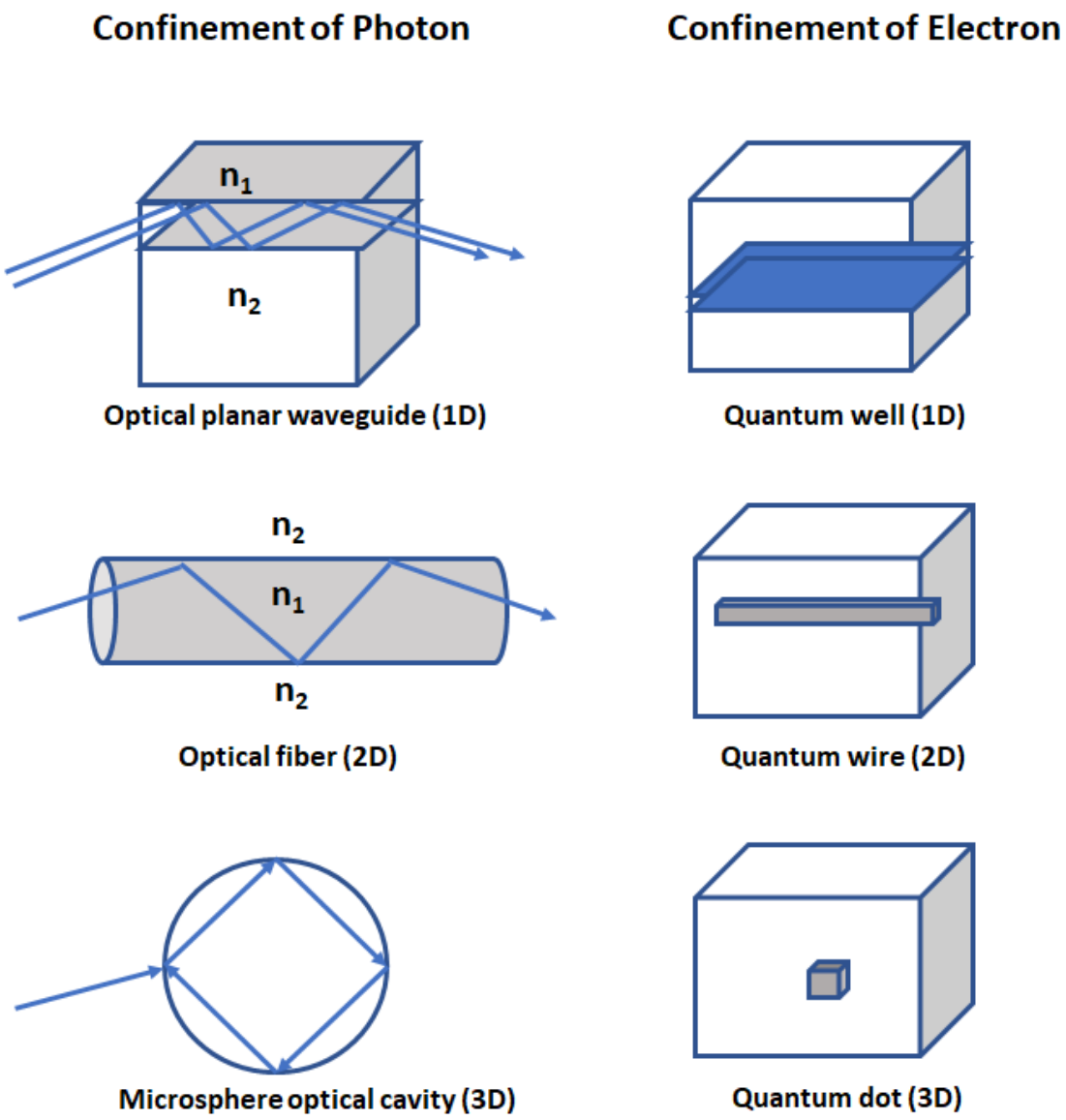

Fig. 1.1: Confinement of photon and the confinement of electron in different dimensions.

Like electrons, photons can be trapped by confining light in an area with a large refractive index or with a high surface reflectivity. (Yu and van de Lagemaat, 2011) A planar optical waveguide is an example of photon confinements in one dimension. (Johnson et al., 1998) When the refractive index of the light-guiding layer, n_1, is greater than the refractive index of the surrounding medium, n_2, light propagation is constrained in the high refractive index layer or thin film. For a optical fiber or a channel waveguide, the confinement is in two dimensions. Example for an optical medium that confines light in all directions is a microsphere optical cavity. (Wongcharoen et al., 1996) This type of optical confinement may be due to the

difference in the refractive indices between the guiding medium and the surrounding medium. So, the contrast n_1/n_2 creates a scattering potential and a barrier, to the passage of light. (Berg, 2018) Fig. 1.1 represents the confinement of photon and the confinement of electron in different dimensions.

Nanomaterials are often characterized as materials with at least one dimension smaller than about 100 nm and exhibiting unique physical and chemical features at the nanoscale. (Stucky and Mac Dougall, 1990) Nano thin film, nano filaments, quantum dots, nanotubes, nanocables, nanowires, composite materials, and other materials besides nano powder are examples of common nanomaterials. (Kostoff et al., 2006) Nanomaterials differ from microscopic atoms, molecules, and macro-objects in terms of physical, electrical, chemical and magnetic characteristics due to their unique nanoscale (1-100 nm) size. Because of the size decrease, the characteristic properties of macroscopic materials quickly shift to certain remarkable other properties. (Asha and Narain, 2020)

Multilayer nano thin films are now common elements of many optoelectronic and photonic devices, and the technological growth of these materials has resulted in the production of active and passive optical elements, which are often found in all types of optical characterization configurations. Multi-layered thin films are structures made up of numerous repeats of two alternating layers, as well as structures made up of a stack of unique layers. Optical multilayer thin films offer a wide range of uses in science and technology. A variety of strategies have been investigated for the design of multilayer thin films. Numerical simulation is the most versatile method. Thin film coatings can create optical surfaces with any desired reflectance and transmittance. (Hiller et al., 2002)

Multilayer thin films with nanoscale layer thicknesses have a unique geometry that leads to a variety of innovative features and behavior not observed in the bulk. When electromagnetic radiation incident on a multilayer thin film, a number of reflections may take place from each interface. Depending on the layer thicknesses, refractive index of the materials, and wavelength of the light sources, the reflected rays may be coherent or interfere with one another. This optical interference can be used in many opto-electronic and photonic devices. (Hammond, 2004)

Multi-layered thin film coatings can be used to create various optical filters such as anti-reflection coatings, highly reflective mirrors, high pass filters, comb filters, and so on. One

of the most common optical materials used in optoelectronics is distributed Bragg reflectors (DBR). A DBR is a mirror structure that consists of alternative layers of high and low refractive index materials are arranged in a periodic manner. They have received a lot of attention due to their unique properties and cost-effective production methods, such as the sol-gel. These extremely reflecting dielectric mirrors are used in waveguides, laser resonators, optical filters, and sensors along with many other applications. (Quaranta et al., 2018) Because of the diverse applications of DBR, we were inspired to create these featured DBRs and combine their usage into photonic and optoelectronic devices.

The multilayers, when linked with an active optical materials like emitting material or quantum dots to generate a cavity-like structure, have a wide range of applications in photonics. Quantum dots are semiconducting nano particles with size less than 10nm. Among the quantum dots, Carbon Quantum Dots (CQDs) are rising stars due to their low cost, intense fluorescence, nontoxicity, flexible luminescence range, great light stability, non-blinking property, and outstanding solubility among other quantum dots and with these important characteristics, CQDs have a wide range of potential applications. (Z. Zhang et al., 2016)

1.2 Multilayer Thin Film

Over the last few decades, there has been a lot of interest in the growth of multilayer thin films, both because of their fundamental features and because of their prospective usage in a variety of innovative applications. A thin film is a layer of material with a thickness that can range from a few micrometres to some fractions of nano meters. Multilayer thin films are periodic array of multiple thin film layers of different refractive indices.

Lord Rayleigh, in the early twentieth century, successfully used electromagnetic theory to describe the properties of multi-layer dielectric films. He established that as the angle of incidence changes, the wavelength of the reflected light from the multilayer thin films will change.(Henderson, 1960) He substantiated his argument by measuring the variance in reflected colour of butterfly wings as a function of angle of incidence. (Henderson, 1960; Tada et al.,

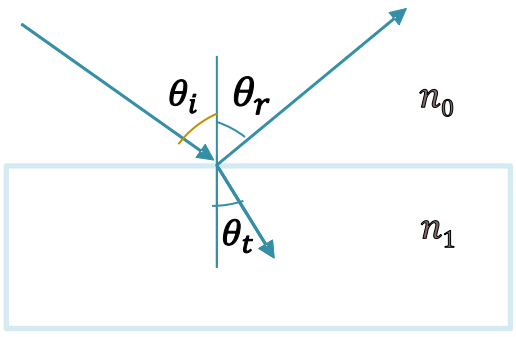

Fig. 1.2: Reflection and transmission in thin film

1999) And he established the fact that this is due to the structural arrangement of material. (Hartmann, 1985; Siddique et al., 2016; Tada et al., 1999)

When a beam of light incident on a thin film of refractive index n_1 from air of refractive index n_0, light is partially reflected and transmitted at the air film interface. Fig. 1.2 shows the reflection and transmission in a thin film. The transmitted wave may again undergo reflection from the bottom of the film. The two reflected light from the top and bottom surface of the thin film, may coherent and interfere with each other. (Blodgett, 1935) Depending upon the path difference between the two rays reflected from the top and bottom surface of the film, constructive or destructive interference takes place. (Blodgett, 1935) The optical path difference depends on the thickness of the film, refractive index of the material and the angle of incidence of light.(Huibers and Shah, 1997) Depending on the optical path difference, the film appeared as colored when viewed in white light. (Blodgett, 1935; Huibers and Shah, 1997)

The major optical property of periodic multilayers is their capacity to reflect and transmit light of specific wavelength ranges. (Smirnov et al., 2013) If the light waves reflected from each interface present in the stack interfere constructively, an intense specular reflectance peak will be obtained. (Corso and Pelizzo, 2019) The product of geometrical thickness and refractive index of the material is called optical thickness and this factor controls the optical interference effects of the film, when a beam of light incident on it. (Coppola et al., 2003)

Multilayer thin films, with layer thicknesses on the nanoscale, have a unique geometry that gives rise to novel features and innovative behaviour in the film. (Meng and Keten, 2018) These unique features of multilayered films emerge when the thicknesses of the stack of different layers approaches a specific length. (Wi et al., 2014) The multilayer thin films can be formed in different ways by mixing several different materials, with the resulting characteristics depends on the materials from which their component layers are constructed as well as the layer thickness (Mitzi, 2001), has driven to their use in many sectors of nanotechnology.

1.3 Fabrication Methods

Many different methods can be used for the fabrication of multilayers. Sputter deposition (Tinone et al., 1996), molecular beam epitaxy (Schulze et al., 1988), pulsed laser deposition (Liese et al., 2010), atomic layer deposition (Dameron et al., 2008) and solution

chemistry method (Mendelsohn et al., 2000) are common deposition techniques of thin films, enabled to deposit the layers as thin as a single monolayer, with the potential to build up multiple stacks of diverse layers. (Petrila et al., 2021) Among the thin film deposition techniques, solution chemistry methods provide a simple and adaptable thin film deposition methodology. (Mitzi, 2001) Even for oxides, solution processing enables control over the thickness, optical constants, composition, porosity, doping, tunable optical absorbance or transmission and other complex optical properties. (Glynn and O'Dwyer, 2017) Spin coating is an excellent technology for thin film production due to its low cost, homogeneity, safety, and ease of scaling up. The basic procedure is depositing a small amount of fluid onto the center of a substrate and then spinning the substrate at high speeds. (Tyona, 2013) Dip coating is another basic, low-cost method that may be scaled up for commercial production. (Scriven, 1988) Immersion, withdrawal, and evaporation are the three major technical processes in the dip coating process. (Yimsiri and Mackley, 2006) Spray coating is a potential approach in research and industry for producing thin and thick coatings. (Moridi et al., 2014) It is a simple technology for preparing thin films with uniform distribution at small scales ranging from a few nanometers to micrometers in thickness. (Sun et al., 2020) Inkjet printing is a new potential approach for creating large-scale, flexible thin films. The inkjet printing technology allows for simple customization of a wide range of complicated structures. (Shahrubudin et al., 2019) This type of solution processing methods does not require ultra-high vacuum deposition unit and the method is relatively cheaper and also they can be processed at room temperature (Akedo et al., 2008) We adopted this simple solution chemistry method for the thin film fabrication.

1.4 Materials

The multilayer thin films can be fabricated from inorganic and organic materials. (DiBenedetto et al., 2009) Inorganic materials used in the multilayer fabrications are Magnesium fluoride (n ~ 1.37), Zinc sulphide (n ~ 2.32), Silicon dioxide (n ~ 1.45), Calcium fluoride (n ~ 1.43), Titanium dioxide (n ~ 2.2), Aluminium oxide (n ~ 1.62) etc. (Muallem et al., 2015, p. 2) and the fabrication methods includes physical vapour deposition methods, (Kim et al., 2017) laser ablation, (Liese et al., 2010)sputtering, (Tinone et al., 1996) pulsed charge deposition etc. (Chávez-Valdez and Boccaccini, 2012) The organic materials used in the multilayer fabrications are Cellulose acetate (CA, n ~ 1.46), (Lova, 2018) Poly(methyl methacrylate) (PMMA, n ~ 1.50), (Du et al., 2010) Polyacrylic acid (PAA, n ~ 1.51), (Petersen

et al., 2012) Polyvinyl alcohol (PVA, $n \sim 1.52$), (Morissette et al., 2004) Polystyrene (PS, $n \sim 1.58$) (Gao et al., 2006)etc. and the fabrication methods includes solution chemistry methods like spin coating, dip coating etc.

The selection of a precursor solution is essentially the first part in the preparation of a solution processed thin film material. After preparing the solution, any solution processed method can be adopted for depositing liquid precursors onto substrates in order to generate a thin layer coating. Each approach has advantages and disadvantages that can be influenced by the chemical and adhesion properties of the precursor solution and the substrate. (Song et al., 2005) Spin coating is still one of the most widely used deposition processes for homogenous layers in academics and industry. Multilayers of polymer thin films can be coated on the glass substrate through spin coating method in a simple and cost-effective way (Köhnen et al., 2009)

Multilayer thin films can be employed for the fabrication of the antireflection coatings, distributed Bragg reflectors, comb filters and dichroic filters etc. We had fabricated the flexible Distributed Bragg reflectors (DBR) in a simple cost-effective solution chemistry method by a spin coater. DBR is a mirror structure composed of an alternating sequence of layers with high and low refractive index materials organized in a periodic pattern. (Almeida and Portal, 2003) All of the reflected components from the interfaces interfere constructively, resulting in strong reflection. Previously, DBR was fabricated using inorganic metal oxides or semiconductor thin films. These materials have comparatively high refractive indices and so high refractive index contrast between the pairs can be achieved by using these materials. (Bergström, 1997) Even though they provide high refractive index contrast, the fabrication method have high cost of installation and maintenance. Also, the poor mechanical properties of inorganic metal oxides limiting the possibilities of fabricating flexible, stretchable and bendable opto-electronic and photonic devices. (He et al., 2015) Flexible DBR can be used in opto-mechanical sensing applications. (Pruessner et al., 2011) When creating optoelectronic, optomechanical, and photonic devices, cost reduction and efficiency enhancement are critical variables. Polymer DBRs can produce high reflectivity through simple and cost-effective production processes. (Resende et al., 2018) The use of polymeric materials in the fabrication of DBR has advantages in mechanical sensing applications. (Lova et al., 2018) Polymers are highly flexible under stress and so very beneficial in the manufacturing of flexible DBR. (Kleine et al., 2018) These flexible DBR have very much importance in the fabrication of optical devices such as solar cells, lasers, sensors, ultra-sound receivers etc. (Sethiya et al., 2020)

The optically transparent polymers used for the fabrication of flexible DBRs are

- Fluorinated polymer (n ~ 1.3)
- Cellulose acetate (CA, n ~ 1.46)
- Poly (methyl methacrylate) (PMMA, n ~ 1.50)
- Polyacrylic acid (PAA, n ~ 1.51)
- Polyvinyl alcohol (PVA, n ~ 1.52)
- Polystyrene (PS, n ~ 1.58)
- Poly (N-vinyl carbazole) (PVK, n ~ 1.68) etc.

Using polymers, the DBR fabrication become simple and cost-effective. The fabrication can be done in the solution processing method like spin coating. But the limitations are the refractive index of polymers are comparatively low. (Luk'yanchuk et al., 2017) So, high refractive index contrast between the pairs cannot be achieved. (Luk'yanchuk et al., 2017) So, large number of periods were required to attain the desired reflectivity. (Karim et al., 2000) Also, few works were reported on polymer DBRs. These limitations motivated us in developing a new class of polymer-inorganic nano composite for the high index polymer. The refractive index of the polymers can be increased by forming a metal oxide-polymer nano composite. (Ritchie et al., 2021)

The advantages of using Polymer DBR in the fabrication of flexible DBR (Prontera et al., 2021; Ritchie et al., 2021) are

- Promising alternatives to inorganic materials in the fabrication of flexible DBR
- High refractive index can increase index contrast
- Simple and cost-effective processing methods
- High reflectance can be achieved
- High optical transparency can be achieved
- Stop band can be increased
- Flexible DBR with desired reflectivity and stop band can be fabricated

To increase the refractive index of the polymers, we have chosen TiO_2 as the inorganic metal oxide in our research work. Many studies have been conducted on titanium dioxide films due to their exceptional optical and electrical properties. (Akl et al., 2006) Since TiO_2 is water soluble, we considered water soluble poly vinyl alcohol (PVA) as our polymer. Here TiO_2 and

PVA can be easily mixed together and both are non-toxic. (Ahmed et al., 2020) So, by mixing TiO_2 and PVA in definite proportions, the refractive index of PVA can be increased.

Now a days, multilayer thin films have numerous applications in the field of opto-electronic and photonic devices that can integrate the features of several materials. The most frequent optical elements in solar cells, optical filters, lasers, sensors, and other devices are multilayers of transparent materials repeated in periodically. (Dubey and Ganesan, 2017; Hu et al., 2017; Lova, 2018) Multilayer thin films have significant applications in a variety of opto-electronic and photonic devices, including computer discs, optical filters, sensors, lasers and solar cells etc. (Dubey and Ganesan, 2017; Wu et al., 2019) The distinctive geometry of multilayer thin films with nanoscale layer thicknesses gives birth to a diverse range of applications in opto-electronics. (Hammond, 2004) Numerous optoelectronic and photonic devices use the multilayer thin films as optical filters, antireflection coatings, highly reflective films, etc. (Wu et al., 2019) Multilayer thin films are also used in solar panels and solar cells, in the medical industry as drug carriers, in water filters as desalination membranes etc. (Barhoum et al., 2019)

1.5 Passive optical components

Optical passive components are those devices or components that can produce light modification. They doesn't use any active devices or components for its operations. (Ismaeel et al., 2013) The main role of optical passive devices are

- to connect the optical waveguide or optical path
- to control the direction of light propagation
- to control the optical power distribution
- optical coupling etc.

Examples of optical passive devices are optical filters like anti reflection coatings, distributed Bragg reflectors, dielectric film filters, power dividers, polarization splitters, optical couplers, optical connectors, electro-optic modulators, magneto-optic modulators etc. (Coenning and Caloz, 2017) Some passive optical components are described below.

1.5.1 Antireflection coatings as passive optical component

An anti-reflection (AR) coating is a type of optical coating used to reduce reflection on the surface of lenses and other optical devices. (Krogman et al., 2005) They are made up of thin films of one or more layers of transparent materials that are coated on lenses to reduce the reflection. (Walheim et al., 1999) In AR coatings, the optically transparent multilayers are conveniently used for light modification and can be used as passive optical components. For example, on coating MgF_2 above the glass substrate with optical thickness equal to quarter wavelength thickness, reduced the reflectivity to 4%. (Cox et al., 1954)

1.5.2 Distributed Bragg reflectors (DBR) as passive optical component

DBR is a mirror structure made up of an alternating array of high and low refractive index materials that are stacked in a periodic pattern. (Quaranta et al., 2018) The reflectivity of the DBR increased by increasing the number of periods as well as refractive index contrast between the alternative layers. (Anaya et al., 2016) So, the light modification is possible by using DBR and can be used as a passive optical component. For example, SiO_2/TiO_2 as alternating low and high refractive index materials. (Wu et al., 2007, p. 2)

1.5.3 Comb filters as passive optical component

In comb filters, a thick optically transparent material is sandwiched between two DBRs, by forming cavity like structure. (Chénais and Forget, 2012) As the thickness of the middle layer increases, a number of low reflectance windows were opened and the full width at half maximum of the window decreased. (Persson et al., 2006) So, the light modification is possible by using comb filters and can be used as passive optical component. For example, an optically transparent material like PVA, PMMA etc. sandwiched between two DBR structures.

1.5.4 Dichroic filters as passive optical component

A dichroic filter allows light of a certain wavelength range to pass through while reflecting light of an undesirable wavelength. (Shapiro, 2001) High pass and low pass filters can construct using dichroic filters and can be used as passive optical component. Example, arranging 60 pairs of Nb_2O_5 and TiO_2 in a periodic manner.

1.6 Active optical components

In recent years, there has been a lot of research on new optical active components that can be tuned actively. Optical active materials are those materials that can generate/absorb photo electron or photon. (Dalton, 2000) i.e. Light generation or absorption are possible by these materials. Also, optical active components required a power source to function. The main elements are optical sending and receiving module, optical amplifier, electrical adjustable attenuator etc. The optical active components widely used in optical lasers, optical transceivers, optical receivers etc. (M. Xiao et al., 2020)

1.6.1 Active optical components in laser

Laser dyes are employed as the active medium in dye lasers which can be considered as an active optical component. (Singh et al., 2003) Examples for laser dyes are Coumarins, polyphenyl, Fluorescein, Rhodamine 6G, Rhodamine B, Rhodamine 123, Umbelliferone etc. (Berggren et al., 1997) Each dye emits radiations in the specific region of the electromagnetic spectrum. For example, Rhodamine dyes are employed for emission in the yellow-red spectrum, whereas coumarin dyes emit in the green portion of the spectrum. (Wang et al., 2019) The surrounding media, or the medium in which the laser dyes are dissolved, determines the colour that is emitted by them. There are, however, many laser dyes that can be employed to constantly span the emission spectrum from near ultraviolet to near infrared. (Rurack and Spieles, 2011) Now a days, these laser dyes can be tuned actively.

1.6.2 Quantum dots (QDs) as active optical components

Quantum dots are semiconducting nano particles with size few nano-meters. (Lisichkin and Olenin, 2020) Quantum-dot molecules are quantum-mechanical systems with delocalized electronic states and molecular-like wave functions that are built from linked semiconductor nanocrystals. Electrons behave differently in quantum-confined semiconductor nanostructures than they do in bulk materials. (Zhang, 1997) This allows for the creation of materials with variable chemical, physical, electrical, and optical properties. The characteristic properties of Quantum dots that fall in between those of bulk semiconductors and discrete atoms or molecules. (Zheng et al., 2004) Their optoelectronic properties depend on size and shape. QDs with larger size (5-6 nm diameter) emits colours as orange and red (longer wavelength) (Park et al., 2016) and smaller QDs (2-3 nm diameter) emits shorter wavelength in the blue and green

region of the electro-magnetic spectrum. (Deppe, 2003) The QDs can be actively tuned and used as an active optical component. Some examples for QDs are InGaAs (Indium Gallium Arsenide), CdSe (Cadmium Selenide), PbS (Lead Sulphide), CdS (Cadmium Selenide) etc. Now a days Carbon quantum dots (CQDs) and Graphene quantum dots (GQDs) are widely used QDs from biomaterials. (Zheng et al., 2015)

These optical meta-surfaces have unique properties in the achievement of dynamic tuning due to their optically thin structures. Adding active components to optical nanostructures was a significant step in creating next-generation optical components and devices. Many attempts have been made recently, to develop tuneable optical meta-surfaces with dynamic control of optical properties over amplitude, polarisation, phase, intensity etc. Functions like tuneable focusing, beam steering, tuneable colour filters or absorbers etc. are based on numerous novel active materials and tuneable techniques. (S. Xiao et al., 2020) On incorporating these active meta-surfaces with multilayers have a lot of potential in the real-world applications.

1.7 Transfer Matrix Model (TMM) Simulations

Many different methods can be adopted for the design of multilayer thin films. The most adoptable method for the design is numerical simulation method (Lu et al., 2016)and with proper design, any desired reflectivity and transmittance can be achieved. The transfer matrix model simulations are the best tool for simulating desired reflectivity, absorption and transmission for any number of layers of materials. (Barrios et al., 2015) The transfer-matrix model simulations are based on the Maxwell's equations, and according to this, the electric field and magnetic field should be continuous at the boundaries as it travels from one medium to the other. (Hao and Zhou, 2008) If the field at the beginning of the layer is known, the field at the exit of the layer can be calculated using a simple matrix operation. For the multilayers, the transfer matrix is the product of the individual layer matrices and finally converting the transfer matrix back into reflection and transmission coefficients and from this the reflectivity and transmittance can be found out.

Schematic of multi-layered structure with N layers having refractive indices n_1, n_2, n_3, ... n_j.... n_N are shown in fig. 1.3. Light is partially absorbed, reflected, and transmitted at each interface when it enters to this multi-layered structure. The thicknesses and refractive indices

of the layers can determine whether reflected wave interference is constructive or destructive at a specific wavelength. Transfer matrix model simulations can be used to calculate transmission and reflection of the given structure. (n.d.)

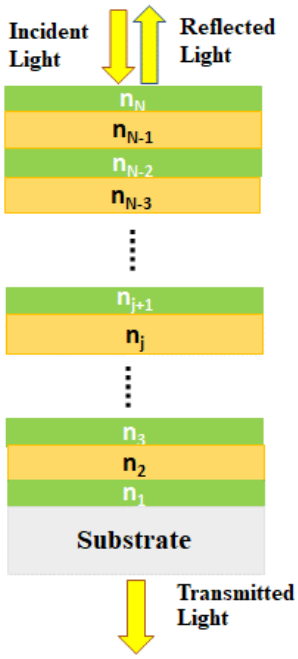

Fig. 1.3: Schematic of multi-layered coating

When an electromagnetic beam of light strikes a thin film of dielectric material with a thickness l and a refractive index of n_l, sandwiched between two infinite media with refractive indices of n_o and n_t (one is air and the other is substrate) respectively. The incident, reflected, and transmitted amplitudes of the electric fields are E_I, E_R and E_T respectively. It is schematically represented as shown in the fig. 1.4.

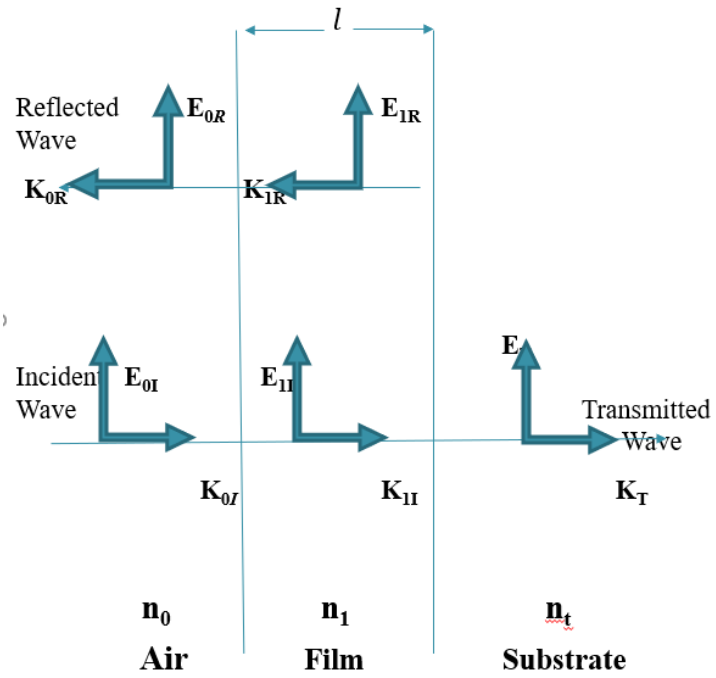

Fig. 1.4: Reflection and transmission in a multilayer thin film

The boundary conditions require that the electric and magnetic fields should be continuous at each interface.

For first interface, $E_{0I} + E_{0R} = E_{1I} + E_{1R}$ (1.1)

$$H_{0I} - H_{0R} = H_{1I} - H_{1R} \quad (1.2)$$

$$n_0 E_{0I} - n_0 E_{0R} = n_1 E_{1I} - n_1 E_{1R} \quad (1.3)$$

For second interface $E_{1I} e^{ikl} + E_{1R} e^{-ikl} = E_T$ (1.4)

$$H_{1I} e^{ikl} - H_{1R} e^{-ikl} = H_T \quad (1.5)$$

$$n_1 E_{1I} e^{ikl} - n_1 E_{1R} e^{-ikl} = n_t E_T \quad (1.6)$$

Eliminating E_{1I} and E_{1R}

$$1 + \frac{E_{0R}}{E_{OI}} = \left[cos\ kl - \frac{in_t}{n_1} sinkl\right] \frac{E_T}{E_{OI}} \tag{1.7}$$

$$n_0 - n_0 \frac{E_{0R}}{E_{OI}} = [-in_1 sinkl + n_t cos\ kl] \frac{E_T}{E_{OI}} \tag{1.8}$$

The equations can then be written in matrix form by applying boundary conditions at the two interfaces and simplifying them as

$$\begin{bmatrix} 1 \\ n_0 \end{bmatrix} + \begin{bmatrix} 1 \\ -n_0 \end{bmatrix} \frac{E_R}{E_O} = \begin{bmatrix} cos\ kl & -\frac{i}{n_l} sinkl \\ -in_l sinkl & cos\ kl \end{bmatrix} \begin{bmatrix} 1 \\ n_t \end{bmatrix} \frac{E_T}{E_O} \tag{1.9}$$

$$\text{Let, r} = \frac{E_R}{E_O}, \quad \text{t} = \frac{E_T}{E_O} \text{ and M} = \begin{bmatrix} cos\ kl & -\frac{i}{n_l} sinkl \\ -in_l sinkl & cos\ kl \end{bmatrix} \tag{1.10}$$

Where r and t are reflection and transmission coefficients respectively and M is the transfer matrix. Then equation (1.9) reduces to

$$\begin{bmatrix} 1 \\ n_0 \end{bmatrix} + \begin{bmatrix} 1 \\ -n_0 \end{bmatrix} r = M \begin{bmatrix} 1 \\ n_t \end{bmatrix} t \tag{1.11}$$

Now suppose that we have N layers numbered as 1, 2, 3, . . . N having indices of refraction $n_1, n_2, n_3, \ldots n_N$ and thicknesses $l_1\ l_2, l_3\ \ldots l_N$ respectively., then we have

$$\begin{bmatrix} 1 \\ n_0 \end{bmatrix} + \begin{bmatrix} 1 \\ -n_0 \end{bmatrix} r = M_1 M_2 M_3 \ldots\ldots M_N \begin{bmatrix} 1 \\ n_t \end{bmatrix} \text{t} \tag{1.12}$$

$$= \text{M} \begin{bmatrix} 1 \\ n_t \end{bmatrix} t \tag{1.13}$$

$$\text{Where M} = M_1 M_2 M_3 \ldots\ldots M_N = \begin{bmatrix} \text{A} & \text{B} \\ \text{C} & \text{D} \end{bmatrix} \tag{1.14}$$

is the overall transfer matrix. Then from eqn. (4) and (6) we have

$$r = \frac{An_0 + Bn_t n_0 - C - Dn_t}{An_0 + Bn_t n_0 + C + Dn_t} \tag{1.15}$$

$$\text{and } t = \frac{2n_0}{An_0 + Bn_t n_0 + C + Dn_t} \tag{1.16}$$

So, reflectance and transmittance are given by $R = [r]^2$ and $T = [t]^2$ respectively.

Using the transfer matrix model simulations, it is possible to design antireflection coatings, distributed Bragg reflectors, different types of optical filters like comb filters, dichroic filters etc.

1.7.1 Theory of Antireflection Coatings

An anti-reflection (AR) coating is an optical coating that reduces reflection on the surface of lenses and other optical devices. This enhances the efficiency of ordinary imaging systems since less light is wasted owing to reflection. The removal of stray light increases the contrast of the picture in complicated systems such as cameras, binoculars, telescopes and microscopes by reducing reflections. (Keller, 2006) In planetary astronomy, antireflection coatings are very essential. Also, a coating on eyeglass lenses that makes the wearer's eyes more prominent to others.

The reflection coefficient is given by,

$$r = \frac{n_1(1 - n_t)\cos kl \; - \; i(n_t - n_1^2)\sin kl}{n_1(1 + n_t)\cos kl \; - \; i(n_t + n_1^2)\sin kl} \qquad (1.17)$$

For AR coatings to achieve zero reflectance at λ, optical thickness is fixed at $\lambda/4$ for each layer and the reflectance is equated to zero in eqn. 7, to obtain the required refractive index matching condition.

If the optical thickness equal to quarter wavelength thickness, $kl = \pi/2$

$$R = \frac{(n_t - n_1^2)^2}{(n_t + n_1^2)^2} \qquad (1.18)$$

For R=0, $n_1 = \sqrt{n_t}$

To achieve a wide range of wavelengths with zero reflectance, a tri-layered structure with optical thickness ($\lambda/4$- $\lambda/2$- $\lambda/4$) has to be chosen. Fig. 1.5 shows the schematic representation of three-layer anti-reflection coatings with multilayers.

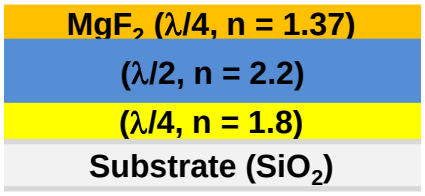

Fig. 1.5: Schematic representation of three-layer anti-reflection coatings

1.7.2 Theory of Highly reflecting mirrors

The transfer matrix method can be widely used in industries for designing highly reflecting mirrors called distributed Bragg reflectors. (Balili, 2012) These distributed Bragg reflectors made up of alternating sequence of layers of high and low refractive index materials of quarter wave thickness arranged in a periodic manner. If the number of pairs of alternating high and low refractive index materials increases, reflectivity also increases. The reflectivity also increased with increasing refractive index contrast between high and low refractive index material. Also, the stop band is determined mainly by the index contrast of the two materials. Between any two DBRs an optical medium is placed, then it will form an optical cavity called microcavity. (Ho et al., 1999) Semiconductor lasers and other optoelectronic devices have this fundamental structure. The Schematic representation of a DBR is as shown in the fig. 1.6.

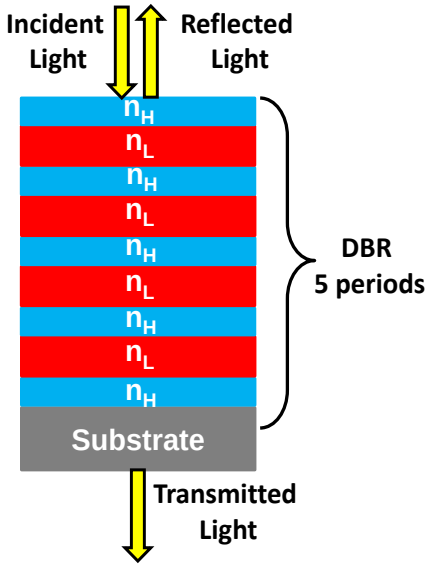

Fig. 1.6: Schematic of a DBR, n_H and n_L are high and low index layers respectively

Alternative layers of high and low refractive indices n_H and n_L were stacked periodically to form a DBR structure.

$$M=\begin{bmatrix} 0 & -\frac{i}{n_L} \\ -in_L & 0 \end{bmatrix}\begin{bmatrix} 0 & -\frac{i}{n_H} \\ -in_H & 0 \end{bmatrix}=\begin{bmatrix} \frac{-n_H}{n_L} & 0 \\ 0 & \frac{-n_L}{n_H} \end{bmatrix} \quad (1.19)$$

$$\text{For 2N layers, } M=\begin{bmatrix} \left(\frac{-n_H}{n_L}\right)N & 0 \\ 0 & \left(\frac{-n_L}{n_H}\right)N \end{bmatrix} \quad (1.20)$$

$$R=\left(\frac{\left(\frac{n_H}{n_L}\right)^{2N}-1}{\left(\frac{n_H}{n_L}\right)^{2N}+1}\right)^2 \quad (1.21)$$

When N is Large, R tends to unity.

Highest reflectance occurs at λ when optical thickness of high index and low index matches the condition,

$$n_L l_L = n_H l_H = \lambda/4. \quad (1.22)$$

1.7.3 Theory of Comb Filters

To realize a comb filter, sandwiching a thick optically transparent layer in between two DBRs by forming a cavity like structure. To get greater number of zero reflectance windows, the cavity length can be increased. As the width of the cavity increases, a number of low reflectance windows were opened and the full width at half maximum of the window decreased. (Shuni Chu and Burrus, 1984) Fig. 1.7 shows the schematic representation of a Comb filter.

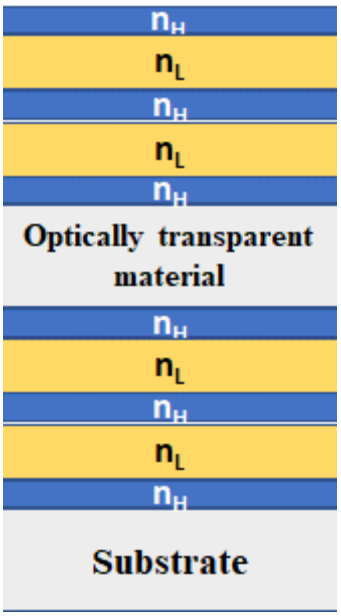

Fig. 1.7: Schematic representation of a Comb filter

1.7.4 Theory of Dichroic Filters

For the design of dichroic filters, a stack of alternative layers of two different optical materials were arranged in a periodic manner similar to DBRs. (Besso et al., 2005; Duan et al., 2007) Here optical thickness of each layer may be varied from quarter wavelength thickness. By changing the number of periods and high index material, we can tune the cut off wavelength of the pass band filters. High pass and low pass filters can be designed using dichroic filters. (Ye Zhou et al., 2009) Fig. 1.8 shows the schematic representation of a Dichroic filter.

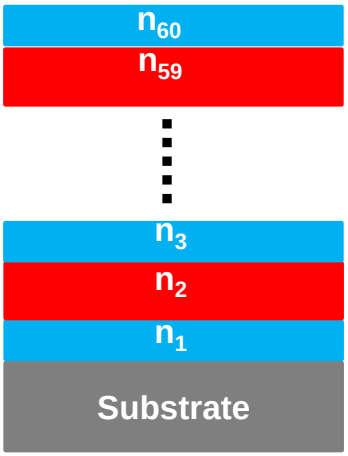

Fig. 1.8: Schematic representation of a Dichroic filter

1.8 Active optical components in our work

In our research work, we considered carbon quantum dots (CQDs) and fluorescein materials as active optical components.

1.8.1 Carbon quantum dots (CQDs)

We present the preparation and characterization method of highly photoluminescent CQDs in a simple, cost-effective way by microwave assisted hydrothermal method. Carbon quantum dots, a rising star of carbon nanomaterials (Wang et al., 2017), have demonstrated remarkable impetus in a variety of sectors such as biosensing, bioimaging, drug delivery, optoelectronics, photovoltaics, and photocatalysis due to their unique physicochemical, optical, and electrical capabilities. (Samantara et al., 2018) The rich optical and electronic properties of CQDs, in particular efficient light harvesting, tunable photoluminescence (PL), extraordinary up-converted photoluminescence (UCPL), and outstanding photoinduced electron transfer, have attracted the attentions of various photocatalytic applications for optimum exploitation of the solar spectrum. CQDs combines the specific optical qualities of quantum dots with the distinctive electronic properties of carbon materials, distinguishing them from standard semiconductor quantum dots or other carbon nanomaterials. (Rani et al., 2020) CQDs have been extensively investigated in various domains, including biosensing, bioimaging, drug delivery, photocatalysis, photovoltaic devices, and optoelectronics. (Wang et al., 2017) These zero-dimensional semiconductor quantum dots (QDs) exhibit optical gain and lasing as well as significant light absorption and brilliant narrowband emission over ultraviolet and visible wavelengths. (Zhang et al., 2019) These characteristics are useful in photography, solar energy harvesting, displays, and communications. (Zhang et al., 2019)

CQDs are frequently described as having a carbogenic core and surface functional groups. Most CQDs have an amorphous to nanocrystalline core composed primarily of sp^2 carbon with lattice spacings compatible with graphitic or turbostratic carbon. (Li et al., 2012) Graphene quantum dots (GQDs), which have comparable structures to CQDs, can be considered one type of CQDs, however they typically have higher crystallinity than CQDs. CQDs are nanoparticles with sp2- or sp3-carbon structures and a high proportion of oxygen- and nitrogen-containing functional groups. GQDs have a quantum-sized effect and are made up of one to several layers of graphene that are commonly functionalized with molecule groups

at the edges. CQDs are usually spherical or quasi-spherical nanoparticles with varying degrees of crystallinity; they frequently exhibit excitation-dependent photoluminescence. (Cao et al., 2013)

It is possible to tune CQD emission across a large spectral range, which may be undertaken at the synthesis stage by altering precursors and reaction conditions. In contrast to most "traditional" Cd- or Pb-based semiconductor QDs, CQDs do not contain any hazardous components and are considered non-toxic materials. Furthermore, the PL quantum yield of CQDs may readily reach extremely high levels, particularly in the blue and green spectral ranges. (F. Zhang et al., 2016) CQDs have been widely employed in bio-imaging, sensing, and other biomedical applications because CQDs are a biocompatible and non-toxic alternative to QDs. (Devi et al., 2019) Phosphorescence has been detected at room temperature in composite materials based on CQDs, which is a valuable characteristic for data encryption. So, the electronic nature of CQDs, and hence their optical transitions, can be regulated and modified over a large spectrum range by adjusting the synthesis conditions and post-synthetic treatment. (Wu et al., 2017)

The CQDs can be incorporated with the multilayers have numerous applications. On incorporating with multilayers Carbon quantum dots can be used as active medium in lasers and distributed Bragg reflectors can be used as fully and partially reflecting mirrors. (Hammond, 2004) CQD's photoluminescence characteristics, band gap, and energy levels can be modified using appropriate structural engineering and so they have wide spread applications in photovoltaic devices. Solar cells are electrical devices that turn light into electrical energy using the photovoltaic (PV) effect; they are made up of a p-n junction, which produces an electric current when the material is illuminated. Because of its low weight, semitransparency, flexibility, and customizable colors, organic photovoltaic devices (OPVs) have become a prime example when compared to silicon and other PV technologies. Toxic and harmful materials are present in photovoltaic devices manufactured with conventional processes. Fluorescent carbon quantum dots might be regarded a low-cost and sustainable alternative to these materials in this scenario. (Lim et al., 2018)

1.8.2 Fluorescein

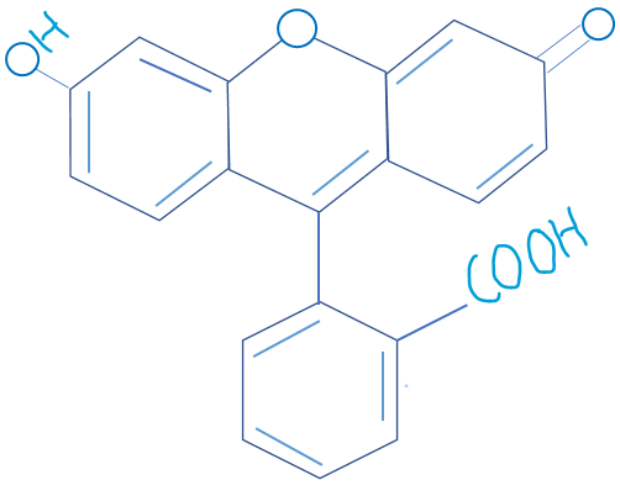

Fig. 1.9: Molecular structure of fluorescein molecule

Another active component we have used in our study and incorporated with multilayers in our work is the fluorescein. Fluorescein is a dye and an organic substance and it comes in the form of a dark orange or red powder that is slightly soluble in water and alcohol. (Sednev et al., 2013) It is generally utilized as a fluorescent tracer in a variety of applications. (Yao et al., 2014) Due to its elevated fluorescence and other photophysical properties, fluorescein and its derivatives form a family of versatile functional dyes that have been widely employed. (Sjöback et al., 1995; Yao et al., 2014) Fluorescein dyes are xanthene dyes with a three-membered ring structure and they share structural similarities with xanthones. (Kalampaliki et al., 2021; Sjöback et al., 1995) The chemical formula of fluorescein is $C_{20}H_{12}O_5$. The molar mass of fluorescein is 332.311 $g \cdot mol^{-1}$ and density is 1.602 g/mL. Fig. 1.9 shows the molecular structure of fluorescein molecule. The important derivative of fluorescein is fluorescein iso-thio-cyanate (FITC). (Kalampaliki et al., 2021)

Because of its very strong molar absorptivity, high fluorescence quantum yield, and excellent photostability, it is a very useful and sensitive fluorescent. (Nakayama-Ratchford et al., 2007) The fluorescein molecules also show PH dependent absorption and emission. (Nakayama-Ratchford et al., 2007) Fluorescein derivatives, which were covalently linked to a variety of functional molecules, have a wide range of applications in biological studies. Fluorescent sensors based on conventional organic and polymeric fluorophores have become very popular in recent years. (Gupta et al., 2005)

The free spectral emission wavelength of Fluorescein is found to be 500nm to 650nm. (Burdette et al., 2001). The Free spectral emission of Fluorescein molecule is presented in the fig.1.10. The peak excitation wavelength of fluorescein in water is 494nm and peak emission is at 521nm. (Ghini et al., 2013) Due to the self-absorption mechanism, the fluorescence

quantum yield is extremely sensitive to sample concentration and excitation wavelength. To avoid the self-absorption effect, the dye concentrations were kept low. (Zhang et al., 2014)

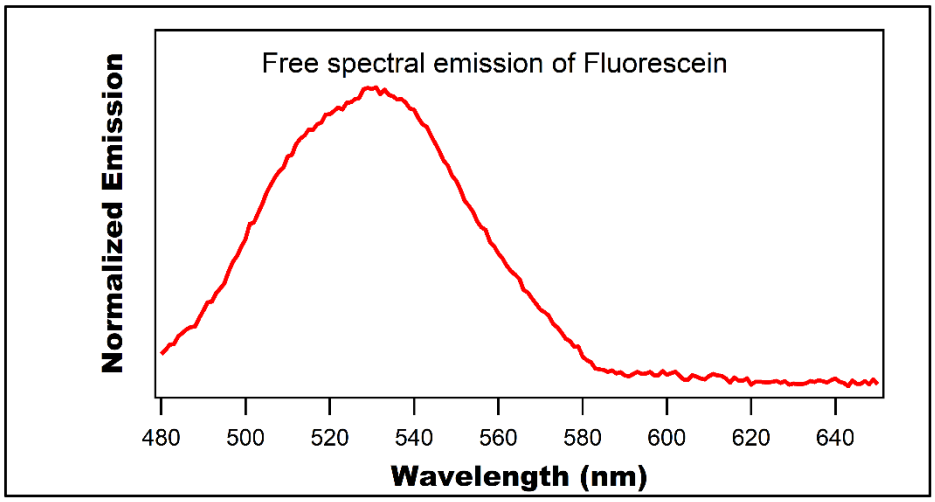

Fig. 1.10: Free spectral emission of Fluorescein molecule

Over the past ten years, the use of fluorescence technology in biology, biotechnology, and medicine has grown significantly. Numerous analyses in sensing, medical diagnosis, biotechnology, and gene expression now use fluorescence as their primary analytical tool. Even though fluorescence detectors have high sensitivity, more sensitivity is always needed to detect fewer target molecules. The sensitivity of fluorescence methods is restricted by a number of factors. The extent of background fluorescence, the efficiency of photon collection, and photolysis of the fluorophores are the three that are most crucial. (Liu et al., 2016) To improve detection sensitivity, there are various ways to alter the emissive characteristics of fluorophores. (Bigdeli et al., 2019)

1.9 Passive optical components in our work

In our research work, multilayer thin films were conveniently used to design and fabricate various passive optical components. We had designed passive optical components like antireflection coatings, distributed Bragg reflectors, comb filters and dichroic filters etc. Also, we had fabricated distributed Bragg reflector by using polymers and a reflectivity of 63% were achieved. The details about the passive optical components were described in the previous sessions.

1.10 Mechanism of Fluorescence Emission

Photoluminescence is a phenomenon that occurs when a molecule is excited by photons of ultraviolet or visible light. (Murthy and Virk, 2013) Depending on the electronic configuration of the excited state and the emission route, photoluminescence might be classified as fluorescence or phosphorescence. The property of some atoms and molecules to absorb light of a specific wavelength and then, after a small period of time, release light of a longer wavelength is known as fluorescence. Similar to fluorescence, phosphorescence happens in a similar way but has a significantly longer excited state lifespan. (Bebb and Williams, 1972)

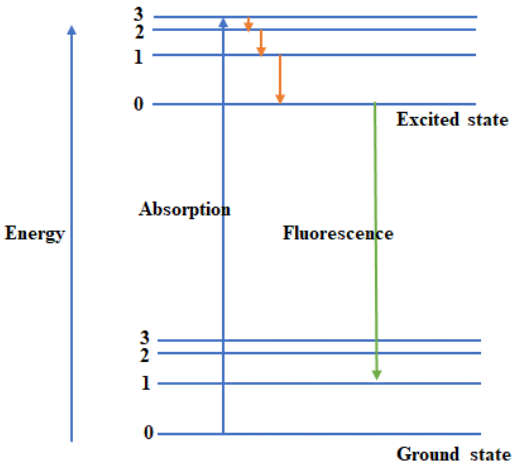

Fig. 1.11: Jablonski diagram

Fluorescence is the emission of a photon by an excited molecule or atom or nanostructure without a change in the electron spin as it relaxes to a lower energy state. (Noomnarm and Clegg, 2009) The phenomenon is known as phosphorescence when the spin of the initial and final states differs. (Murthy and Virk, 2013) In fluorescence, the radiation that is absorbed has a higher photon energy, but the light that is released has a lower energy; so longer wavelength. (Noomnarm and Clegg, 2009) When the fluorescent material absorbed radiation in the ultraviolet (UV) region of the electromagnetic spectrum, even though which is invisible to the human eye, the emission observed in the visible region of the electromagnetic spectrum. (Kontges et al., 2020) This gives the fluorescent substance a distinctive colour that can only be seen when exposed to UV radiation. (Kontges et al., 2020) Unlike phosphorescent materials, which continue to emit light for some time after the radiation source is turned off, fluorescent materials quit glowing almost instantly. (Murthy and Virk, 2013)

A Jablonski diagram in molecular spectroscopy represents a molecule's electronic states and the transitions between them. (Zimmermann et al., 2003) Fig. 1.11 shows the Jablonski diagram represents the vibrational levels of a material describes the absorbance, non-radiative decay, and fluorescence. Here the non-radiate transitions that include vibrational transitions,

internal conversions and intersystem crossings.(Zimmermann et al., 2003) Vibrational relaxation is the process of relaxation of the excited state to its lowest vibrational level. Since this process requires energy to be dissipated from the molecule to its surroundings, it cannot take place for isolated molecules. When a vibrational state from an electronically excited level may couple to a vibrational state from a lower electronic state, internal conversions take place. A transition to a state with a different spin multiplicity is called an intersystem crossing. Intersystem crossing is far more significant in molecules with substantial spin-orbit coupling than it is in molecules with weak spin-orbit coupling. Phosphorescence may come after intersystem crossing. (Kasha, 1950)

1.11 Light matter interaction studies

On incorporating the active and passive optical components with multilayers have wide range of potential applications. (Hammond, 2004) The light matter interaction experiments were accomplished by combining the active and passive optical components with the multilayers. We had performed surface plasmon coupled emission (SPCE) and SPCE tuning experiments by combining fluorescein with multilayers. Plasmons are quanta of plasma oscillations caused by the interaction between photon and electron. Just like light which is made up of photons, the plasma oscillation is made up of plasmons. So, in definition, the collective oscillations of the free electrons in a metal are known as plasmons. Plasmons that are restricted to surfaces and have a strong interaction with light are known as surface plasmons. (Raether, 1988)

The coherent delocalized electron oscillations at the interface between a metal and a dielectric material stimulated by incident light is known as surface plasmons (SPs). (Raether, 1988) So, the surface plasmon can be regarded as a non-radiative electromagnetic surface wave that propagates in a direction parallel to the interface [116]. These oscillations are extremely sensitive to changes in this boundary, such as molecule adsorption etc. on the conducting surface. (Cuevas et al., 2016) The two materials (metal and dielectric) are chosen in such a way that at the interface, the real part of the dielectric function reverse the sign.

Silver and gold are two common metals that can create surface plasmons, and both have a negative dielectric constant. Surface plasmon is also supported by copper, chromium, titanium and certain other metals. Surface plasmon resonance (SPR) refers to the resonant oscillation of conduction electrons at the interface of negative and positive permittivity materials (metal and dielectric) stimulated by incoming light. (Deng et al., 2022) In order for SPR to occur, the incoming radiation's momentum must match that of the plasmon, and when this occurs, the intensity of the reflected light falls drastically. (Deng et al., 2022) Fig. 1.12 shows an example of SPR curve that have minimum reflectivity at 60^0. For the S- polarized light due to the polarization happens perpendicular to the plane of incidence, cannot excite surface plasmons. (I. Gryczynski et al., 2004a) The surface plasmon resonance is extremely sensitive to the medium's effective refractive index. (Homola, 1997) Any desorption or adsorption activities at the metal surface alter the effective refractive index of the medium, causing the surface plasmon resonance angle to vary. So, by analyzing surface plasmon resonance angle desorption or adsorption activities at the metal surface can be detected. (Shumaker-Parry and Campbell, 2004)

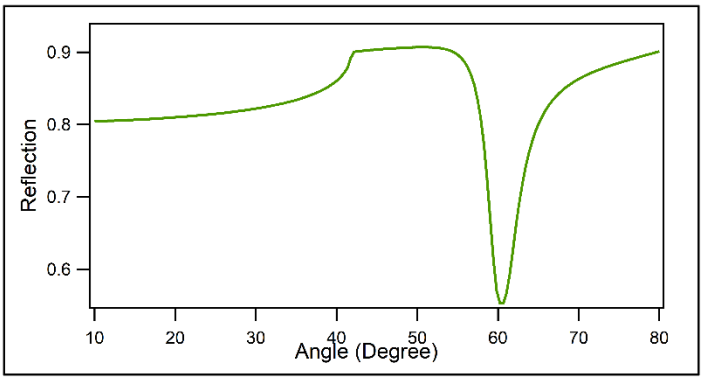

Fig. 1.12: SPR curve

There are two well-known arrangements for employing light to trigger SP waves.

(1) **Otto configuration**

(2) **Kretschmann configuration**

The schematic representation of Otto configuration is presented in the fig. 1.13. In the **Otto configuration**, the light incident on a glass block, generally a prism, and is totally internally reflected. A thin layer of gold or silver (approximately thickness 50nm) is placed near to the prism wall, allowing an evanescent wave to

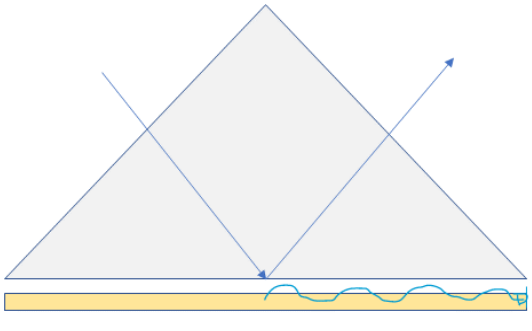

Fig. 1.13: Otto configuration

interact with the plasma waves on the surface of the metal and thereby excite the plasmons. (Zhu et al., 1986)

The schematic representation of Kretschmann configuration is presented in the fig.1.14. In the **Kretschmann configuration** (KR), the metal film (approximately thickness 50nm) is directly coated on the glass block (Gryczynski et al., 2006) and when light incident on the glass block, an evanescent wave passes through the metal coating and the plasmons are stimulated by the light. (Lakowicz et al., 2008) In most practical situations, this setup is employed. (Lakowicz et al., 2008; Naraoka et al., 2005) This configuration is also known as the Kretschmann-Raether configuration.

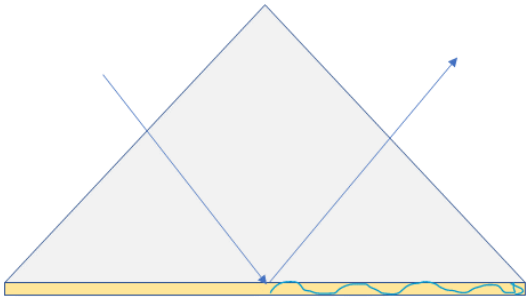

Fig. 1.14: Kretschmann configuration

Surface plasmon resonance method has wide range of applications in medical diagnosis and in biosensors. Imaging of pediatric bone tumors, imaging of pediatric thyroid tumors, liver tumors etc. can be diagnosed by this method. The SPR sensing technology have been used almost three decades ago, and its applications in biosensors can be widely used for characterizing biomolecular interactions. In complementary to SPR in reflection mode, recently studies are emerging based on surface plasmon coupled emission by coating an emitting or fluorescent material. The near-field interaction of the fluorophore to the metal-dielectric interface results in high-efficiency emission. (Yuk et al., 2010) i.e., The coupling of the fluorophore with the surface plasmon in the thin metal film result into strongly directional emission, which refer to as surface plasmon-coupled emission (SPCE). (Yuk et al., 2010) This amazing occurrence is generated by the near-field interaction of fluorophore with the neighbouring surface plasmon, which provides a new mechanism for the creation of far-field radiation. (Lakowicz et al., 2008) Depending on the characteristics of the optical system, the resulting SPCE is highly polarized with precisely specified direction either back into the substrate or into the sample media. (Z. Gryczynski et al., 2004) With very simple optics, this innovative technique may deliver 50% light collection efficiency and inherent wavelength resolution. These qualities can lead to a large range of simple, low-cost, and reliable devices with broad applications in biology and medicine. (Haleem et al., 2021) We emphasise that the directional SPCE is caused by the fluctuating dipoles of the excited fluorophores interacting

with surface plasmons on the metallic surfaces, which then radiate into the substrate or material. (Lakowicz, 2006)

In Kretschmann configuration, light incident through the prism. But in reverse Kretschmann configuration, light incident from the sample side. In our experiment we used a semi cylindrical prism on which the substrate is attached by means of glycerin which was used for the momentum matching. Initially, the metal film was coated on the substrate and then the fluorescent material was coated above the metal film. The light was incident on the sample side and the direction of light opposite to the incident direction is taken as the reference angle (0^0). A detector was placed on the prism side. Fig. 1.15 shows the geometrical representation of SPCE measurements in KR and RK configuration. Thus, the emission intensity was measured in a simple set up. By analyzing the fluorescence emission spectrum, any change on the metal surface can be studied.

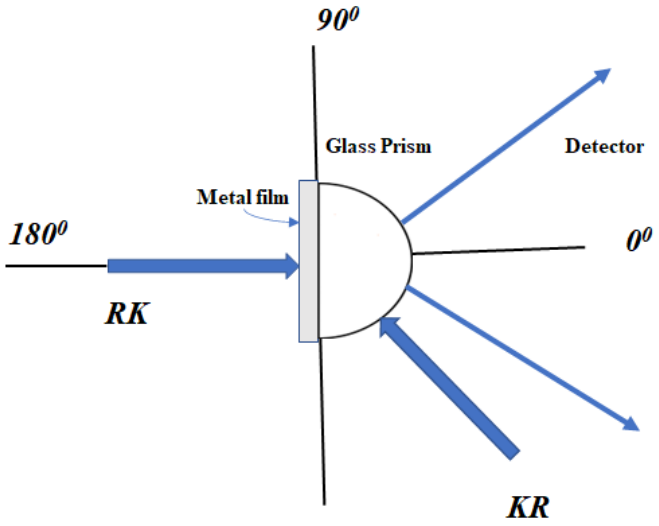

Fig. 1.15: Geometry for SPCE measurements

When light incident on the sample, the fluorescent material gets excited and emits light in all directions. But when the momentum matching conditions are satisfied, the photon emitted by the fluorescent material coupled with the surface plasmon in the metal leading to surface plasmon coupled emission. This interaction of fluorophores with surface plasmon that results into SPCE, which substantially boosts detection sensitivity. (Chowdhury et al., 2008) By linking the emission to surface plasmons on the metallic surfaces, this innovative technique permits a large fraction of the emission to be directed toward the detector. The coupling angle and efficiency of SPCE are greatly influenced by the interface conditions. (Haleem et al., 2021; Lakowicz, 2004) This unique technique will be particularly beneficial for detecting biomolecular binding on surfaces, interaction, and conformational changes in biomolecular systems, as well as providing a novel platform for biomedical assay development. (Haleem et al., 2021)

We have studied the light matter interactions of fluorescent materials and its effect on multilayer fabrication. In our work, we have performed surface plasmon coupled emission experiment in reverse Kretschmann configuration (RK). Surface plasmon coupled emission (SPCE) is a physical process that differs from traditional surface plasmon resonance (SPR) with Kretschmann configuration in that, if a molecule is sufficiently near a metal surface, the photons produced by its excitation will be coupled to the SPR mode, which will then be transformed into a far-field beam moving at the resonance angle. (I. Gryczynski et al., 2004a) Recently, SPCE has been employed in fluorescence and Raman spectroscopies as a potent surface-selective analytical approach. (Calander, 2004; Hobson et al., 2002) It has several benefits, including reproducible field enhancement, high collection efficiency and excellent surface selectivity etc. (Cialla et al., 2012)

1.12 Motivation of the Present Work

Previously DBR was fabricated by complex and expensive methods from inorganic metal oxides. The inorganic DBR layers limit the possibilities of fabricating flexible, stretchable, or bendable opto-electronic devices. (González-García et al., 2010; Lova, 2018; Stueber et al., 2009) Our motivation of the present work is to fabricate the multilayers in a simple, eco-friendly and cost-effective method. Also, few research works were reported on multilayers by polymer- inorganic nano composites. DBR fabricated from inorganic metal oxides are not flexible. Flexible DBR can be used in opto-mechanical sensing applications. Flexible DBR can be fabricated using polymer multilayers. (Anaya et al., 2016; Shekar et al., 2013) Also, DBR fabricated from polymers have optical limitations and optical limiting properties of the commonly used high refractive index polymers motivated us to develop a new class of metal oxide inorganic composite polymer for the DBR fabrication. Since the cost reduction and efficiency enhancement are the important factors while developing opto-electronic and photonic devices and hence we were inspired to prepare the active and passive optical components in a simple, cost effective and eco-friendly method.

1.13 Objectives of the Study

The objectives of our investigation include

1. To develop non-toxic carbon quantum dots/emitting materials for bio and photonic applications

2. To develop high index polymers and hence to fabricate polymer multilayers (Distributed Brag Reflectors) for flexible dielectric mirrors

3. Structural and Optical studies of carbon quantum dots/emitting materials and polymer multilayers including absorption/reflection/transmission and emission studies.

4. Study the light matter interaction/energy transfer mechanism of carbon quantum dots by incorporating carbon quantum dots/emitting materials with multilayers.

5. Explore potential applications of the above fabricated structures for bio photonic applications.

1.14 Outline of the study

Thin films of two different materials of high refractive index contrast are arranged periodically in the DBR and have the ability to deal the light waves in a specific manner. Traditionally, DBRs were made from inorganic metal oxides or semiconductor thin films, and the preparation techniques were expensive to install and maintain. (Stueber et al., 2009)Now a days, flexible optoelectronic devices, such as solar cells or light emitting diodes, are becoming increasingly important, and this has been complemented by the development of flexible optical and electrical materials. Because of the poor mechanical properties of inorganic DBR layers, it is difficult to fabricate flexible, stretchable, or bendable optoelectronic devices. (González-García et al., 2010; Venckatesh et al., 2012) Polymer DBRs provide high reflectivity, versatility, and simple and cost-effective processing methods. (Lova et al., 2018; Shekar et al., 2013) We used solution chemistry method to synthesize optically transparent titania doped poly vinyl alcohol nano composite polymer as the high refractive index polymer by changing the quantity of TiO_2 in PVA. (Anaya et al., 2016; Shekar et al., 2013) This nano composite polymer can be used in the DBR fabrication as a high refractive index polymer, and any

refractive index contrast, thus stop band and reflectivity, can be achieved by simply varying the concentration of TiO2 in PVA without varying any other thin film processing or DBR fabrication parameters.

As an active optical component, CQDs were synthesized from commercial glucose in a cost-effective way via solution chemistry route by microwave enabled hydrothermal method. (Hallaj et al., 2015) CQDs prepared in this manner, possessed all the advantages of quantum dots prepared commercially. The use of glucose as the sole reagent makes this process more appealing when compared to other CQD synthesis methods. The resulting CQDs are extremely photoluminescent, water soluble, environmentally friendly, and non-toxic. In addition, the consumption of chemicals and other waste output has been greatly reduced during the synthesising operations. (Hess et al., 2017; Tang et al., 2012) CQDs can be converted into a thin film by simply mixing with PVA and coated on a glass plate and which has a wide range of bio-photonic and opto-electronic applications. (Hess et al., 2017)

Finally, we had examined surface plasmon coupled emission studies and the influence of Poly Methyl Methacrylate layer (PMMA) on surface plasmon coupled emission tuning on multilayer fabrication by introducing PMMA as a buffer layer between metal and dielectric material and as a multilayer on coating on top of the Fluorescein layer. Angle tuned emission measurements of the sample can be performed in a practical and cost-effective manner. The investigation of light-matter interaction or energy transfer mechanisms using carbon quantum dots or emitting materials with multilayers has wide range of opto-electronic and bio-photonic applications. Fig. 1.16 shows the block diagram of the outline of our study.

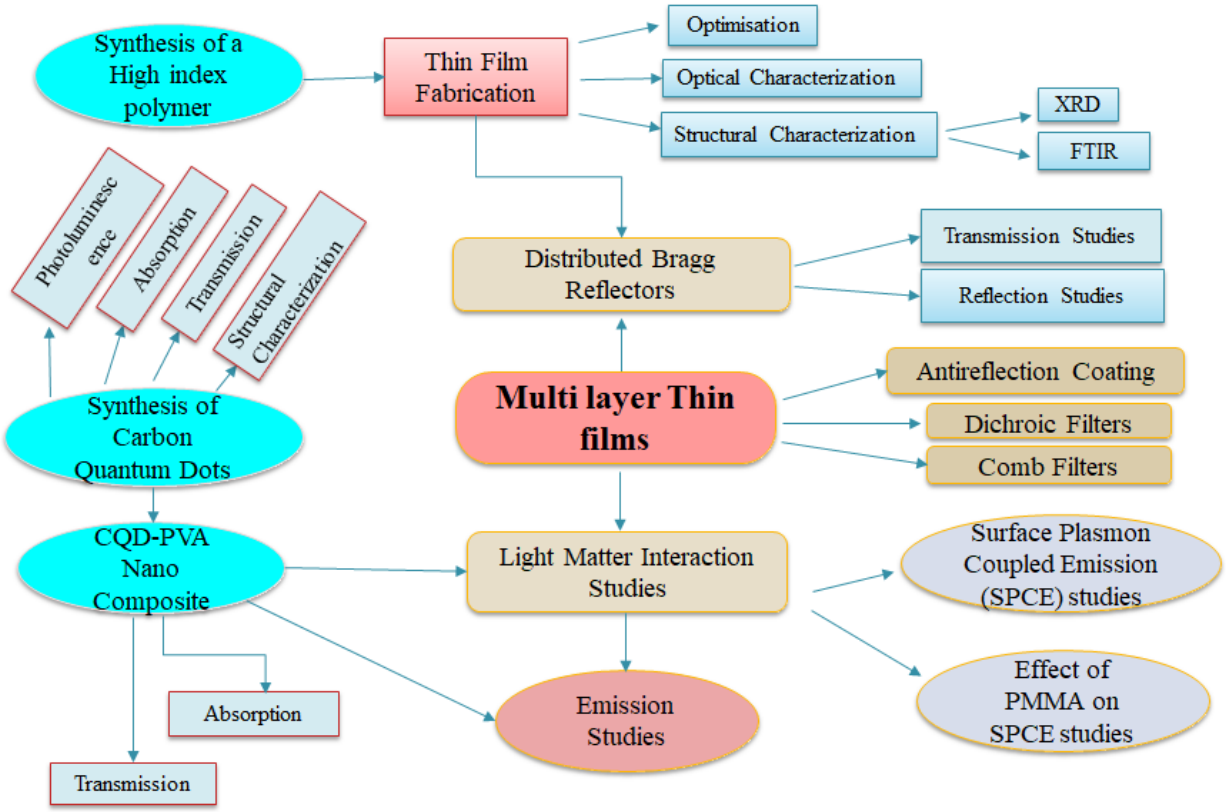

Fig. 1.16: The block diagram of the outline of our study

So, in our research, we had realized a highly stable, optically transparent, and variable refractive index polymer-inorganic nano composite, in a solution chemistry method and multilayers were fabricated using this polymer by a spin coater. We had realized an active optical material experimentally, highly luminous carbon quantum dots from glucose in a microwave assisted hydrothermal process. We have investigated the influence of PMMA film on surface plasmon coupled emission (SPCE) by forming multilayers and observed plasmon coupled fluorescence tuning in metal dielectric multi-layered structures using the reverse Kretschman configuration. We adopted simple, low-cost, eco-friendly and green assisted method to prepare all the samples, and our findings will open up new avenues for the development of opto-electronic and photonic devices.

Chapter – 2

Experimentation and Characterization Tools

Experimentation and Characterization Tools

We have conducted our research on an experimental basis. We have used some numerical simulations also in our work. It is a significant task to validate what has been learnt in theory by the experiment. How theory and experiment are combined and used at the application level determines if the effort is successful. We have realized active and passive optical components either experimentally or simulation method. These works can be used in many opto-electronic and photonic applications.

2.1 Introduction

We have mentioned briefly the experimental methodologies employed in this study endeavour in this chapter. This includes experimental techniques for fabricating passive optical components (single layer and multilayer fabrication), techniques for evaluating their properties, methods for preparing and characterization of active optical components (carbon quantum dots), and applications of multilayers in surface plasmon coupled emission tuning. We also briefly discussed the functioning of the instruments utilised in the research.

Also, optical studies of the fabricated film were done by numerical simulation method. In our work we have adopted the transfer matrix model simulation (TMM) for the design of multilayer thin films. It is the most effective tool for designing multi-layer thin films with any number of layers. If the field intensity at the layer's starting is known, the field intensity at the layer's exit may be calculated using a simple matrix operation known as transfer matrix operations.

2.2 Experimental Techniques

The experimental component of this study covers the fabrication of multilayer thin films, the preparation of carbon quantum dots, and the plasmon coupled fluorescence tuning experiment. Each one is discussed further below.

2.2.1 For the fabrication of multilayer thin film

In both academic and industrial sectors, spin coating is one of the most common deposition techniques for homogenous layers. (Nisticò et al., 2017) In our work of DBR fabrication, polymer thin films were coated on the glass substrate by using a spin coater. The model: SpinNXG-P1 Apex Instruments, that we used in our lab is presented in the fig. 2.1. Spin coating is a method for uniformly coating polymer solutions onto a substrate. (Nisticò et al., 2017) For decades, spin coating could be used in the deposition of thin films. A typical procedure is placing a small amount of fluid resin in the centre of a substrate and then rotating the substrate at a high speed. The resin will spread due to centripetal acceleration and spread to the substrate's surfaces, leaving a thin coating of resin on the surface. (Tyona, 2013) The substrate is mounted on a spinning table in a spin coater, and as the polymer solution is deposited on the substrate, it can be rotated swiftly, causing the solution to spread on the substrate and forming a thin film coating. Depending on the spinning speed and solution concentration, the resulting film thickness can range from 10nm to micrometres. In order to hold the substrate on the spinning table, a small vacuum pump can be used. (Tyona, 2013) The substrate should be properly cleaned with an ultra-sonicator before coating, and make sure the solute was completely dissolved in the solvent. A magnetic stirrer can be used for this purpose. The thickness and qualities of the spin casted film are determined by a number of factors. The thickness and qualities of the multi-layer thin films were affected by variables such as spinning speed, solution concentration or viscosity, and solution nature (organic or inorganic) etc. This is a simple method to coat single layer or multilayer polymer thin films on a substrate. This method is quick and does not require an ultra-high vacuum for thin film applications. (Yuan et al., 2014) In addition, as compared to other thin film coating devices, a spin coater is quite inexpensive. The coated film had been dried by using an oven or IR lamp.

Fig. 2.1: Spin Coater

Advantages of Spin Coating Method

- Simple and ease of use
- Provides both homogeneity and speed
- Provides quality consistency across applications
- Cost effective fabrication method
- The fabricating time is fast.

In many industrial circumstances, having this type of consistent speed and quality is critical, and this coating procedure is one of the finest methods to achieve both. (Scriven, 1988)

Even though the spin coating method have many advantages, may have some limitations also. Spin coated thin films are not as much uniform as compared to other fabrication techniques. The thickness of the fabricated thin films may vary from centre to outward. Also, in the multi-layer thin film fabrication of polymers, the adjacent thin films of polymers may adhere and this leads to inhomogeneity in the thickness of the layers. So, the efficiency of the coated film is low as compared to other coating techniques.

In DBR fabrication, high and low refractive index materials were spin coated alternatively on a glass substrate. The thickness of the deposited film was estimated by fitting the transmission spectra with the TMM simulations. Here, the optical thickness of each film was fixed at the quarter wavelength thickness. So, the reflectivity maximum obtained at the central maximum. Reflectivity was found to be increased with the refractive index contrast of the alternative layers and also with the number of pairs.

2.2.2 For the preparation of Carbon quantum dots

In our research, we have synthesized highly photoluminescent carbon quantum dots (CQDs) by microwave assisted hydrothermal method. The CQDs were prepared from commercial D-glucose (from Alfa Aesar) and the solvent was de-ionised water. 8wt% glucose solution was prepared by dissolving 8g glucose in 100mL de-ionised water. CQDs were synthesized in a simple method by microwave heating of the solution. The microwave oven model: BAJAJ 1701 MT 17L SOLO was used for this purpose and it is presented in the fig.2.2. The glucose solution taken in different glass bottle was subjected to microwave heating at different times 5, 6, 7, 9, 11 and 13 minutes at a certain power of 350W. During this process

of microwave heating, the solution changed its colour from transparent to pale yellow and brown, as a result of formation of CQDs.

Fig. 2.2 : Microwave oven (model: BAJAJ 1701 MT 17L SOLO)

Microwave oven operates on the premise of electromagnetic energy being converted to thermal energy. (Whittaker and Mingos, 1994) In electromagnetic radiations, electric field and magnetic field oscillating perpendicular to each other. When a polar molecule, that is, one with opposite charges, comes into contact with these EM radiations, it oscillates to align itself with them. (Israelachvili and Wennerström, 1996) As a result of friction and collision between molecule, energy is lost from the dipole, resulting in heating. When water molecules (polar molecules) inside the food products come into contact with microwave radiation, they undergo a similar reaction, heating the food. So, microwave heating provides fast heating of the material. (Piyasena et al., 2003) In glucose solution as a result of these microwave heating CQDs were formed.

Advantages of microwave heating

- Provide simultaneous, homogeneous, fast heating (Oghbaei and Mirzaee, 2010)
- Uniform size distribution of quantum dots.
- Simple and cost-effective method.
- Eco-friendly and non-toxic method
- Time-saving etc.

2.2.3 For the Plasmon coupled fluorescence tuning Experiment

Plasmon coupled fluorescence tuning was observed in metal-dielectric multi-layered structures in reverse Kretschmann configuration. In the surface plasmon coupled emission tuning, we have performed the experiment on three samples.

- Ag/PVAF or Metal-Fluorescin (MF)

- Ag/PMMA/PVAF or Metal/PMMA/Fluorescin (MPF)
- Ag/PVAF/PMMA or Metal/Fluorescin/PMMA (MFP)

The sixth chapter contains more information on surface plasmon coupled emission tuning studies. Only experiment techniques are discussed here.

Thermal vapour deposition method was used to deposit thin silver film of thickness ~45nm on the clean glass slides maintaining a vacuum of $5x10^{-5}$ mbar. The deposition rate was kept at around 10 Å /s by adjusting the LT current primary and secondary. The thin film of fluorescein and PMMA were coated by using a spin coater.

Fig. 2.3 shows the picture of a Thermal evaporation unit that we used in our lab. Thermal evaporation is a PVD technique that involves heating the depositing material to the point of evaporation and exposing the substrate to the vapour to develop a thin film coating on the substrate. (Shahidi et al., 2015) PVD operations are usually performed between medium vacuum and high vacuum, with the vacuum system being a vital part of the deposition. It is essential that the deposition material should have a clear path to the substrate, which can be accomplished by running the process in high vacuum. (Schou, 2009) Thermal evaporation occurs at pressures less than 10^{-5} Torr. The vacuum systems require two pumps in series. This is for the high vacuum pump should exhaust to a medium vacuum. The deposition rate of a point on the substrate is proportional to $1/r^2$, if a point evaporation source and constant rate of evaporations are assumed. Where r is the distance from the evaporating source to the substrate. (Powell et al., 2001)

Fig. 2.3 : Thermal evaporation unit

The source is heated by Ohmic resistance via a specially designed heating element called a boat. The boat must be made of refractory metals like tungsten, molybdenum and tantalum or

alloys therewith to avoid contamination of the thin film. (Kern and Schuegraf, 2001) Refractory metals are heat resistant because they have high melting points and enthalpy of vaporizations, which are essential parameters of a thermal evaporation boat. (Heimann, 1996)

The deposition process is managed by adjusting the current flowing through the boat and comparing it to the response from a crystal thickness monitor. This can be accomplished manually or through the use of a closed loop control circuit. The crystal thickness monitor can monitor the thickness and rate of deposition when the film being deposited. A quartz crystal microbalance (QCM) is employed in a crystal thickness monitor, and vibrations in the crystal causes the stress to oscillate at the mechanical resonance of the crystal. The oscillating stress induces an oscillating electric charge, which produces a detectable signal, because quartz is a piezoelectric material. By evaluating the change in the crystal's mechanical resonance, this signal is used to determine the rate of mass deposited on the quartz resonator. The mechanical resonance of the crystal decreases as mass is deposited on it, in a proportion roughly proportional to the mass per unit area of the deposited film. The thickness of a film can be calculated if the density of the film is known.(Reichelt and Jiang, 1990)

The substrate is hidden from the source by a shutter when the evaporation begins. Once a suitable deposition rate has been established (in the angstroms per second scale) the shutter is lifted to expose the substrate to the source. When the thin film has reached the appropriate thickness, the shutter is closed, and the evaporation is halted. (Boone, 1986)

For the first sample, a metal thin film of silver (Ag) of thickness ~45nm was coated on the glass substrate by using thermal vapour deposition method and 2wt% PVA solution was prepared by dissolving an appropriate amount of PVA in distilled water and stirring constantly with a magnetic stirrer for 45 minutes at 80^0C. The Fluorescein (FL) solution was prepared by dissolving 0.5wt% Fluorescein in iso-propyl alcohol. The PVA and FL solutions were then mixed in a 100:1 ratio using a magnetic stirrer, and the resulting PVAF solution was coated on the Ag film using the spin coater with a spinning speed of 5000rpm.The PVAF film formed were dried by an oven kept at 100^0C. Two more samples were formed by coating 0.5wt% Poly Methyl Methacrylate (PMMA) in toluene as a buffer layer between Ag and PVAF, and depositing PMMA layer after the PVAF layer with the same spinning of 5000rpm. After conducting the surface plasmon coupled emission tuning experiment we have found the influence of PMMA on the SPCE tuning.

2.3 Characterization Techniques

2.3.1 Optical Characterization

Optical characterization was done by Ocean Optics Maya 2000-Pro UV compact spectrometer, white light source, laser source (450nm, 540nm and 640nm) and necessary optical fibres and lenses. Fig. 2.4 shows the picture of high sensitivity spectrophotometer and fig. 2.5 shows picture of the white light source that we used in our lab.

Fig. 2.4 : High Sensitivity Spectrometer

The UV-Visible absorption, transmission and photoluminescence studies were carried out using Ocean Optics Maya 2000-Pro UV compact spectrometer, white light source, laser source (450nm, 540nm and 640nm) and necessary optical fibres and lenses. Spectra suit software is used to control the spectrometer.

Fig. 2.5 : White Light Source

Spectroscopy is essentially concerned with the interaction of light with matter. (Rigosi et al., 2015) When light is absorbed by matter, the energy content of the atoms or molecules is increased. The excitation of electrons from the ground state to a higher energy state occurs when UV radiations are absorbed. Molecules with π electrons or non-bonding electrons (n-electrons) can absorb ultraviolet light energy and excite these electrons to higher anti-bonding molecular orbitals. (Akash and Rehman, 2020) When a chemical substance

absorbs ultraviolet light, it produces a characteristic spectrum that can be used to identify the compound. (Koutchma, 2009)

The wavelength is inversely proportional to frequency. As a result, shorter light wavelengths carry more energy while longer wavelengths carry less. To excite the electrons in a substance to a higher energy state, a precise quantity of energy is required, which we can detect as absorption. In a substance, electrons in different bonding environments require a distinct amount of energy to jump them to a higher energy state. This is why different wavelengths of light are absorbed by different substances. (He et al., 2008) By locating the particular wavelengths corresponding to maximum absorbance, UV-Vis spectroscopy can be used to analyse or identify various compounds. (Barbosa-García et al., 2007)

The schematic of the main parts of UV-Visible spectrophotometer assembled in our experimental set up as shown in the fig. 2.6. Light from the source incident on the sample and the sample absorb certain amount of radiations. A part of light was transmitted and the other part reflected from the sample. The transmitted energy was fed to a highly sensitivity spectrophotometer through the optical fibre. The spectrometer was computer controlled using Ocean Optics spectra suit software.

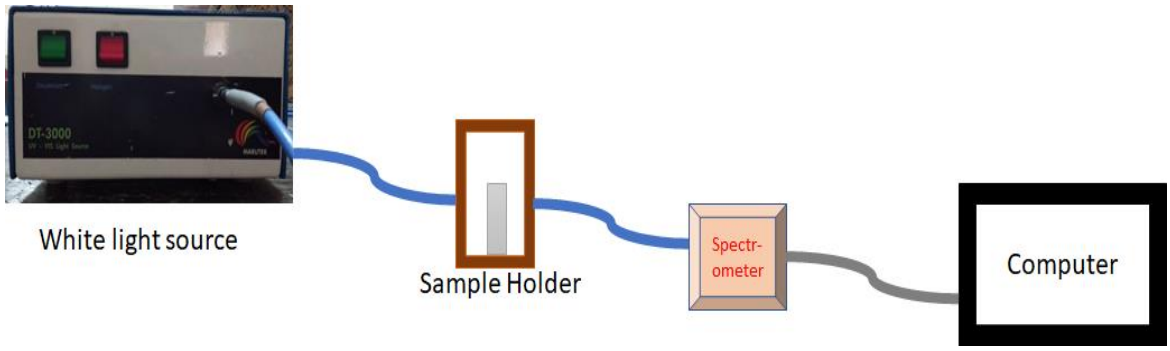

Fig. 2.6 : Schematic of the experimental set up for the transmission studies

We have used single beam spectrophotometer in our lab to record transmittance and absorbance. Hence, reference spectrum was recorded first by placing only substrate in the sample holder and then substrate with sample was placed on the sample holder. Then the software provides the resultant transmittance/absorbance spectrum of the sample by processing reference and sample spectrum.

The thickness and refractive index of the coated film was estimated by fitting the transmission spectra with transfer matrix model simulations. For this, the refractive index of

the deposited film was first estimated by Brewster's angle method. The estimated values were then used in TMM simulations to get the optimized values for refractive indices and film thicknesses.

2.3.2 Structural Characterization:

2.3.2.1 X-ray Diffraction

The phase identification of the prepared nanocomposite was done by using X-ray diffractometer (XRD). Fig. 2.7 shows the picture of X-ray diffractometer (Make: Malvern Panalytical Aeries Research) that we used. In materials science, X-ray diffraction analysis (XRD) is a method for determining a material's crystallographic structure. XRD is a technique that involves irradiating a material with incoming X-rays and then measuring the intensities and scattering angles of the X-rays that exit the substance. (Bunaciu et al., 2015) The identification of materials based on their diffraction pattern is one of the most common applications of XRD analysis. In addition to phase identification XRD provides information on how the actual structure of the material differs from the ideal one due to internal stress and defects.

Fig. 2.7 : X-Ray Diffractometer

The bending of light around the corner of an object is known as diffraction. For diffraction to occur the size of the object must be almost equivalent to the wavelength of light employed. (Davison and Simpson, 2006) X-rays, like other electromagnetic waves, can be diffracted. The size of the obstacle for diffraction of X-rays should be a few angstroms (about 1 Å) which is the wavelength of X rays. Crystal provides the ideal alternative for studying X-ray diffraction because the atomic spacing in the crystal is almost comparable to wavelength of X-rays [176]. As a result, X-ray diffraction gives important information on the structure and characteristics of both crystalline and non-crystalline materials. (Toby and Egami, 1992)

In crystals, the atoms are arranged in a regular pattern. When X-rays incident on the crystal, the scatterers in the crystal produce a regular array of spherical waves. These waves undergo constructive interference, as indicated by Bragg's law: $n\lambda = 2\,d\,Sin\,\theta$, where d is the interplanar spacing, θ is the glancing angle, n is an integer and λ is the wavelength of X-rays. If the condition for constructive interference from the crystalline sample is satisfied that direction appeared as spots on the diffraction pattern (Widjonarko, 2016).

Single crystal and Powder XRD are the two most common configurations used in X-ray diffractometer. The important component parts of x-ray diffractometers are very standard and include: Source of x-rays, Sample stage and Detector. A plot of the intensity of X-rays scattered at different angles by a sample is called an X-ray diffraction pattern. (Chung, 1974)

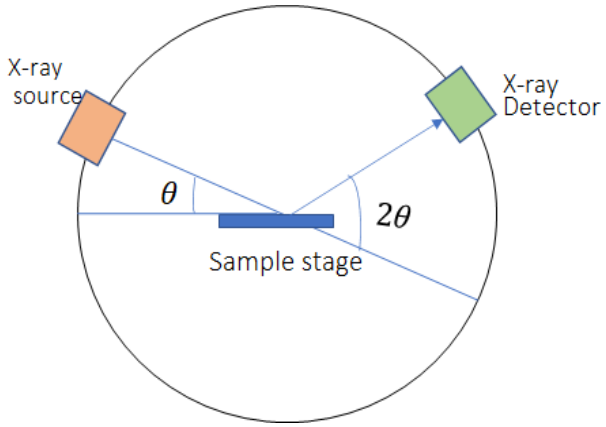

Fig. 2.8 : Schematic arrangement of X-ray Diffractometer

The schematic arrangement of X-ray Diffractometer is as shown in the fig. 2.8. The detector can rotate in a circle around the sample and the detector's position is recorded as the angle 2θ. The detector counts the number of X-rays seen at each angle 2θ. The X-ray intensity is commonly reported in "counts" or "counts per second". (Chung, 1974) The sample can also rotate to ensure that the X-ray beam is properly focused. The X-ray tube, rather than the sample, may rotate in some instruments. To determine which phases are present in the sample, experimental XRD data is compared to reference data. (Widjonarko, 2016) All main peaks specified in the reference pattern should be present in the experimental data.

2.3.2.2 FTIR Spectrometer

The composition of the prepared sample was done by an FTIR spectrometer. FTIR spectra of the prepared high index material were recorded by using Perkin Elmer Spectrum Two FT-IR Spectrometer. Fig. 2.9 shows the picture of the FTIR Spectrophotometer that we used. In the infrared region (IR) of the electromagnetic spectrum which has longer wavelength and shorter frequency than visible light. When a sample is exposed to infrared radiation, the chemical bonds between different elements absorb light at different wavelength. (Jelle and Nilsen, 2011) The range of wavelengths in the infrared region that are absorbed by a material is measured via FTIR analysis. The absorbance of infrared radiation at different wavelengths gives information about the material's molecular composition and structure. (Jelle and Nilsen, 2011) By comparing the spectrum to a database of reference spectra, unknown compounds can be recognised. Unknown components, additives within polymers, surface contamination on a material, and more can all be identified via FTIR Analysis. (Chércoles Asensio et al., 2009)

Fig. 2.9 : FTIR Spectrophotometer

2.3.2.3 Optical Microscope

An optical microscope was used to find out the surface quality of the coated film. i.e., any cracks or in-homogeneities that appeared in the film. This helped to conduct a comparative study of homogeneity of the film as the thickness increased. Fig. 2.10 shows the picture of an optical microscope in our lab.

Optical microscopy is a technique for closely examining a sample using a magnifying lens and visible light. (Reddick et al., 1989) This is the classic type of microscopy, which was

Fig. 2.10 : Optical Microscope

developed before the 18th century and continues to be used today. The optical microscope, often known as a light microscope, is a type of microscope that employs visible light and a lens system to magnify pictures of tiny objects with one or more lenses. (Lu et al., 2013) The lenses are positioned between the sample and the viewer's eye to enlarge the picture and allow for more detailed examination. There are several kinds of optical microscopes. (Kaneda et al., 1992) They can range from extremely simple to highly complex designs with increased resolution and contrast. Some types of optical microscopes listed below:

- A simple microscope consists of a single lens that magnifies the picture of the sample, like a magnifying glass.
- Compound microscope: a collection of lenses used to magnify the sample picture to a greater resolution.
- Digital microscopes can feature simple or compound lenses, but they use a computer to display the picture rather than an eyepiece to see the sample.
- The stereo microscope produces a stereoscopic picture that is beneficial for dissections.
- A comparison microscope allows you to see two different samples at the same time to compare.
- Inverted microscope: examines the sample from below, which is beneficial for studying liquid cell cultures.

Using conventional light-sensitive cameras, an optical microscope can create an image. Traditionally, photographic film was used to capture the photographs. With the advancement of technology, optical microscopes can now take digital pictures with CMOS and charge-couple device (CCD) cameras. (Flores-Moreno et al., 2020) These digital microscopes provide real-time image projection onto a computer screen for sample examination. Because eyepieces are no longer required, using this device is more convenient. Numerous scientific fields, such as microbiology, microelectronics, nanophysics, biotechnology, and pharmaceutical research etc. frequently employ optical microscopy. (Grieshaber et al., 2008)

2.3.2.4 Transmission Electron Microscopy

Transmission electron microscopy images were carried out by JEM 2100 having resolution 0.24nm and an acceleration voltage of 200kV used to realize morphological, compositional and crystallographic information about the sample. Fig. 2.11 shows the picture of the transmission electron microscope that we used. Transmission electron microscopy (TEM) creates a 2D image with the best possible resolution by transmitting electrons through a sample with a high-energy beam of electrons. (Inkson, 2016) TEM may be used to examine nanomaterials and provide information about their structure and composition at the atomic level. (Frenkel et al., 2001) To acquire the more detailed information, it is critical to choose the correct sample holder (TEM grid) for different types of nanomaterials. When samples are excessively thick, they must first be thinned to allow electrons to pass through them, ideally to less than 100 nano meters. (Inkson, 2016) These TEM samples are then put on a TEM grid and analysed with a concentrated, strong electron beam under ultra-high vacuum conditions. (Inkson, 2016; Kik and Brongersma, 2007)

Fig. 2.11 : Transmission Electron Microscope

2.3.3 Plasmon coupled fluorescence tuning

The schematic representation of the experimental setup for the surface plasmon coupled emission tuning is presented in the fig. 2.12 below. The sample was coupled to a hemi cylindrical prism (n=1.5) by using glycerine as the coupling agent (index-matching liquid to maintain the optical index continuity between the prism and the glass substrate). (Kik and Brongersma, 2007) A diode laser of wavelength λ=450nm was allowed to fall normally to the sample to excite the fluorescein molecules within the PVA matrix and the emission studies were done by Reverse Kretschmann configuration (RK). The fluorescein molecule get excited and emits light in all directions. To filter the excitation wavelength a high pass (HP) filter can be used. The collection optics were mounted on a rotational platform to record the spectra at

different angles from 20^0 to 90^0 with an interval of 1^0. The direction opposite to the excitation laser was taken as the reference angle (0^0).

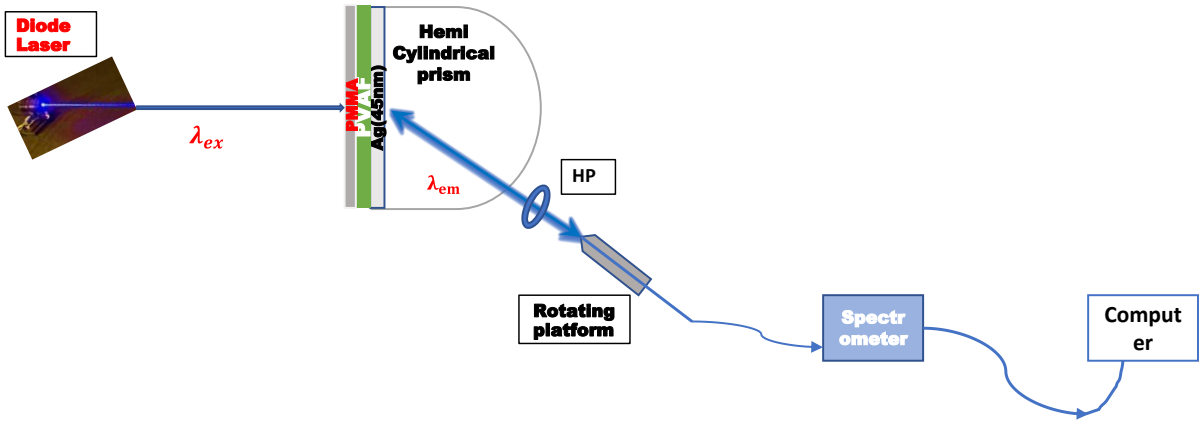

Fig. 2.12 : Schematic of the experimental setup for surface plasmon coupled emission tuning

The emitted light then fed to the high sensitivity spectrometer (from Ocean Optics; Model: Maya2000Pro) through the optical fibres. Ocean optics Spectra Suite software was used to control and collect the emission spectra. For modelling the SPR for more than one layers, we can choose transfer matrix model simulations (TMM) or other commercial software. For the present work we have used WINSPALL software (version 3.02) to simulate SPR curves of Ag/PVAF layers.

The reflectivity curves generated in surface plasmon resonance studies must be fitted using theoretical models. WINSPALL, a free software (for non-commercial usage), performs just that. WINSPALL is a PC-based free software that evaluates the reflectivity of optical multilayer systems and that can predict the SPR angles. (Pérez-Ocón et al., 2022) It is founded on Fresnel equations and matrix formalism. It is useful for analysing surface plasmon investigations. (Ji et al., 2014) The Knoll group invented this WINSPALL software and it is available for free download from the MPI website. It is not permitted to be utilised for commercial purposes. [181]

2.4 Conclusion

In this chapter, we had exhibited different types of techniques used for the experimentation and characterization in our research work. The single layer and multilayer thin films were fabricated in a simple spin coating method. The optical and structural

characterization of the fabricated film had done in different methods and it was discussed here. We had also described the preparation methods of carbon quantum dots in a simple, eco-friendly and cost-effective microwave assisted hydrothermal method. The optical and the structural characterization techniques also discussed here. In the last session we had discussed the applications of multilayers in surface plasmon coupled emission tuning. We had also exhibited a simple experimental set up for the surface plasmon coupled emission tuning experiment. We had also briefly described the working principles of different instruments used in the research work. All our works were done in simple, eco-friendly, non-toxic and cost-effective method. So, in our work we had adopted simple, low cost and green assisted method for the preparation of all the sample and these works will create wide possibilities in the fabrication of opto-electronic and photonic devices.

Chapter -3

Passive Optical Filters- Design

Passive Optical Filters- Design

In recent years, multilayers have inevitable importance in the field of photonics and optoelectronic devices and they offer fine control over light transmission and reflection, have attracted the attention of many scientists and technologists. On fabricating multilayer thin films, the designer has to be conscious about the parameters like number of layers, film thicknesses and the refractive indices of the individual layers and the surrounding media. In this chapter, we have designed the multi-layered thin film coatings using transfer matrix model (TMM) simulations. Also, these multi-layered thin films were conveniently used to realise anti-reflection coatings, highly reflecting mirrors, high pass filters, comb filters etc. This paper had been communicated in the journal Materials Today proceedings.

3.1 Introduction and Motivation

Now a days, multilayer thin films are common elements of many opto-electronic and photonic devices and the industrial development of these materials has led to the realization of passive and active optical elements and commonly found in all kinds of optical characterization setups. The optical thin films have numerous applications in many fields of science and technology. Many different methods have been developed for the design of multilayer thin films. Numerical simulation methods are the most flexible method because they can be applied to problems with complex specifications that required a large number of multilayers for their solutions. These complicated spectral problems can be solved by using matrix theory of optical multilayer system.

In this chapter, number of optical filters were designed and modeled to aid the fabrication of optical filters which are essential from both industrial and scientific perspective. The multi layered thin film coatings were conveniently used to realise various optical components like anti-reflection coatings, highly reflecting mirrors, high pass filters, comb filters etc. AR coatings were demonstrated using one, two- and three-layered optical coatings. To increase the zero-reflectance window, a tri-layered optical coating with central layer having an optical thickness of $\lambda/2$ may be chosen. With this design, reflectance was highly reduced (~0.04%) within the visible wavelength region. DBRs were designed using alternating

sequence of layers of high and low refractive index materials to get highly reflecting mirrors. Results show that, for a high index contrast (~0.87) DBR, ten periods were adequate to get reflectance of ~ 99.7%. Comb filters were designed by sandwiching a thick transparent layer between two DBRs. As the thickness of the middle layer increases, a greater number of low reflectance windows were opened and the full width at half maximum (FWHM) of the window decreased. Dichroic filters were also designed by multilayers of alternating high and low refractive index materials in a periodic pattern. Studies show that for a design with the ratio of thicknesses of high and low index layer ~0.11, pass band was increased and the ripple in the transmission spectra was minimised.

An optical filter, like an electrical filter, can be designed to selectively pass on one portion of the optical spectrum while blocking the other portions. Optical filters can be made in a variety of ways, and their properties may or may not be affected by the wavelength of light used. External electric or magnetic fields, temperature, illumination level, and other factors can alter the properties of thin-film filters. (Rack and Holloway, 1998) Optical filters such as beam splitters, highly reflecting mirrors, and various optical pass band filters (high, low, and band) are essential components of various optical devices such as lasers, microscopes, and Michelson interferometers, as well as optical setups such as holography and photonic setups. (Glebov et al., 2012) The transmittance, reflectance, absorbance spectra, and optical density curves can provide more information about an optical filter's properties. The desired spectral intensity can be achieved by arranging many optical filters in parallel or in series. (Liu et al., 2018)

Optical thin film filters can be designed in different ways and have numerous applications. Antireflection coatings, cut-off filters, narrowband transmission or rejection filters, beam splitters and comb filters are some of them. There is an ongoing effort to reduce reflection by using some coating and patterns on the reflective surfaces, which is known as anti-reflection (AR) coating. (Walheim et al., 1999) Optical thin films coated on optical surfaces to reduce the reflectivity is called the antireflection coatings. Anti-reflection (AR) coatings are used in optical devices such as camera lenses, regular spectacles, optical windows, and so on. (Garlisi et al., 2020) Even with a single layer able to achieve a zero reflectance at a particular wavelength. However, due to a shortage of suitable low-index coating materials, this cannot be achieved in practise for substrates with refractive indices less than 1.9. Nonetheless, even with the available materials, all popular glass types materials achieve a highly helpful reduction in reflection in a broad spectral area. Rayleigh proposed in 1879 that the reflectivity

of an object's outer surface could be reduced if the transition of refractive index (RI) between the object and the surrounding medium was small and AR grew from there. (Cui et al., 2016) Following the proposal of Rayleigh, English lens designer H. Dennis Taylor in 1892 discovered that tarnished camera lenses permit photography with less exposure. (Joo et al., 2010) He discovered a decrease in reflection that was linked to the tarnish on a glass surface. F. E. Wright turned this observation into an AR development method. He explained how the coating's anti-glare properties are achieved by a gradual RI transition from glass to air due to tarnishing. (Ye et al., 2016) There have been a lot of methods and strategies developed over the last century to reduce the reflection. An effective zero percent reflection at a specific wavelength can be achieved when a single-layer quarter-wave optical material coating is applied to flat substrates. Bi- and tri-layer coatings can improve the zero percent reflection. Modern optoelectronic devices, such as displays, touchscreens, and ultra-compact cameras, are rapidly evolving, putting new demands on the AR industry. (Chen, 2001) By reducing reflective losses at interfaces over a wide range of wavelengths, broadband antireflective (AR) coatings have attracted a lot of attention in imaging devices, solar cells, display panels, and laser systems. (Liu et al., 2018; Tan et al., 2018)

Another optical component is distributed Bragg reflector (DBR). The most common optical elements used in the fabrication of high reflectivity distributed Bragg reflectors are multilayers of transparent materials repeated in a periodic pattern (DBR). DBR is made up of layers of two different optical materials that alternate in order. In DBR all the reflected components from the interfaces interfere constructively, that leads to strong reflection. (Sridharan and Waks, 2011) The photonic stop band refers to the wavelength range that is reflected. The stop band is determined by the difference in refractive index between the two materials. (Dong et al., 2016; Sridharan and Waks, 2011) DBRs have an important role in opto-electronic and photonic devices due to their high reflectance and wavelength selectivity similar to metallic mirrors. (Dong et al., 2016; Yang et al., 2019) DBRs with such great features can be used in photovoltaic devices, exciton-polariton lasers, vertical cavity surface-emitting lasers (VCSELs), light-emitting diodes (LEDs), sensors, solar cell actuators, optical switches, in data communication, etc. (Christopoulos et al., 2007; Johnson et al., 2001) The responsiveness of DBR to electric, magnetic, mechanic and chemical stimuli makes them very appealing for a variety of different applications. [90,195–197]

Third optical component design in this work is comb filter. Comb filters are the basic building blocks for digital audio effects and are used in wavelength division multiplexed (WDM) systems, multi-channel dispersion compensation, fibre sensors, and multi-wavelength lasers. (He et al., 2017; Li et al., 2015; Liu et al., 2014) Researchers improve the filter performance in two ways in order to improve filter efficiency. The first is to precisely control the filter channel spacing, while the second is to tune the transmission spectrum of a comb filter to a desired wavelength. (Jin et al., 2013; Kwon et al., 2005) To create a comb filter, a thick optically transparent layer was sandwiched between two DBRs. (Huang et al., 2016; Tan et al., 2017)

Dichroic filter is the fourth optical component design using multilayers. A dichroic filter is a type of colour filter that selectively passes light of a narrow wavelength range while reflecting other colours. This filter transmits light in one wavelength range while blocking light in another. Unwanted wavelengths are reflected in dichroic filters, while desired portions of the spectrum are transmitted. (Glukhov et al., 2020) It is also possible to separate light into two sources based on wavelengths using dichroic filters. These can also be achieved by layering varying refractive index materials in a single or multiple layers. These filters are suitable for both high and low pass filtering. (Madsen and Lenz, 1998; Weng et al., 2019)

For the design of optical filters, inorganic metal oxides or semiconductor thin films such as magnesium fluoride (n~1.38), silicon dioxide (n~1.46), zinc sulphide (n~2.35), titanium dioxide (n~2.1), calcium fluoride (n~1.43), aluminium oxide (n~1.77) etc. can be used. Here we have considered the refractive index of the inorganic materials at 632nm. These inorganic materials can achieve high transparencies and high refractive index contrasts of up to $\Delta n = 1$. For the design of flexible, stretchable, or bendable optical filters, organic materials, such as fluorinated polymer, ($n \sim 1.3$), poly (methyl methacrylate) (PMMA, $n \sim 1.50$), cellulose acetate (CA, $n \sim 1.46$), poly vinyl alcohol (PVA, $n \sim 1.52$), polyacrylic acid (PAA, $n \sim 1.51$), polystyrene (PS, $n \sim 1.58$), poly (N-vinyl carbazole) (PVK, $n \sim 1.68$) etc., are auspicious substitutes to inorganic materials. These flexible multilayers can be used to make highly transparent, bendable and flexible optical filters. (Kou et al., 2020; Lova et al., 2018) For multilayer fabrication, low-cost methods such as spin coating, chemical vapour deposition (CVD), or sol gel methods can be used. [205,206]

In our present work, transfer matrix model (TMM) simulations were used to design multi-layered thin film coatings. The design parameters like optical thicknesses, number of

pairs and refractive indices were optimised to get desired transmission or reflection windows within the desired region. AR coatings, DBR mirrors, comb filters, and dichroic filters are all made possible with these multi-layered thin films. One, two, and three-layered optical coatings were used to demonstrate AR coatings. Using an alternating sequence of layers of high and low refractive index materials, highly reflecting DBR mirrors were designed. A thick transparent layer was sandwiched between two DBRs to create comb filters so that a cavity like structure was formed. As the cavity length was increased, a number of low reflectance windows were opened. Multilayers of high and low refractive index materials were arranged in a periodic pattern to create dichroic filters. A stack of alternative layers of two different materials were arranged in a periodic manner. Here optical thickness of each layer may be varied from quarter wavelength thickness. Six sets of dichroic filters were designed with 60 pairs of alternating high and low index materials. In all dichroic filters, the low index material was fixed as SiO_2 and high index material was chosen from Nb_2O_5, TiO_2 and Al_2O_3. By changing the optical thickness and high index material, we can tune the cut off wavelength of the pass band filters.

3.2 Results and Discussions

3.2.1 Anti-reflection (AR) coating

Anti-reflection coating was designed using single layer, bi-layer and tri-layer optical coatings as shown in Fig. 3.1(a-d). Corresponding reflectance spectra is shown in Fig. 3.1(e). Reflectance of 3.8% was observed for a normal glass with a refractive index of 1.45. A coating of MgF_2 (n=1.37) with optical thickness ($\lambda/4$) on the top of a glass substrate drastically reduced the reflectance to 2% around the wavelength 500nm. For a double layer coating with each layer having an optical thickness of ($\lambda/4$) satisfying the condition of destructive interference in the reflection mode, the reflectance percentage reduced to below 2% around 500nm. But for wavelengths away from the central wavelength, reflectance increased above that of glass reflectance.

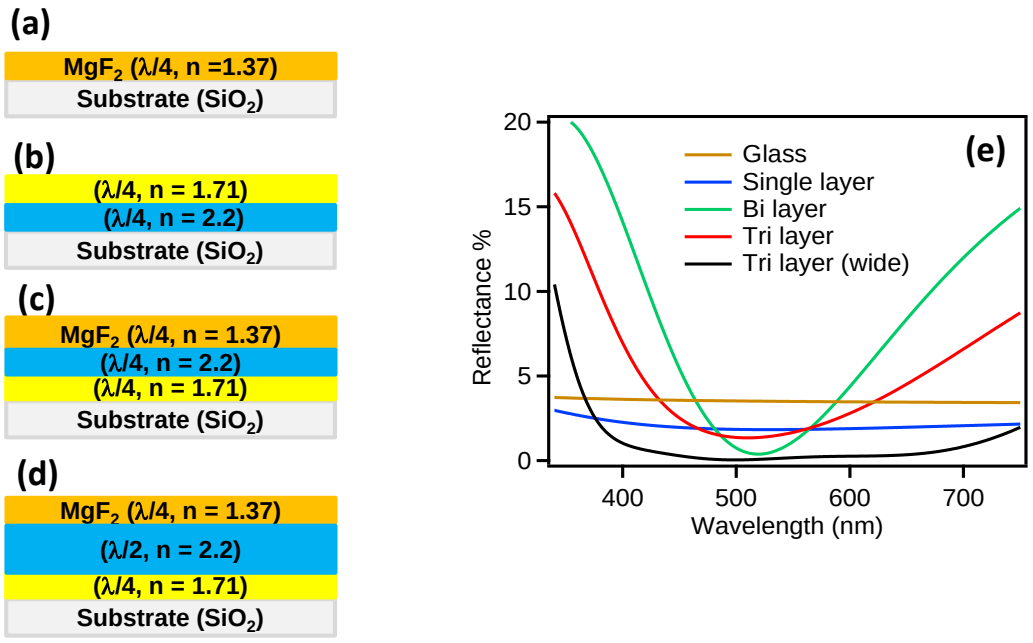

Fig. 3.1: (a) to (d) Schematic of single, bi-, tri- (narrow) and tri-(wide) layered AR coating and (e) corresponding reflectance spectra

A tri-layered optical coating can be used to get low reflectance for a wider range of wavelengths. While ($\lambda/4$- $\lambda/4$- $\lambda/4$) optical thickness stacking could reduce reflectance to nearly zero (1.35%) around central wavelength, the reflectance increased beyond 4% for wavelength away from central wavelength (λ < 450 nm and λ > 590 nm). However, to increase the zero-reflection window, we can opt for a tri-layered optical coating where the central layer has an optical thickness of $\lambda/2$. With this design, a reflectance of ~0.04% was observed for a wavelength range of 400nm to 700nm. This type of coating reduced the reflectance to a very low value over the entire visible region. Hence to get an antireflection coating with near zero reflectance within visible region, we can go for ($\lambda/4$- $\lambda/2$- $\lambda/4$) multi-layered optical coatings. The choice of materials is also an important point to get a better anti-reflection coating and high transmittance. AR design and the corresponding parameters are tabulated in Table 3.1.

Table 3.1: AR design parameters for central wavelength 500 nm

No. of layers	Materials (from top to bottom)	Refractive index	Optical thickness	Reflectance %
One	MgF_2	1.37	$\lambda/4$	2
	Substrate	1.45		
Two	Polymer2	1.71	$\lambda/4$	0.38
	Polymer1	2.2	$\lambda/4$	
	Substrate	1.45		
Three	MgF_2	1.37	$\lambda/4$	1.35
	Polymer1	2.2	$\lambda/4$	
	Polymer2	1.71	$\lambda/4$	
	Substrate	1.45		
Three	MgF_2	1.37	$\lambda/4$	0.04
	Polymer1	2.2	$\lambda/2$	
	Polymer2	1.8	$\lambda/4$	
	Substrate	1.45		

3.2.2 Distributed Bragg Reflectors (DBRs)

In a DBR alternative layers of high and low refractive index materials are arranged periodically. One pair of low and high refractive index layers is called a period and to get a high reflectivity number of periods may be increased. The refractive index contrast between high and low index layers is the basic parameter deciding the span of wavelengths with high reflectivity.

For DBR1, MgF_2 (n=1.38) was selected as the low refractive index material and SiO_2 (n=1.46) as the high refractive index material. The refractive indices of each film were considered at 632nm wavelength (Wavelength of Ruby laser). The central wavelength was fixed at 500nm and the thickness of each layer was designed for quarter wavelength thickness. The refractive index contrast between low and high index material were Δn =0.08. Reflectance spectra of the designed DBRs were presented in fig. 3.2(a). We have designed the DBR1 for 5,

10,15,20,30 and 40 pairs. As the number of periods of high and low refractive index material increases reflectivity also increases. For 5 periods of DBR, the maximum reflectivity at the central maximum was found to be 19%. But for 10 periods of DBR, the maximum reflectivity increased to 40%. In order to achieve 93% reflectivity, about 40 periods were required.

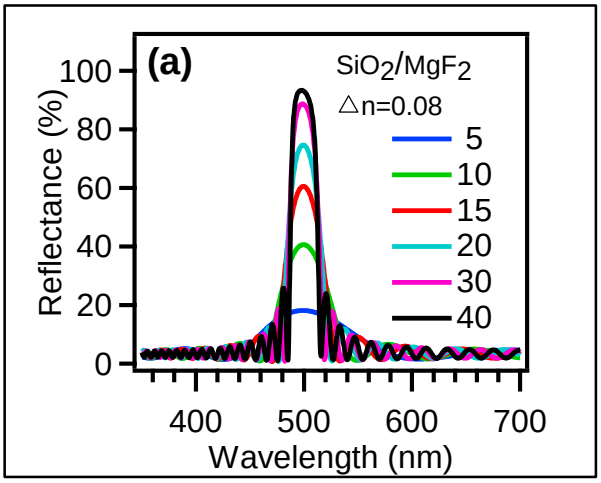

Fig. 3.2(a): simulated reflectance spectra of DBR1

In DBR2, SiO_2(n=1.46) was selected as the low refractive index material and Al_2O_3 (n=1.77) was chosen as the high index material. The refractive index contrast between high and low refractive index material was 0.31. The reflectance spectra designed by transfer matrix model simulations were as shown in the fig. 3.2(b). For 5 periods, the reflectivity found to be 41%. But as the number of periods increased to 10, reflectivity also increased to 79%. For 15 periods, reflectivity increased to 93%. For 20 periods, reflectivity increased to 97%. As the number of periods increased to 30, reflectivity increased to 98%. On further increase in number of periods, not much increase in reflectivity.

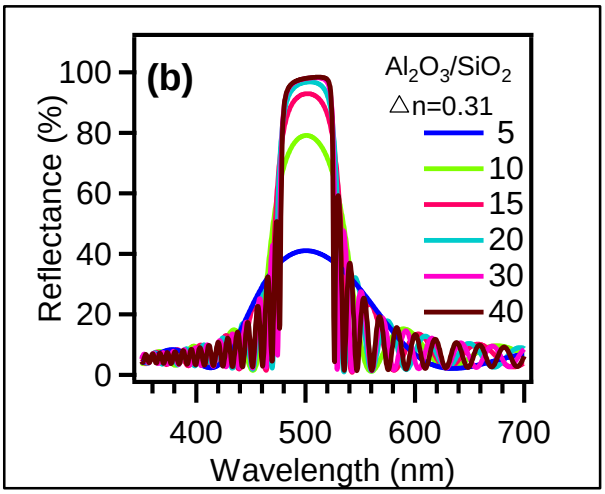

Fig. 3.2(b): simulated reflectance spectra of DBR2

In DBR3, SiO_2(n=1.46) was selected as the low refractive index material and TiO_2 (n=2.1) was chosen as the high index material. The refractive index contrast between high and low refractive index material was 0.64. The reflectance spectra designed by transfer matrix model simulations were as shown in the fig. 3.2(c). In DBR3, the reflectivity found to be greater than 90% with 5 periods. As the number of periods increased to 10, reflectivity also increased to 99%.

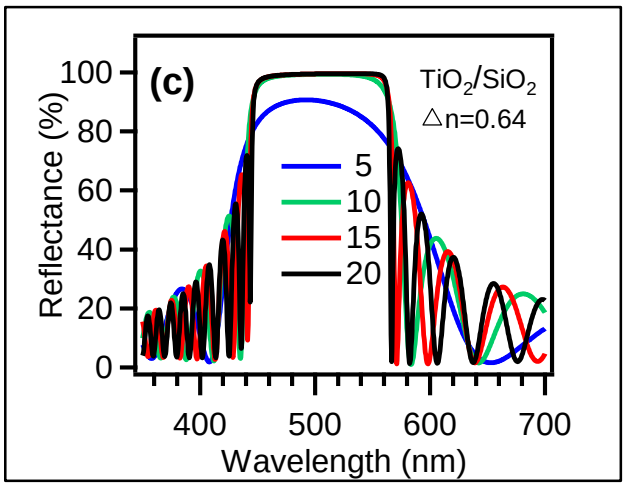

Fig. 3.2(c): simulated reflectance spectra of DBR3

In DBR4, SiO_2(n=1.46) was selected as the low refractive index material and Nb_2O_5 (n=2.32) was chosen as the high index material. The refractive index contrast between high and low refractive index material was 0.87. The reflectance spectra designed by transfer matrix model simulations were as shown in the fig. 3.2(d). The reflectivity found to be greater than

95% with 5 periods. The reflectivity found to be increased with increasing number of periods and also with increasing refractive index contrast of the low and high refractive index materials. High refractive index contrast between the two consecutive layers will also benefit in having a relatively broad stop band.

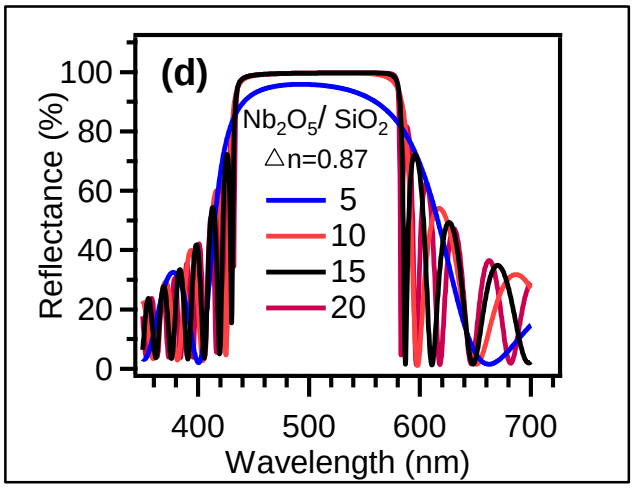

Fig. 3.2(d): simulated reflectance spectra of DBR4

For an index contrast of 0.08, 5 periods of DBR shows a reflectance of less than 20%. But as the number of periods increased to 10, 15 and 20, reflectance also increased to 40, 60 and 74% respectively. From the table 2, it is clear that in DBR1 in order to achieve 90% reflectance, almost 40 pairs of high and low refractive index layers were required. In contrast to increase in reflectance, FWHM decreases from 93nm to 25nm and the curve edges get sharper as periods increases. Similar trend was observed for all the DBRs. DBR parameters are determined and tabulated in Table 2. It is to be noted that as the index contrast increases, very few periods were sufficient to get a reflectance of more than 99%. For example, DBR4 with an index contrast of 0.87 a reflectance of 99.7% could be achieved for 10 periods. Further increase in the periods has very little effect on the reflectance. But the curve edges become more step like function as period increased to 10, 15 and 20. So, the reflectivity of the DBR can be increased either by increasing the number of pairs of DBR or by increasing the refractive index contrast between the pairs. The various parameters determined from DBR design is presented in the table 3.2.

Also, these high index contrast DBRs could be used as laser mirrors for a laser operating within visible region [226]. So, in the fabrication of DBR, the optical thickness of each layer

can be easily changed and so possible to get a high reflectance at any desired range of wavelengths.

Table 3.2: Various parameters determined from DBR design

DBR design	**Materials**	**index**	**Δn**	**No. of periods (N)**	**Peak reflectivity (%)**	**Stop band FWHM (nm)**
DBR1	SiO_2	1.46	0.08	5	18	93
	MgF_2	1.38		10	40	49
				15	60	36
				20	74	32
				30	89	27
				40	93	25
DBR2	Al_2O_3	1.77	0.31	5	41	118
	SiO_2	1.46		10	79	71
				15	93	61
				20	97	55
				30	98.4	51
				40	98.4	48
DBR3	TiO_2	2.1	0.64	5	91	173
	SiO_2	1.46		10	99.4	141
				15	99.4	130
				20	99.4	126
DBR4	Nb_2O_5	2.32	0.87	5	95.8	203
	SiO_2	1.46		10	99.7	164
				15	99.7	154
				20	99.7	150

3.2.3. Comb filters

To realize a comb filter, we have designed multilayered optical coatings in a different way, by sandwiching a thick optically transparent layer in between two DBRs, by forming cavity like structure. In our work, we have chosen MgF_2 and ZnS as the low and high refractive index material for the DBR designing and the refractive index contrast between these two materials are 0.95. Four periods of multilayers have been chosen for both the DBRs. In Fig. 3.3(a), the cavity length was fixed at 182.5 nm to get a single zero reflectance window at ~500 nm. As the cavity length increased to 500 nm, two peaks with low reflectance were observed, one at 600 nm and the other at 470 nm (Fig. 3.3(b)).

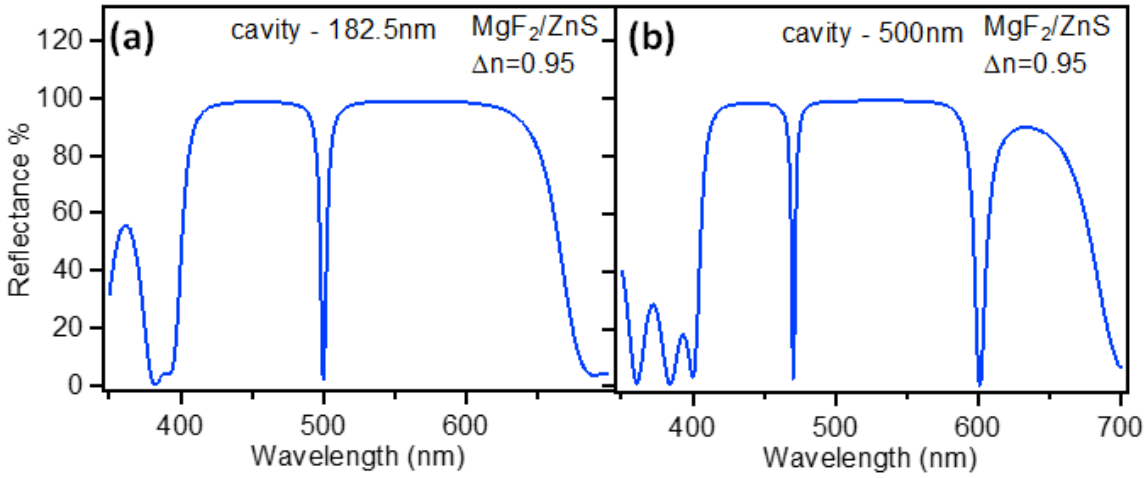

Fig. 3.3: Simulated comb filters for middle layer thickness (a) 182.5 nm and (b) 500 nm.

On increased further to 1μm and 3 μm, number of low reflectance windows increased to four and ten respectively (Fig. 3.3 (c)&(d)). While number of peaks increased for higher cavity length, the FWHM of each peak decreased with increase in cavity length. Thus, to get a high-resolution filtering we prefer larger cavity length. Multi wavelength lasers can also be designed by using the comb filter along with a florescent material incorporated within the cavity. (Hofmann et al., 2010)

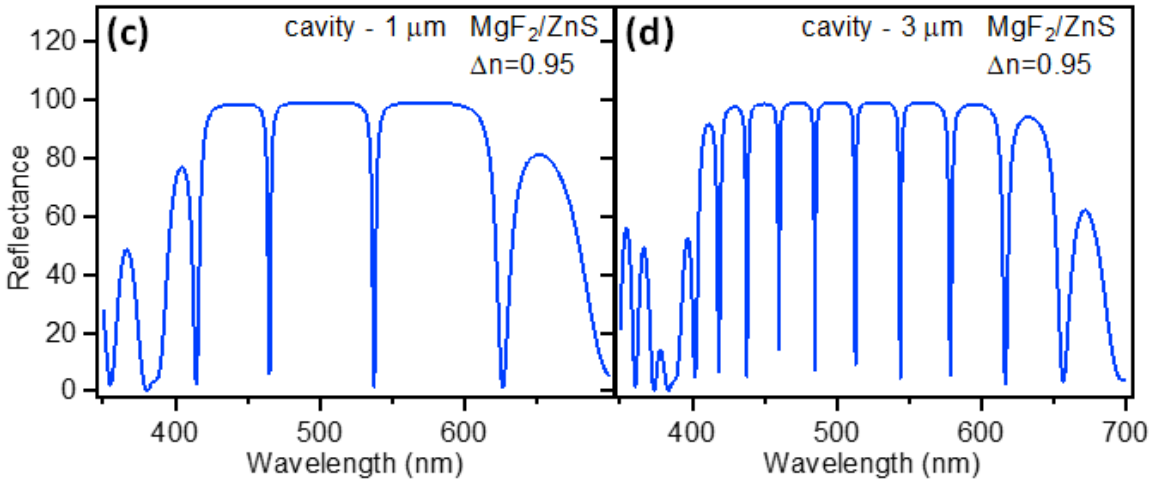

Fig. 3.3: Simulated comb filters for middle layer thickness (c) 1μm and (d) 3 μm

3.2.4. Dichroic Filters

A dichroic filter allows light of a specific range of wavelength to pass through while reflecting light of undesired wavelength. Unwanted wavelengths are reflected in dichroic filters, while desired portions of the spectrum are transmitted. In our study, we have designed six sets of dichroic filters by coating three pairs of different refractive index materials in a periodic manner and with different optical thicknesses. The designed dichroic filters were named as DC1, DC2, DC3, DC4, DC5, DC6. All dichroic filters were designed for 60 pairs of alternating high and low index materials and for a central wavelength of 500nm. And in all dichroic filters, the low index material was SiO_2.

In DC1 and DC2 the materials selected were Nb_2O_5 ($n_H = 2.32$) and SiO_2 ($n_L = 1.456$) as the high and low refractive index material respectively and the refractive index contrast between high and low index material is 0.87. The optical thickness of each layer in DC1 were fixed at quarter wave optical thickness (named as Quarter wavelength filter-QWF) and in DC2 the thickness of high and low index layers was fixed at $0.21(\lambda/4n_H)$ and $1.16(\lambda/4n_L)$ respectively (named as non-quarter wavelength filter-NWF). Where $\lambda/4n$ is the quarter wave optical thickness. Simulation results of transmission spectra of the dichroic filters with H and L are quarter wave thickness of high and low index layers respectively are presented in fig. 3.4(a) and 3.4(b). All dichroic filters were modelled for 60 pairs and the central wavelength were chosen at 632nm (wavelength of He-Ne laser). For DC1 and DC2 the cut off wavelengths are 580nm and 400nm respectively showing a higher pass band for DC2 as compared to DC1. It is observed that, when the optical thickness was deviated from quarter wavelength thickness the cut off wavelength and the ripple in the transmission spectra decreased.

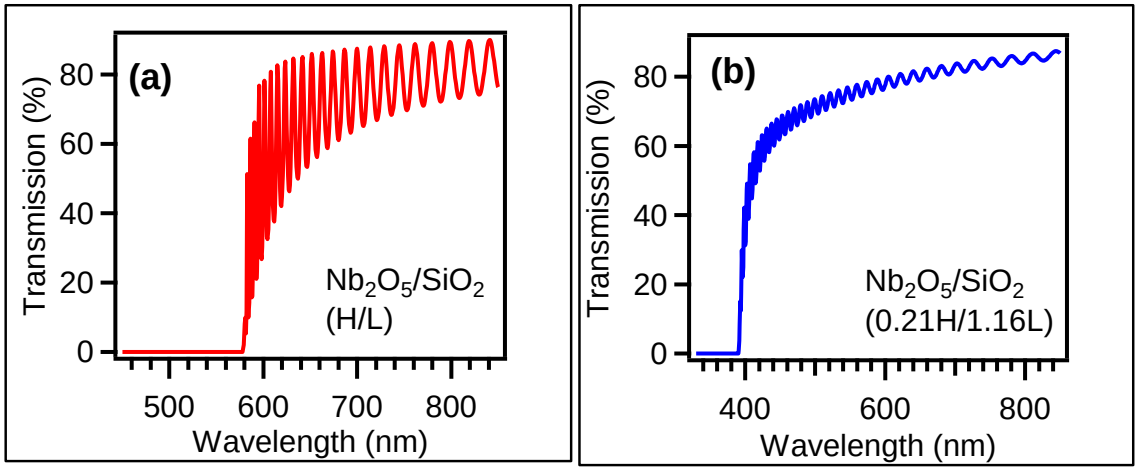

Fig. 3.4: (a) and (b) are the simulated transmission spectra of the dichroic filters of Nb_2O_5/SiO_2 pairs for QWF and NWF respectively.

In DC3 and DC4, TiO_2 (n_H = 2.1) and SiO_2 (n_L = 1.456) were selected as high and low refractive index materials respectively. Refractive index contrast of the two materials were 0.65. In DC3, the optical thickness of each layer was fixed at the quarter wave optical thickness and in DC4, the thickness of high and low index layers was fixed at $0.18(\lambda/4n_H)$ and $1.16(\lambda/4n_L)$ respectively. Simulation results of transmission spectra were presented in fig. 3.4(c) and 3.4(d) shows that the cut-off wavelength is shifted from 560 nm to 380 nm as we go from QWF to NWF. It is also observed that the ripple on the transmission curve of NWF is minimised.

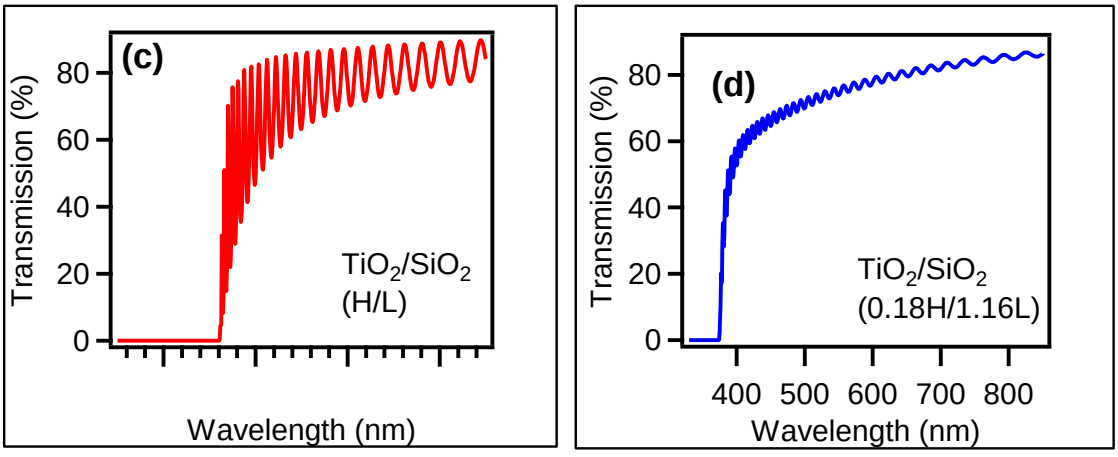

Fig. 3.4: (c) and (d) are the simulated transmission spectra of the dichroic filters of TiO_2/SiO_2 pairs for QWF and NWF respectively.

Similar results were observed for third set of dichroic filters (DC5 and DC6) where the high and low index materials selected were Al_2O_3 (n_H = 1.77) and SiO_2 (n_L = 1.456)

respectively. The refractive index contrast of the two materials was 0.31. DC5 is a QWF and DC6 is NWF. The thicknesses of high and low index layers of DC6 were fixed at $0.16(\lambda/4n_H)$ and $1.16(\lambda/4n_L)$ respectively. Transmission spectra of DC5 and DC6 are presented in fig. 3.4(e) and 3.4(f). Similar trend was observed when we go from QWF to NWF. DC6 shows high band pass as compared to DC5 and the ripple on the transmission curve is minimised further for the NWF (DC6) as compared to any other designed filters.

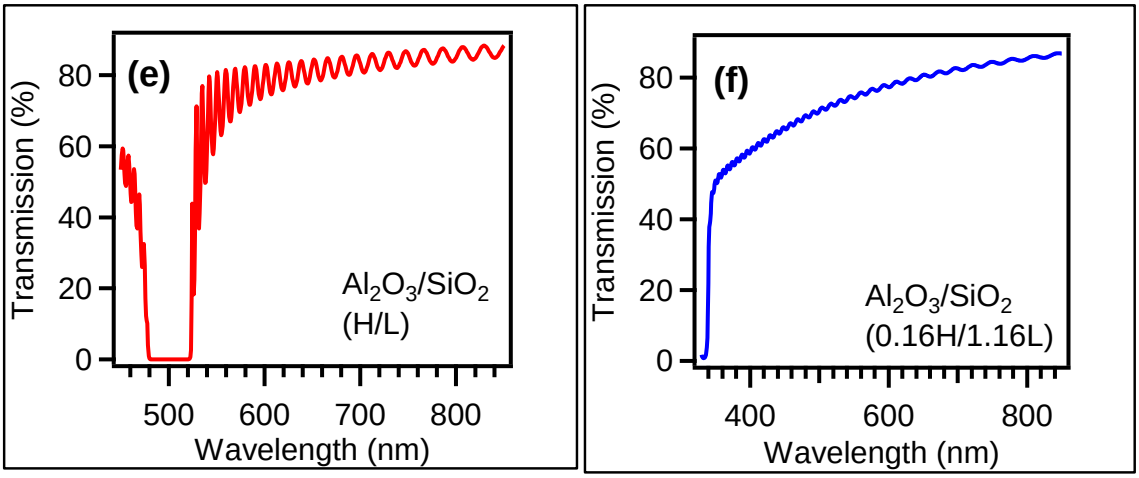

Fig. 3.4: (e) and (f) are the simulated transmission spectra of the dichroic filters of Al_2O_3/SiO_2 pairs for QWF and NWF respectively.

From our simulation results it is clear that the cut off wavelength depends on the refractive index contrast and optical thickness of the high and low refractive index materials. As the refractive index contrast of high and low refractive index material was decreased, cut off wavelength decreased and the dichroic filters show higher pass bands. In addition to this, the fringes appeared in the transmitted light were found to decrease when the ratio of the thickness of high and low index layers were approximately maintained around ~0.11. Dichroic filter parameters are given in Table 3.3.

Table 3.3: List of dichroic filters, materials used for high and low index layers and the corresponding parameters. The refractive indices of the film were chosen at 632nm wavelength. (QWF-Quarter wavelength filter, NWF-Non-quarter wavelength filter, t_H/t_L-thickness ratio of high and low index layers)

Dichroic filter	**High and low index layers**	**Refractive index contrast (Δn)**	**QWF or NWF**	**t_H/t_L ratio**
DC1	Nb_2O_5/SiO_2	0.87	QWF	0.63
DC2	Nb_2O_5/SiO_2	0.87	NWF	0.11
DC3	TiO_2/SiO_2	0.65	QWF	0.69
DC4	TiO_2/SiO_2	0.65	NWF	0.11
DC5	Al_2O_3/SiO_2	0.31	QWF	0.83
DC6	Al_2O_3/SiO_2	0.31	NWF	0.11

3.3 Conclusions

Multi-layered thin film coatings were designed using transfer matrix model (TMM) simulations. Multi-layered thin films were used to realise anti-reflection coating, highly reflecting mirrors, comb filters and dichroic filters. Anti-reflection (AR) coatings were demonstrated using single layer, bi layer and three-layered optical coatings. While one and two layered coatings show high transmission for a narrow range of wavelengths, three layered coating shows high transmission for a wide range of wavelengths. The width of the zero-reflectance window can be increased if a tri-layered optical coating with central layer having an optical thickness of $\lambda/2$ may be chosen. Distributed Bragg reflectors (DBR) were designed using alternating sequence of layers of high and low refractive index materials in a periodic manner. Simulation results showed that, to achieve reflectivity of more than 90%, 40 periods were required for an index contrast of 0.08 and periods reduced to 15 for an index contrast of 0.31. For an index contrast of 0.64 and 0.87, reflectivity above 90% was achieved for just 5 periods. High index contrast of alternative layers will also benefit in having high reflectivity for a broad range of wavelengths. Comb filters were designed by sandwiching a thick transparent layer between two DBRs. As the thickness of the middle layer increased, a greater number of low reflectance peaks were opened and the full width at half maximum (FWHM) of each window decreased. Dichroic filters were designed by arranging multiple layers of different refractive index materials in a periodic manner with different optical thicknesses. The

optical thicknesses of the filters were selected for both the quarter wave thicknesses and non-quarter wave thicknesses. The cut off wavelength depends on the refractive index contrast and optical thicknesses of the high and low refractive index materials. As the refractive index contrast of high and low refractive index material was decreased, cut off wavelength shifted towards lower wavelengths and hence have higher pass band. In addition to this, the ripple in the transmitted light was minimised. When the ratio of the thicknesses of high and low refractive index material was approximately equal to 0.11, the dichroic filter shows higher pass band and very low ripples in the transmission spectra. By choosing appropriate material and optical thickness, the cut-off wavelength can be tuned to any desired wavelength. These optical filter designs can be employed to realize various optical components and hence could be utilized for wide range of practical applications.

Chapter - 4

TiO_2-PVA Nano Composite Polymer Thin Film for Flexible DBR

TiO_2-PVA Nano Composite Polymer Thin Film for Flexible DBR

In the previous chapter, multi-layered thin film coatings were conveniently used to design different types of optical filters using transfer matrix model (TMM) simulations. Anti-reflection coating, highly reflective mirrors, comb filters, and dichroic filters were all designed using multi-layered thin films. These optical filter designs may be used to generate a variety of optical components and hence have a wide range of practical applications. Now, in this chapter, we have fabricated Polymer Distributed Bragg Reflectors by coating titania doped PVA polymer matrix composite and poly methyl methacrylate polymer as alternating high and low index layers respectively. The reflectivity of the fabricated DBR was increased by increasing number of periods. The experimental results were in agreement with transfer matrix model (TMM) simulations. The present work suggests that fabricating flexible polymer DBRs with any desired reflectivity and stop band can be achieved by simply varying the concentration of TiO_2 in PVA without altering any other thin film processing and DBR fabrication parameters. This paper had been communicated in Optical Materials (Elsevier).

4.1 Introduction and Motivation

During the last decade, researchers are very much interested towards the optoelectronic and photonic devices. Flexible and transparent optoelectronic devices have unique physical properties and infinite possibilities to design hetero-structures. Multilayers of transparent materials repeated in a periodic way are the most common optical elements used in the fabrication of high reflectivity distributed Bragg reflectors (DBR).(Brudieu et al., 2014) A DBR is a mirror structure which consists of an alternating sequence of layers of two different optical materials. (Schubert et al., 2007) The design is such a way that all reflected components from the interfaces interfere constructively, which results in a strong reflection. (Jambunathan and Singh, 1997) Distributed Bragg Reflectors have great importance and acceptance in opto-electronic and photonic devices due to their unique properties and cost-effective fabrication process like sol-gel method. DBR have plenty of applications in opto-electronic and photonic devices and a lot of research work going on in this area. These highly reflecting dielectric mirrors which are used as waveguides, laser resonators, antireflection coatings, optical filters, sensors, etc. (Qiao et al., 2018) Because of these diverse applications of DBR, motivated us to

fabricate these featured DBRs and incorporate its applications into photonic and optoelectronic devices.

In DBR, thin films of two distinct material with high refractive index contrast are arranged periodically and they have the capability to deal light waves in a particular manner. On arranging periodically, these periodic structures affect photons properties as the crystal potential in a semiconductor affects the properties of electrons. (Lim et al., 2019) Many different methods have been developed for the design of multilayers. Traditionally, DBRs were fabricated from inorganic metal oxides or semiconductor thin films. (Kedawat et al., 2013; Muallem et al., 2015; Weng et al., 2019) Inorganic DBRs offer dielectric contrasts as large as $\Delta n = 1$. Fabrication methods include vacuum evaporation technologies, sputtering, metal organic chemical vapor deposition, electron-beam evaporation, molecular beam epitaxy, atomic layer deposition, etc. (Alias et al., 2018; Çetin et al., 2013) These methods have high cost of installation and maintenance.

Now a day's flexible optoelectronic devices, such as solar cells or light emitting diodes, have so much importance and it been accompanied by that of flexible optical and electronic materials. Integration into such type of devices, require the stability of their properties upon bending and stretching, adaptability to different types of substrates and durability etc. Among optical materials employed in opto-electronics, distributed Bragg reflectors (DBRs) play a central role. In order to attain the flexible version of the DBRs, a common strategy is taken that stack the thin polymer layers of varying refractive index alternatively. In order to improve performance and functionality of the optoelectronic and photonic devices Flexible Distributed Bragg reflectors have an important role. (Brudieu et al., 2014) Flexible Distributed Bragg reflectors have a self-standing and flexible structure with high mechanical stability. The flexible DBR's can be used as photon frequency filters, optical cavities to enhance spontaneous or stimulated emission or simply as mirrors to increase the time of residence of photons in absorbing electrodes and thus improve their photovoltaic performance. (Calvo et al., 2015) Recent optoelectronic research works aim at developing flexible optoelectronic devices including tuneability of optical filters, mirrors, vertical cavity surface emitting lasers (VCSELs), LEDs etc. (Ji et al., 2016; Yao et al., 2016)

Optically transparent polymers such as fluorinated polymer, ($n \sim 1.3$), cellulose acetate (CA, $n \sim 1.46$), poly (methyl methacrylate) (PMMA, $n \sim 1.50$), polyacrylic acid (PAA, $n \sim 1.51$), poly vinyl alcohol (PVA, $n \sim 1.52$), polystyrene (PS, $n \sim 1.58$), poly (N-vinyl carbazole)

(PVK, n ~ 1.68) etc. are promising alternatives to inorganic materials in the fabrication of flexible DBRs (Kou et al., 2020; Lova et al., 2018, 2015) Fabrication of high index and highly transparent polymers can increase index contrast (Ho et al., 2009) and hence the stop band of polymer DBRs. Fabrication of flexible DBRs from high index contrast polymers has the advantages in opto-mechanical sensing applications.

Cost reduction and efficiency enhancement are the important factors while developing optoelectronic, opto-mechanical and photonic devices. Polymer DBRs have the ability to achieve high reflectance, simple and cost-effective processing methods. (Resende et al., 2018)

While there are reports on the fabrication of high index polymer-inorganic nanocomposites, achieving high index with high transparency is more challenging. (Lee and Chen, 2001; Liu et al., 2011, p. 2; Liu and Ueda, 2009) One of the works reported is on the fabrication of polymer DBRs by Poly vinyl (N- carbazole) (PVK) and cellulose acetate (CA) as high and low index layers respectively. (Takeuchi and Sakata, 2008) But PVK is a toxic polymer and also takes long time to become completely soluble. CA is not a good transparent material as compared to other transparent polymers like PVA, PMMA, PS etc.

Also, while fabricating DBR using CA and PVK as low and high index polymer layers respectively, a refractive index contrasts greater than 0.15 cannot be achieved, and this limiting the photonic band gap width. So, a very large number of periods are required to achieve the desired reflectance. These limitations motivated us in developing new class of metal oxide polymer composite materials for high index polymer layers in polymer DBRs.

For optical applications such as DBR, individual thin film layers of DBR must have high transparency in the visible region. Metal oxides with wide optical band gap act as highly transparent medium for light wavelengths within visible region. Also, high refractive index contrasts greater than $\Delta n = 0.5$ can be easily achieved if we choose certain metal oxides in the fabrication of DBR. This will reduce periods of the DBR and high reflectivity can be easily achieved. Hence the choice of metal oxide for a polymer composite must have high refractive index, high transparency and a wide band gap.

For such optical applications, metal oxides such as TiO_2 and ZnO are commonly used as suitable additives (Jeong et al., 2004; Shetty B et al., 2019). TiO_2 is one such metal oxide with exceptional electrical, optical, chemical and photo catalytic properties. (Haider et al., 2017; Yildiz et al., 2008) It has widespread applications in many areas such as transparent

conducting electrodes, photo catalysis and sensor applications. (Bai and Zhou, 2014; Zhu et al., 2016) TiO_2 semiconductor has a band gap of 3.2eV and refractive index of 2.72 (@550nm for rutile phase). (Bendavid et al., 1999) Also, optical band gap of nanostructured TiO_2 is higher as compared to its bulk counterpart. Moreover, TiO_2 is non-toxic, have strong catalytic activity, powerful self-cleaning characteristics and low cost. These properties led us to choose TiO_2 as a suitable metal oxide for the synthesis of metal oxide polymer composite.

In this work, we have developed a variable refractive index and optically transparent TiO_2 doped PVA polymer composite film (TPMC) by solution chemistry method. TiO_2 of varying concentrations was mixed to PVA solution and then spin-coated to get high index optically transparent polymer thin films. One such high index polymer was then used as high index layer to fabricate DBR. Highly transparent water insoluble poly methyl methacrylate (PMMA) was chosen as low index layer. PMMA was chosen as the low index polymer layer due to its high transmittance of over 92%. Polymer DBRs of up to five periods (one period equals a pair of TPMC and PMMA layers) were fabricated by cost effective spin-coating method. Refractive indices and thickness were estimated by fitting the transmission curves of polymer thin films and DBRs by Transfer Matrix model (TMM) simulations. The TMM simulations were extended to identify number of periods necessary to get DBR reflection higher than 90% and feasible refractive index contrast to reduce number of periods to as low as possible. The present work suggests fabricating flexible polymer DBRs using highly transparent and cost-effective polymers (TPMC and PMMA). Moreover, any desired refractive index contrast, and hence stop band, can be achieved by simply varying the concentration of TiO_2 in PVA without altering any other thin film processing and DBR fabrication parameters.

4.2 Materials and Methods

The pigmentation, refractive index and structural arrangement of materials may change the optical properties of various optical devices. So, for the fabrication of DBR, the material chosen have to be optically transparent and should have sufficient refractive index contrast between the layers. Also, the materials must be capable of being processed into a defect free photonic structure. Initially, we have chosen the materials Poly (9- Vinyl Carbazole) (PVK) and Cellulose Acetate (CA) as high and low refractive index materials. PVK was dissolved in Chlorobenzene and CA was dissolved in Diacetone alcohol. PVK takes long time to become completely soluble in the solution Chlorobenzene. Again, CA is not a good transparent material as compared to other transparent polymers like PVA, PMMA, PS etc. The

refractive index of PVK is approximately 1.6 and CA is 1.48. On fabricating DBR using CA and PVK as low and high index polymer layers respectively, a refractive index contrasts greater than 0.12 cannot achieved. This limiting the photonic band gap width and so very large number of periods are required to achieve the desired reflectance. On increasing the number of periods, the fabrication becomes more challenging. Moreover, PVK was a toxic material and Chlorobenzene was less environment friendly. Also, the coated film was rugged and not in uniform and transmittance spectra obtained was not wave like as expected. The transmittance spectra obtained was as shown in fig. 4.1.

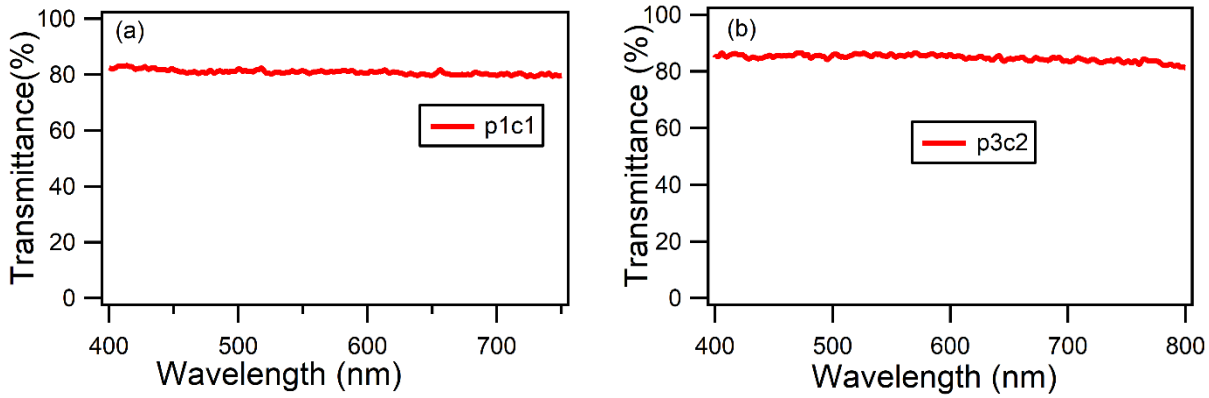

Fig. 4.1. (a) single layer of PVK and CA coated on glass substrate (b) 3 layers of PVK and 2 layers of CA coated on glass substrate.

Due to these reasons, we were forced to change our materials. Thus, began the search for materials with high transparency and high refractive index contrast. On considering the advantages of flexible DBR, we decided to fabricate a nanocomposite polymer, mixture of inorganic metal oxides like titanium dioxide (TiO_2) and a polymer like poly vinyl alcohol (PVA). The reason for choosing TiO_2 as our inorganic material is that

- TiO_2 have exceptional electrical, optical and chemical properties
- Good photo catalytic properties
- High refractive index (2.72 @550nm for rutile phase)
- Water soluble nature
- Optical band gap of nanostructured TiO_2 is higher as compared to its bulk counterpart.
- TiO_2 can be mixed with polymer by simple solution chemistry method
- TiO_2 is non-toxic inorganic metal oxide
- Preparation method is eco-friendly
- Cost effective

- High optical band gap (3.2eV) and dielectric constant
- TiO_2 have high transparency in the visible region

Its high refractive index and huge band gap make it ideal for multilayer thin films. (Khan et al., 2017) It is important to investigate the optical and structural features of TiO_2 films in order to successfully promote their uses. A critical demand for industrial use is the low cost and vast area deposition of TiO_2 thin film on diverse substrates. Even though TiO_2 films can be deposited using a variety of processes, including sputtering, (Löbl et al., 1994) chemical vapour deposition, (Martinet et al., 1997) and the sol–gel process (Garzella et al., 2000) etc., we prefer the solution chemistry method. Here TiO_2 can be easily mixed with the polymer for depositing the thin films. It offers many advantages over other processes, such as low processing temperature, easy composition control, broad area coatings and low equipment cost.

Titanium dioxide nanomaterials have numerous photonic and biomedical applications ranging from common products to advanced devices, such as solar cells, bio-sensors etc. (Sanchez et al., 2011) TiO_2 is an excellent material with outstanding properties and had wide variety of photonic and opto-electronic applications. And PVA is a good and optically transparent polymer which is easily soluble in water. Again, PVA is a non-toxic polymer. Also, both TiO_2 and PVA are water soluble and easily can be mixed. This motivated us to prefer TiO_2 doped PVA as our high refractive index material. The prepared titania doped polyvinyl alcohol nano composite was highly stable, optically transparent and high refractive index contrast can be achieved using these materials.

4.2.1 Material preparation

Solutions of titanium dioxide (TiO_2) doped polyvinyl alcohol (PVA) polymer composite of varying TiO_2 concentrations were synthesised via solution chemistry route. Poly-vinyl alcohol (PVA) (from Sigma Aldrich) was chosen as the polymer matrix and commercial 1 molar Titanium tetra chloride ($TiCl_4$) in toluene solution (from Sigma Aldrich) was used as initial precursor. Initially, titania solution was prepared through a controlled hydrolysis of $TiCl_4$ solution by injecting 1.5 ml of $TiCl_4$ slowly into 10ml deionized water maintained at 0^oC. The mixture was maintained at room temperature with constant stirring for 5 hours to ensure full reaction. Otherwise, white precipitates will sediment at the bottom. 2 wt% PVA solution was then prepared by dissolving 0.2g PVA in 10 ml deionized water (DI) and maintaining at 80^oC for an hour by constant stirring. Freshly prepared titania solution was added to the freshly

prepared PVA solution at a ratio 1.4:1 and stirred the mixture for 20 minutes at room temperature to get transparent TiO_2 dispersed PVA solution (T-PVA solution). T-PVA solutions with varying concentrations of TiO_2 in PVA were prepared by following the above procedure but by increasing the initial volume of $TiCl_4$ from 1.5ml to 2ml, 2.5 ml, 3 ml and 4 ml. The molar concentrations of TiO_2 in PVA solution is presented in Table 1. Solutions thus prepared were named as T-PVA1, T-PVA2, T-PVA3, T-PVA4 and T-PVA5 respectively. The prepared TPVA solutions were highly stable, optically transparent, non-toxic and varying refractive index. While synthesizing T-PVA solutions with higher concentrations of TiO_2, the reaction time to prepare titania solution may be increased considerably to ensure complete reaction. Thin films of varying thicknesses were deposited by spin coating method and the films were named as TiO_2-polymer matrix composites (TPMCs). Thin films from the above T-PVA solutions were named as TPMC1, TPMC2, TPMC3, TPMC4 and TPMC5 respectively. DBRs (named DBR1 and DBR3) were fabricated on cleaned glass substrates by choosing TPMC3 and TPMC5 as high index layers respectively. Poly (methyl methacrylate) (PMMA) (purchased from Alfa Aesar) was chosen as low index layer in both the DBRs. 2 wt% PMMA solution was prepared by dissolving 0.2g PMMA in 10 ml Toluene and maintaining at 90^oC for an hour by constant stirring. Clear and optically transparent PMMA solutions were obtained. For thin film fabrication, the obtained PMMA solution was spin coated with rotational speed 5000rpm. All thin films were dried by using IR lamp to remove excess solvent.

4.2.2 Thin film deposition and characterisation

Thin films were deposited on a glass plate by spin coater (Apex instruments spinNXG-P1). The UV-Visible absorption and transmission studies were carried out using Ocean Optics Maya 2000-Pro UV compact spectrometer, white light source and necessary optical fibres and lenses. The phase identification of the prepared nanocomposite was done by using X-ray diffractometer (XRD) (Make: Malvern Panalytical Aeries Research) and FTIR spectra were recorded by using Perkin Elmer Spectrum Two FT-IR Spectrometer. The Igor software and the TMM simulations were used for the analysis.

4.2.3 Transfer Matrix Model (TMM) Simulations

The thin film designer has to be designed the multilayer thin films in such a way that the transmittance, reflectance and absorbance values should be specified for the particular wavelength of the incident light. This is achieved by regulating the thickness and the refractive

indices of the individual layers. The transfer matrix method is a method used to analyse the propagation of electromagnetic waves through the multilayers of different refractive indices. When electromagnetic wave falls on multilayer thin films of different refractive indices, optical reflections will take place from each interface. Depending on the wavelength of the light source and thickness of the layer, the reflected beams interfere with one another. In transfer matrix model simulations, the optical interference spectra of the reflected beam analysed and then design the optical multilayers with widely varying spectral characteristics. So, transfer matrix model simulations can be used for the design of optical multilayers, distributed Bragg reflectors, optical filters and antireflection coatings etc. Detailed description of the TMM simulations were described in the previous chapter.

Schematic of a DBR made of multiple layers of two transparent media with refractive indices n_H and n_L ($n_H > n_L$) is shown in fig. 1.6. When light enters into this structure, light is partially absorbed, reflected and transmitted at each interface. The thicknesses and refractive indices of the layers define whether the interference among reflected wave is constructive or destructive at a specific wavelength. This can be calculated using transfer matrix model simulations [35].

We have realized that, for alternative layers of high and low refractive indices n_H and n_L and number of periods N, the highest reflectance occurs at λ when

$$n_L l_L = n_H l_H = \lambda/4 \qquad (4.1)$$

When the optical thickness of each layer equal to quarter wavelength of the light used, constructive interference occurs and the layers act as a high-quality reflector.

4.3 Results and Discussions

4.3.1 Structural characterisation

To identify the presence of TiO_2 before and after mixing titania solution with PVA polymer solution, XRD patterns of thin films deposited from titania solution and TPMC4 were recorded and is presented in fig. 4.2. Both the films were spin coated at 3000rpm with dwelling time of 60s on cleaned glass substrate. The broad amorphous background in XRD patterns of thin films from titania solution and TPMC4 might be due to background reflections from both the substrate and polymer matrix. Both the XRD patterns show peak at 28.6^o corresponding to

(110) plane of rutile phase TiO_2. Standard XRD pattern of TiO_2 rutile phase is also presented in Fig.4.2 for reference. (Bae et al., 2009; Howard et al., 1991)

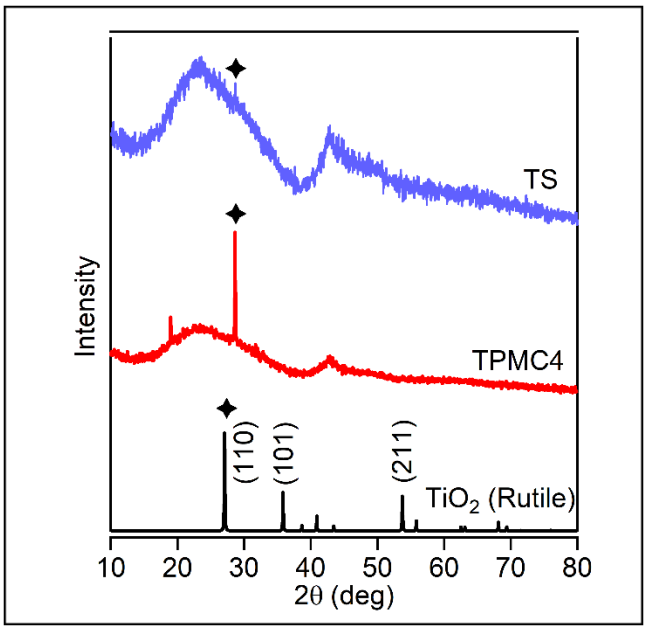

Fig. 4.2: XRD patterns of thin films fabricated from titania solution (TS) (blue) and TPMC4 (red) and standard rutile phase of TiO_2.

As compared to other phases of TiO_2, (Reyes-Coronado et al., 2008) the strongest XRD peak of TPMC4 well matches with rutile phase. This confirms the formation of TiO_2 rutile phase during hydrolysis of $TiCl_4$. The peak is more prominent in TPMC4 film as compared to titania film. This is due to the crystallization of TiO_2 particle within the PVA matrix during thin film formation and post processes such as drying. Crystallite size and d-spacing were determined using Debye Scherer formulae (eqns. 10 and 11). The crystallite size and d-pacing thus estimated were found to be 37.7nm and 3.12 Å respectively. The various parameters determined from XRD pattern is presented in the table 4.1.

$$D = \frac{0.9\lambda}{\beta cos\theta} \tag{4.2}$$

$$\text{and } d_{spacing} = \frac{n\lambda}{2sin\theta} \tag{4.3}$$

Where λ is the wavelength of X-rays, β is the full width at half maximum of the diffraction peak, n is the order of the spectrum- and θ is the angle of diffraction.

Table 4.1: Various parameters determined from XRD pattern

Sample	2θ	θ	FWHM	β in radian	cosθ	sinθ	D in A^0	d spacing (A^0)
TPMC4	28.6230	14.31150	0.21730	0.00379	0.969	0.2472	377	3.115

The infrared spectrum of a molecule provides information about the characteristic properties of the molecule. So, the infrared spectrum can be used as a fingerprint for identification of the structural features of the molecule, and the functional groups attached to the molecule. From the structural features of the molecule, or the functional groups attached to the molecule, we can analyse characteristic properties of the material. FTIR spectra of TPMC4 thin film is presented in fig. 4.3. The largest singlet peak in the wavenumber ranging between 3000 cm^{-1} to 3600 cm^{-1} and the peak around 1650 cm^{-1} are due to the stretching and bending vibrations of -OH group and this indicates the normal polymeric OH presence. The broad peak extending from 400 cm^{-1} to 1000 cm^{-1} shows stretching vibrations of Ti-O and Ti-O-Ti framework bonds. (Kumar et al., 2000)

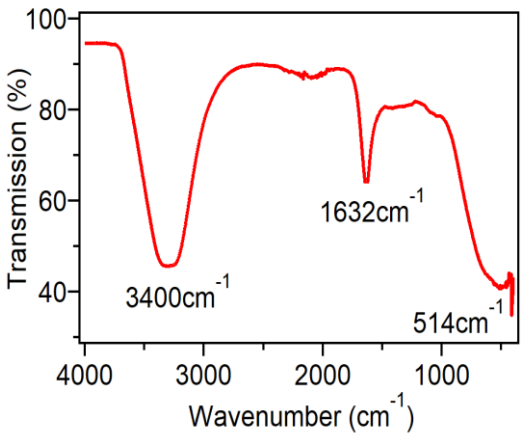

Fig. 4.3: FTIR spectra of TPMC4

4.3.2 Optical characterisation

The transmittance spectra of a TPMC thin film obtained from UV-Visible Spectro-photometer is as shown in fig. 4.4. The transmittance spectra appeared like a wave with a dip in certain wavelength region. At this region, the reflectivity goes to a high value.

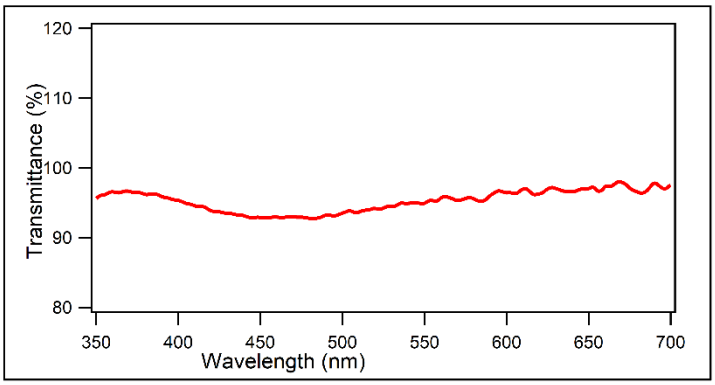

Fig. 4.4 : Transmission spectra of TPMC thin film

The transmittance spectra of TPMC thin films with different concentrations of TiO_2 in PVA were deposited on glass substrates as shown in the fig. 4.5. The different concentrations of TPVA solutions were obtained by increasing the concentrations of $TiCl_4$ as 2ml, 2.5ml, 3ml and each corresponds to a concentration of TiO_2 in PVA as 231, 266, 295 mmol/lit respectively. From the fig.6, it is clear that, the transmittance decreases and so the reflectance increases with increasing concentration of TiO_2 in PVA. Here, we have assuming R%=100-T%, assuming very low absorption over the entire visible region. From the table 4.1, it is obvious that as the concentration of TiO_2 in PVA increases, refractive index of the TPVA solution increases. This implies that as the refractive index of the TPVA solution increases, reflectivity of the film also increases.

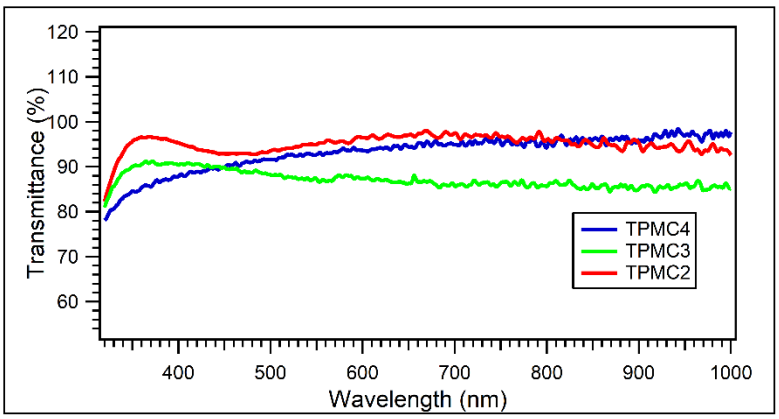

Fig. 4.5: Transmission spectra of the TPMC film by increasing $TiCl_4$ concentration

The estimated refractive indices of samples with varying TiO_2 concentrations were presented in Table 4.2. The refractive indices were found to increase monotonically with an increase in TiO_2 concentrations.

Table 4.2: Polymer film id, TiO_2 concentration
and corresponding refractive indices (estimated by TMM simulations)

Sample id	**Conc. of TiO_2 (mmol/lit)**	**n (@ 632nm)**
PVA	0	1.48
TPMC1	194	1.52
TPMC2	231	1.58
TPMC3	266	1.66
TPMC4	295	1.75
TPMC5	442	1.80

TPMC thin films of various thicknesses were deposited on glass substrates by varying the spinning speeds. Spinning speeds were between 2000 rpm and 7000 rpm, with a spinning time of 60 sec. A set of transmission spectra recorded for TPMC4 thin films is shown in fig. 4.6. Refractive indices were first estimated by Brewster's method. Using these refractive index values in TMM simulations to get optimised values for refractive indices and film thicknesses. Thicker TPMC4 films (Fig. 4.6(c) and 4.6(d)) were deposited from T-PVA solution prepared as mentioned in section 4.2.1 except 2wt% PVA solution was replaced with 3wt% PVA solution.

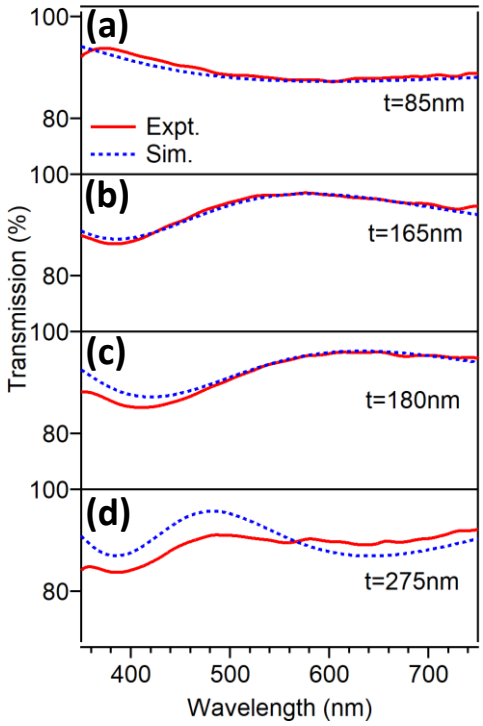

Fig 4.6: Transmission spectra of TPMC4 thin films (a) 2wt% PVA, 7000rpm, (b) 2 wt% PVA, 3000rpm, (c) 3 wt% PVA, 6000rpm and (d) 3wt% PVA, 2000rpm. (t-thickness)

To perceive the overall quality of the spin coated film the optical microscopy images were taken. The pictures taken by an optical microscope is presented in the fig. 4.7. From the optical microscopy images, it is clear that the deposited film was almost uniformly coated on the glass substrate.

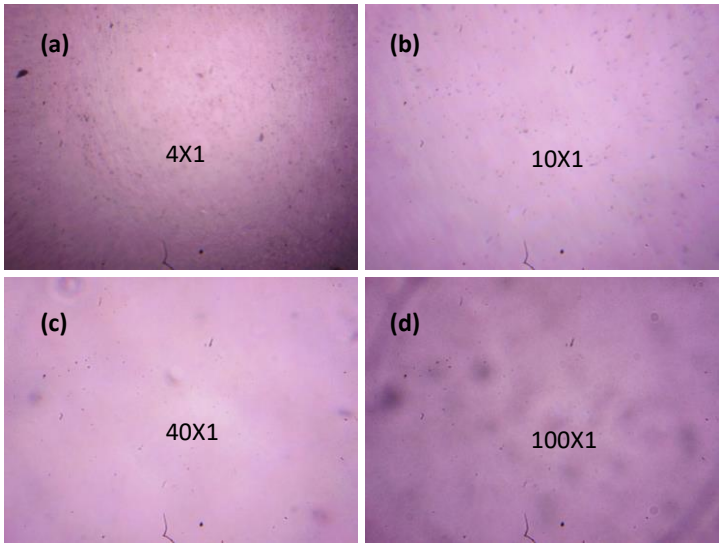

Fig. 4.7: Optical microscopy images of the spin coated TPMC film at various resolutions

But as the thickness of the film increased by increasing the concentration of PVA, uniformity of the film lost to a certain extent. As the number of pairs increased, cracks were observed on the film. Fig. 4.8 shows the optical microscopy images of the spin coated TPMC film with higher thickness at various resolutions.

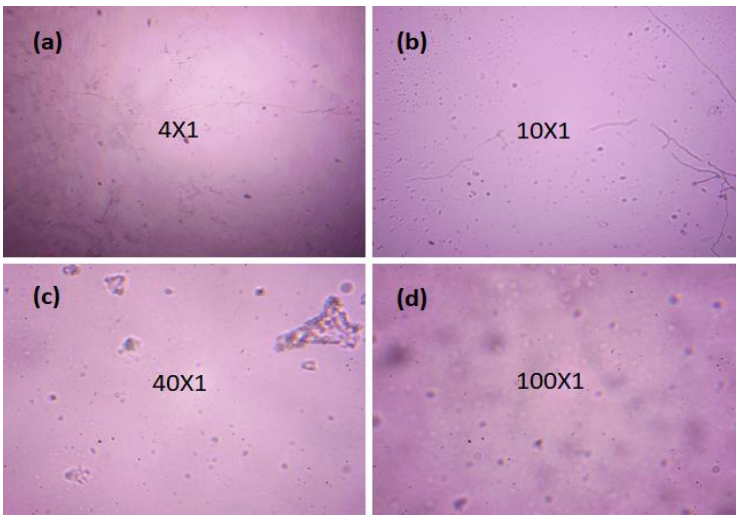

Fig. 4.8: Optical microscopy images of the spin coated TPMC film with higher thickness at various resolutions

4.4 Distributed Bragg Reflectors (DBR)

Distributed Bragg reflectors were fabricated by spin coating T-PVA and PMMA solutions on a glass substrate using a spin coater. TiO_2-polymer matrix composites (TPMCs) were used as high index polymer and PMMA were used as low index polymer. DBR1 was fabricated with TPMC3 (n_H-1.66) and PMMA (n_L-1.49) as high and low index layers respectively.

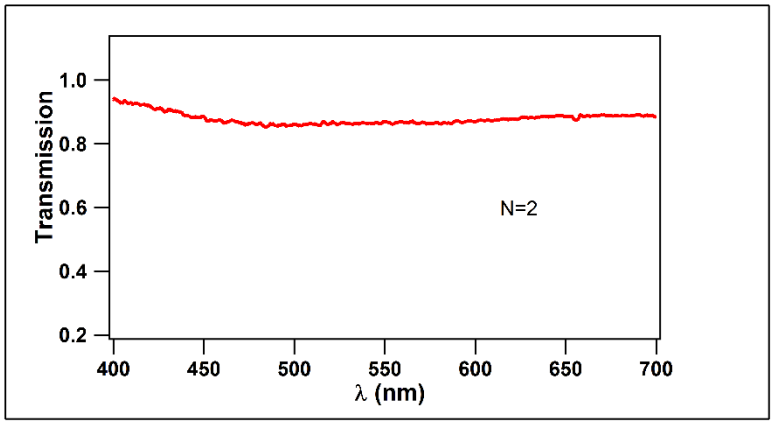

Fig. 4.9 Transmission spectra of DBR1 for N=2

The transmission spectra were recorded and from the transmission spectra, reflection spectra were calculated by R%=100-T%, assuming very low absorption over the entire visible region. The transmission spectra of DBR1 with N=2 was obtained as shown in fig. 4.9. As the number of periods (N) in DBR was increased from 2 to 5, a stop band between wavelength range 500 nm and 700nm was observed and the reflection increased from 12% to 33% around the central wavelength 600nm. Fig. 4.10[(a)-(d)] represents the experimental and simulation results of reflection spectra of DBR1 with increasing periods and fig. 4.10(e) is the simulation results of DBR1 for periods N = 5, 10, 15 and 20.

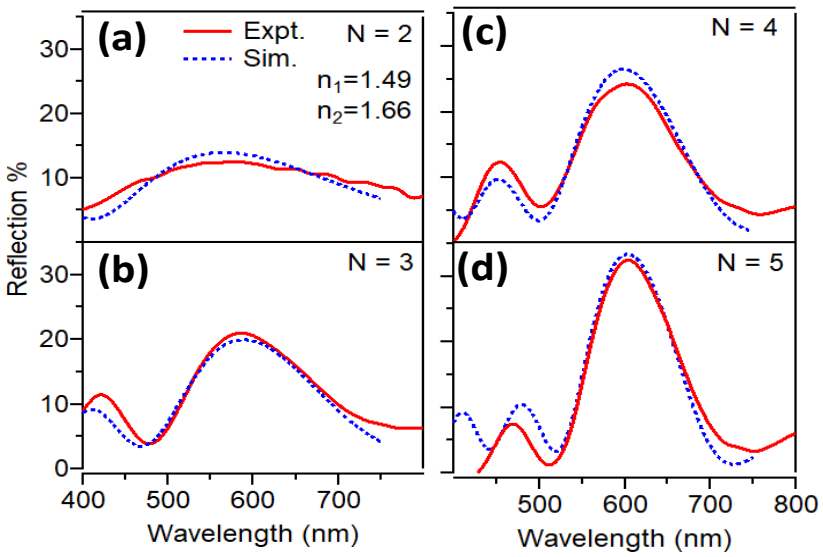

Fig. 4.10: (a) to (d) Experimental and simulation results of reflection spectra of DBR1 with increasing periods

.

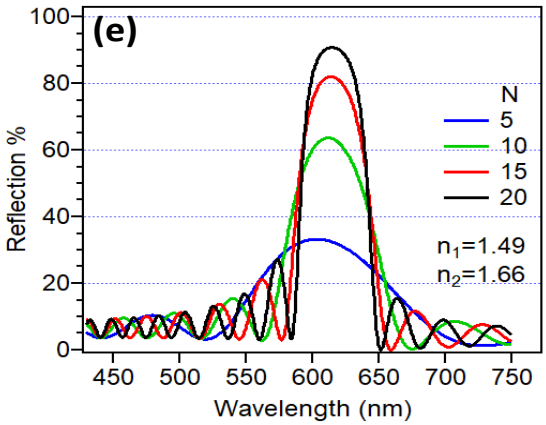

Fig. 4.10: (e) Simulation results of DBR1 for periods N = 5, 10, 15 and 20.

TMM simulations perfectly match with the experimental results. From TMM simulations the thickness of high index and low index were estimated to be 60 nm and 140 nm. We have extended the simulation results to observe the increase in reflection (%) by increased N from 5 to 20. From fig. 4.10(e) it is clear that the reflection band increases up to 90% with a DBR having 20 periods. It is also observed that the central wavelength red shifts with increase in N. This is due to the mismatch in the condition $n_L l_L = n_H l_H = \lambda/4$. Thicknesses of high index and low index layers within DBR1 structure do not exactly match optical thickness as mentioned in the above equation. Hence, we observed peak shift of 46 nm as N was increased from 2 to 20. To reduce this shift and to get a DBR with a central wavelength of 600nm, the thickness of TPMC3 and PMMA layers must be fixed at 90.4 nm and 100.7 nm respectively. The deposition parameters like rotation speed and time and PVA wt% are to be optimised to get the above estimated layer thicknesses for n_H and n_L. Thus, by fixing the optical thickness of each layer to 1/4th of central wavelength the peak shift with increase in N can be minimised.

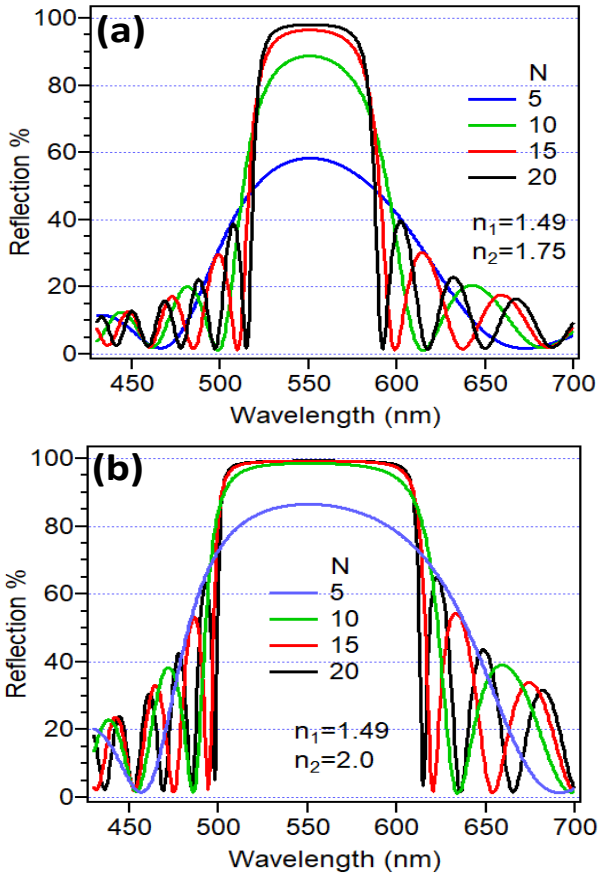

Fig. 4.11: Simulation results of (a) DBR2 and (b) DBR4 for no. of periods (N) = 5, 10, 15 and 20.

Simulations were carried out for DBR structures with higher TPMC indices 1.75 and 2.0 (named as DBR2 and DBR4). The results are presented in fig. 4.11. DBR parameters

estimated from simulations are tabulated in Table. 4.3. It is clear that as N increases reflectivity increases. For DBR1 (Δn ~ 0.17), the peak reflectivity increased from 12.5% to 90.8% as N was increased from 2 to 20. For an index contrast of 0.26 (DBR2), peak reflectivity of 88.8% was achieved for N=10 and the reflectivity increased to ~98% for 20 periods. As the index contrast was increased to 0.51 (for DBR4), within 5 periods a peak reflectivity of 86.5% was achieved. This DBR structure could deliver a reflectivity of as high as 99.3% within 15 periods. Reflectivity was not increased much for N above 15 periods. DBR2 and DBR4 were designed with optical thicknesses of each layer exactly equal to quarter wave (central wavelength 550nm). These structures do not show any peak shift. Full width half maximum of stop band can be increased by increasing the index contrast. For a 20 periods DBR structure, stop band of 50 nm was estimated for Δn of 0.17. This was increased to 70 nm and 115 nm for Δn of 0.26 and 0.51 respectively.

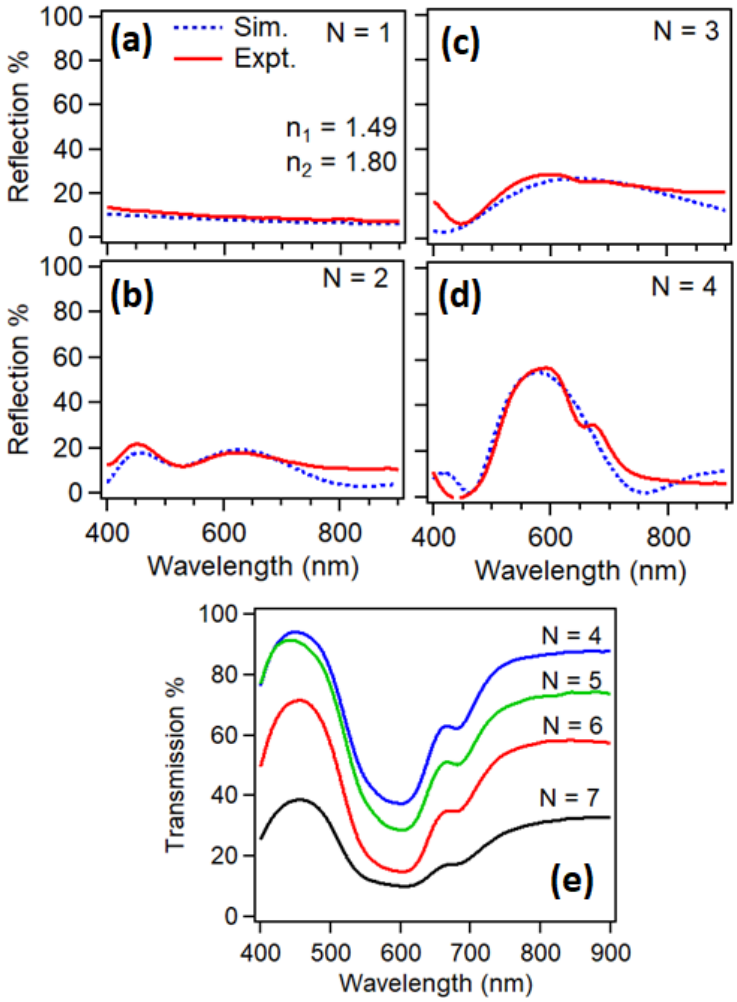

Fig. 4.12: (a) to (d) Experimental and simulated reflection spectra of DBR3 with N = 1 to 4 and (e) transmission spectra of DBR3 with N=4, 5, 6 and 7.

Further we have extended our studies by fabricating DBR (named DBR3) using TPMC5 (n=1.8) and PMMA as high and low index layers respectively. Reflection spectra of the fabricated DBR3 are presented in Fig. 4.12. The index contrast between high and low index layers in DBR3 is 0.31 and hence a wide stop band and high reflectivity is expected even for low N values as compared to DBR1 and DBR2. DBR3 shows a reflectivity of 62.3% for number of periods 4. This is much better than the reflectivity of 24.6% achieved for DBR1 for the same number of periods. Unfortunately, as the number of periods was further increased in DBR3, the reflectivity was found to decrease. For seven pairs of layers, reflectivity decreased to 28.6% (Fig. 4.12(e)). Cracks were observed for DBRs having number of pairs more than 4 when viewed with optical microscope. This led to more surface roughness and hence to a low reflectivity. The base line of the transmission spectra was found to decrease for N values above 4 as shown in Fig. 4.12(e). This implies that, apart from transmission and reflection, a fraction of light gets scattered due to surface roughness. From fig. 4.12(e), the scattering percentage was estimated to be 61% for seven periods. From our designs, peak reflectivity of 80% or above is achievable with high index contrast layers in DBR. Our fabrication is limited to DBRs with 5 periods due to reduced surface quality on depositing a greater number of layers. Fabrication process needs to be optimised to identify the origin of cracks and hence on reducing scattering effects. Nevertheless, high reflectivity and a broad stop band may be achieved by choosing high index contrast layers and minimal number of periods to avoid scattering losses. We propose TPMC and PMMA as high and low index layers for a flexible polymer DBR mirrors. Here TPMC index can be changed by simply varying the concentration of TiO_2 in PVA without altering any other thin film processing and DBR fabrication parameters. Hence any desired stop band range and any desired peak wavelength and reflectivity can be designed using the proposed DBR structure. The various parameters determined from DBR design were tabulated in the table 4.3.

Table 4.3: Various parameters determined from DBR design and fabrication

DBR design	TPMC index	Δn	No. of periods (N)	Peak reflectivity (%)	Peak λ (nm)	Stop band FWHM (nm)	Expt/ Sim
DBR1	1.66	0.17	2	12.5	570	350	Expt.
			3	21.0	585	165	Expt.
			4	24.6	600	140	Expt.
			5	32.5	605	110	Expt.
			10	63.7	612	70	Sim.
			15	82.0	615	55	Sim.
			20	90.8	616	50	Sim.
DBR2	1.75	0.26	5	58.3	550	120	Sim.
			10	88.8	550	90	Sim.
			15	96.5	550	80	Sim.
			20	98.1	550	70	Sim.
DBR3	1.8	0.31	2	28.0	596	310	Expt.
			3	34.9	598	205	Expt.
			4	62.3	602	173	Expt.
			5	62.8	602	160	Expt.
DBR4	2.0	0.51	5	86.5	550	165	Sim.
			10	98.6	550	135	Sim.
			15	99.3	550	125	Sim.
			20	99.3	550	115	Sim.

4.5 Conclusions

Thin films of variable refractive index from a single polymer were developed by doping titanium dioxide (TiO_2) in poly-vinyl alcohol (PVA) by solution processing. A refractive index of up to 1.80 was achieved by increasing the doping levels of TiO_2 in PVA. Further increase in TiO_2 could increase the refractive index of T-PVA to 2.0 or even more. DBRs were fabricated by titania doped PVA polymer matrix composite (TPMC) and poly methyl methacrylate (PMMA) polymers as alternating high and low index layers respectively. The reflectivity of DBR was increased by increasing number of periods. The experimental results were in agreement with transfer matrix model (TMM) simulations. TMM simulation results showed that, to achieve reflectivity of more than 90%, number of periods can be increased or refractive index contrast can be increased. With a high index contrast of 0.51,

number of periods can be reduced to 5 as compared to 20 periods in a DBR with an index contrast of 0.17. High index contrast of alternative layers will also benefit in having a relatively broad stop band. The present work proposed that fabricating flexible polymer DBRs from highly transparent and cost-effective polymers TPMC and PMMA in a simple solution chemistry method. Moreover, any desired refractive index contrast, and hence stop band, can be achieved by simply varying the concentration of TiO_2 in PVA without altering any other thin film processing and DBR fabrication parameters.

Chapter -5

Carbon Quantum Dots Dispersed PVA Thin Films

Carbon Quantum Dots Dispersed PVA Thin Films

In the previous chapter, we had proposed TPMC and PMMA polymers as high and low refractive index materials for the fabrication of flexible DBR using a simple, cost-effective solution chemistry approach. Using these pairs, any desired refractive index contrast and hence stop band and reflectivity can be achieved by simply varying the concentration of TiO_2 in PVA. In this chapter, we discussed the synthesizing method of highly photoluminescent carbon quantum dots in a simple microwave assisted hydrothermal method. The CQDs were prepared from Commercial D-glucose, a simple monosaccharide sugar. The solvent was de-ionised water. CQDs were synthesized in a simple, green assisted method by microwave heating of the solution. CQDs can exhibit different emission colours when they are excited at different excitation wavelengths. Also, the emission wavelength of CQDs independent of size of the CQDs. We found that CQDs show strong optical absorption in the UV region. ie. CQDs are effective photon-harvesting agents especially in short-wavelength region. In order to form a thin film of CQDs we had mixed CQDs with PVA and CQD-PVA nano composite thin film had done. This work presented in the international conference of Optical Society of America and published in OSA Technical Digest as "Photoluminescent glucose derived carbon quantum dots for photonic and optoelectronic applications".

5.1 Introduction And Motivation

Carbon quantum dots are carbon based zero dimensional materials with size less than 10nm. Carbon is one of the fundamental elements of all living things, have an important role in modern science and technology. Among the quantum dots CQDs are rising stars due to their low cost, intense fluorescence, low toxicity, flexible luminescence range, excellent light stability, non-blinking features and outstanding solubility. (Wang et al., 2017) With these significant features CQDs have wide range of potential applications. (Kandasamy, 2019) In addition, CQDs have appealing qualities like high stability, strong conductivity, environmental friendliness, straightforward synthetic processes, and optical features that are equivalent to other quantum dots. Therefore, CQDs are fascinating class of carbon nanoparticles. (Lim et al., 2015)

When purifying single-walled carbon nanotubes from arc-discharged soot, Xu et al. unintentionally found this fascinating class of fluorescent CQDs. (Wang et al., 2017) Following that, many synthesis routes have been created for the preparation of CQDs, and many of them

are simple, affordable, and size-controllable procedures. Furthermore, a variety of techniques may be employed for the synthesis of large-scale CQDs. (Chen et al., 2016)

Mainly, there are two different approaches for the synthesis of CQDs. One is top-down approach and the other is bottom-up approach. Top-down approaches use chemical oxidation, laser etching, and other techniques to reduce the size of massive carbon structures such as graphite and carbon nanotubes. This technique necessitates expensive and time-consuming equipment. (Yang et al., 2022) Controlling the size and properties of the CQDs is also challenging in this procedure. In the bottom-up approach, a variety of techniques including the microwave-assisted hydro-thermal method, can be used to generate the CQDs from small carbon particles or molecules, which is relatively straightforward and simple to manage. Reliable row materials are often employed in the bottom-up approach for CQD synthesis. As a result, this strategy is cost-efficient, environmentally friendly, and successful in reducing waste creation. (Singh et al., 2018) Schematic illustration of CQD preparation via 'top-down' and 'bottom-up' approaches is presented in the fig. 5.1.

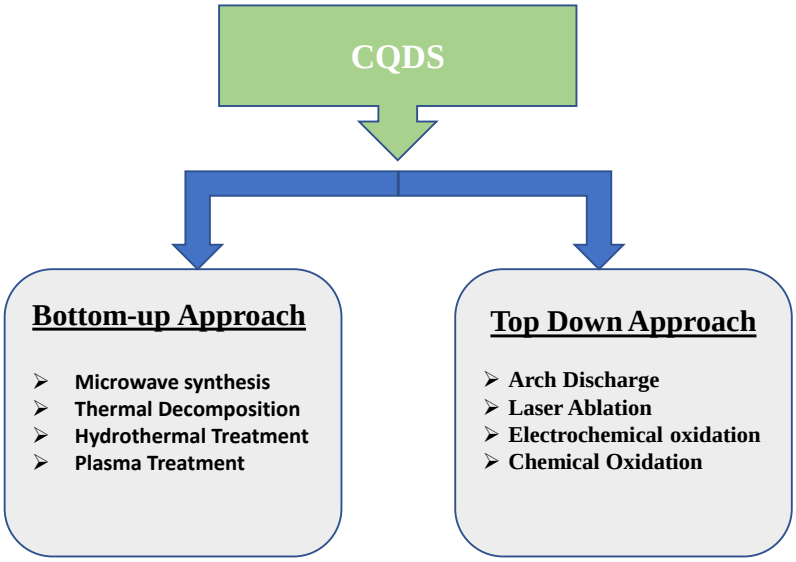

Fig. 5.1: Schematic illustration of CQD preparation via 'top-down' and 'bottom-up' approaches

The raw materials used in the synthesis of CQDs are naturally occurring various carbon containing materials such as citric acid, denatured milk, dried leaves, sodium hydroxide, broccoli, food wastes, ammonium citrate, grass, ascorbic acid, vegetables, gelatine etc. (Rani et al., 2020) Carbon is one of the essential elements of organism and because of the wide extensive resources of carbon, the production cost of CQDs is much lowered. Also, CQDs possess attractive properties such as high stability, good conductivity, environmental

friendliness, simple synthetic routes as well as comparable optical properties to quantum dots. (Liu et al., 2020) In most cases, CQDs are synthesized from naturally occurring plants, vegetables or other carbon sources. (Fan et al., 2020) So, the method is cost effective, low toxic, eco-friendly and the raw materials are widely available. Also, in the synthesizing processes, the consumption of chemicals and waste production has been greatly reduced.

Carbon quantum dots (CQDs) or graphene quantum dots (GQDs) may be the two types of carbon-based quantum dots that are synthesised. The major difference between CQDs and GQDs are in CQDs excitation dependent emissions are happened; but in GQDs excitation independent emission are happened. In CQDs size may be below 10nm, but in GQDs size lies between 1-100nm. CQDs may be amorphous in nature; but GQDs are crystalline. For the preparation of CQDs , we have wide range of resources including all biomaterials; but in GQDs we have only limited number of precursors including carbon nanotube, graphene oxide, carbon black etc. (Ghosh et al., 2021; Li et al., 2019)

Although there are various methods for producing carbon quantum dots, the microwave-assisted hydrothermal (MAH) method combines hydrothermal and microwave techniques. Intense energy can be provided by microwave radiation to break the molecule's chemical bonds. So, this method can effectively reduce the reaction time and so provide simultaneous, homogeneous fast heating, which leads to uniform size distribution of quantum dots. Additionally, by adjusting the microwave heating time, the size of the CQDs can be easily controlled using this method. The formation of highly photoluminescent carbon quantum dots is done in an easy, non-toxic and economical way. Also, CQDs obtained using this method are highly stable and water soluble. (Xu et al., 2020)

The mechanism for CQD formation includes dehydrating glucose molecules to produce the nucleus of the CQDs. Then the growth of CQD occurs at the spherical surface with increasing microwave heating time. As the microwave heating time increases, the source molecules reach the surface of the CQD and generate new C-C by dehydration. By this way CQD becomes larger as heating time increases. Owing to the high pressure induced by the hydrothermal condition, the newly formed C-C is orderly arranged and that causes the growth of CQDs. The newly formed surface functional groups in CQDs causes to absorb the UV Visible light. So CQDs act as an effective photon harvesting agents especially in the UV Visible region. (Rani et al., 2020) The mechanism of CQD formation is schematically represented in the fig.5.2.

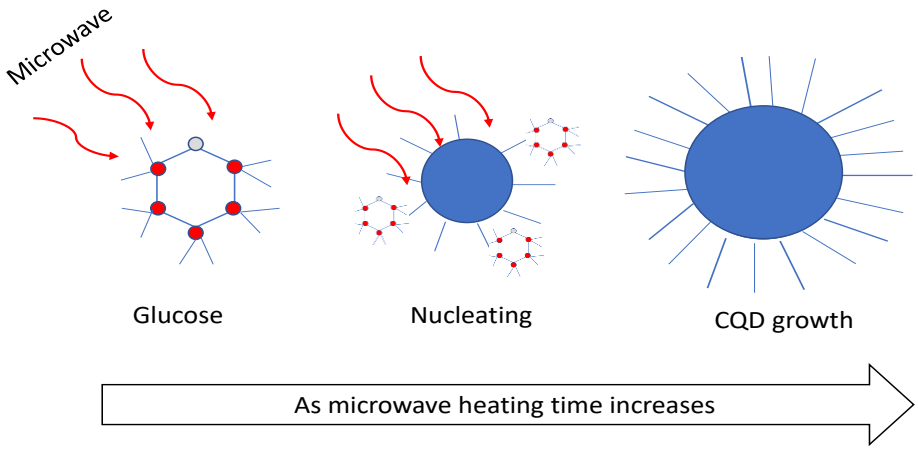

Fig. 5.2 Mechanism of CQD formation

CQD's remarkable features such as low toxicity, inexpensive and strong biocompatibility make them attractive materials for photocatalysts, UV absorbers, bioimaging, biosensors, photosensitizers, electron mediators and spectral converters etc. (Mehta et al., 2019) CQDs have superiority in water solubility, chemical stability and low toxicity over common photocatalysts ZnO, TiO_2, CdS etc. Also, after specific surface modification, CQDs exhibit excellent and tuneable optical properties particularly absorbance and photoluminescence. (Heng et al., 2021) Main challenges facing the photo-catalyst materials are fast recombination of charges and limited light utilisation properties. In CQD-based nano composite photocatalysts materials, CQDs can be easily dispersed into the surfaces of other nanocomposites. Also, CQDs have an excellent electron-transfer property that can improve charge separation. (Khan et al., 2020) Conventional photocatalysts, TiO_2 and ZnO have wide-bandgap and can be excited only by UV light and this limits their practical applications. (Zhang et al., 2009) When conventional TiO_2-based photo catalyst coupled with narrow-bandgap semiconductors like CdS and CdSe etc. the composite system exhibits photo-excitation by wide range of wavelength from the full solar spectrum. (Zheng et al., 2020) But in practical applications they are restricted because of their toxicity and instability. CQDs/TiO_2 composite photocatalyst system exhibits higher photocatalytic activity than pure TiO_2 because CQDs trade as a spectral converter in CQD-based composite photocatalysts system. i.e., CQDs can extend the light utilisation range of photo-catalyst from UV-light to visible-light range. (Zhang et al., 2017)

Other applications of CQDs are adsorption treatment using CQDs. CQDs can remove organic and inorganic pollutants or unwanted materials from a solution. This is because CQDs have large surface area and these surfaces or edges of CQDs can interact with other functional groups. i.e., CQDs increases the physical or chemical interactions among the materials. So, the precipitate formed can be easily removed. (Rani et al., 2020) It is also possible to tune the energy bandgap of quantum dots and this leads to increase of adsorption capability. This captivating property of CQDs makes them an efficient adsorbent in the removal of pollutants from waste water. (Wu et al., 2018)

CQDs can be used as an antimicrobial agent for the degradation of bacteria and the CQDs/TiO_2 nanocomposite has sustainable antibacterial property. The CQDs/TiO_2 nanocomposite can effectively use as an antibacterial agent than pure TiO_2 because in pure TiO_2 due to the agglomeration, antibacterial efficiency will degrade. CQDs/TiO_2 nanocomposite may produce more free radicals, and these free radicals will decompose the organic materials in the bacteria cells causing decay of these bacteria. (Yan et al., 2019) CQDs can be used as an excellent antibacterial agent because of their fascinating properties like controlled-size, well-dispersed in water and good antimicrobial properties. CQDs antibacterial activity enhanced by UV-light irradiation, because of their fluorescent properties and resistance to photo-bleaching. (Budimir et al., 2021)

Due to the outstanding features of CQDs as biocompatibility, good solubility in aqueous solution, non-toxicity and desirable optical properties, they have many attractive biomedical applications. (Azam et al., 2021) The tuneable fluorescence and quantum size effect of CQDs make them to choose as promising material in the biological imaging of various cellular processes. (Jin et al., 2011)

In our research, we initially intended to develop CdSe quantum dots. But it is toxic. CQDs were developed after it was realized that they offered all of the advantages of CdSe or other quantum dots. We had synthesized highly photoluminescent, water soluble, eco-friendly, non-toxic CQDs in a cost-effective way by microwave assisted hydrothermal method. CQDs were synthesized from glucose via solution chemistry route and Deionized water was used as solvent. This method has the advantages of microwave and hydrothermal techniques. This method does not require any surface passivation agents or inorganic additives. The sole reagent is glucose, which makes this method more attractive as compared to other CQD synthesis methods. Also, all our works were polymer related and using CQDs polymer matrix can be easily formed. So, more applications can be done in polymers. We had prepared different sized

CQDs by changing the heating time and the concentrations of glucose solutions. It was found that size of the CQDs increased with increasing heating time as well as with the concentrations of CQDs. From the photoluminescence spectra it was found that the emission wavelength of CQDs is independent of size of the CQDs but depends on the excitation wavelengths. Also, CQDs show strong optical absorption in the UV region. ie. CQDs are effective photon-harvesting agents especially in short-wavelength region.

5.2 Materials and Methods

CQDs were synthesized from commercial glucose via solution chemistry route. Deionized (DI) water which is used as solvent. Both the materials used in the synthesis process are easily available and non-toxic. Here glucose is used as the carbon source. Microwave-irradiation of the sample was done by model: BAJAJ 1701 MT 17L SOLO microwave oven. We considered a straightforward synthetic method involving microwave heating of the material. This microwave heating provides simultaneous, homogeneous, fast heating, leading to uniform size distribution of quantum dots. Since the ingredients are glucose and DI water, the method is cost effective and eco-friendly. Also, in the synthesizing processes, the consumption of chemicals and other waste production has been very much reduced.

We had synthesised water soluble CQDs from glucose solution (8wt% concentration) by using glucose and DI water as source and solvent respectively. 8.0g glucose was dissolved in 100ml DI water, and the resulting glucose solution was collected in a 5ml glass bottle. Microwave heating of the solution contained in the glass bottle for different time such as 5, 6, 7, 9, 11 and 13minutes at a certain power of 350W. We had repeated the experiment by changing the microwave power, microwave heating time, concentration of the solution and volume of the solution. It was found that the experimental parameters such as microwave power, heating time, source concentration as well as solution volume have a distinct effect on the growth of CQDs. i.e., these experimental parameters will affect the size of the CQDs. In the process of microwave heating, the solution changed its colour from transparent to pale yellow and brown, as a result of formation of CQDs [5,6]. The procedure of CQD formation diagrammatically represented as shown in the fig. 5.3.

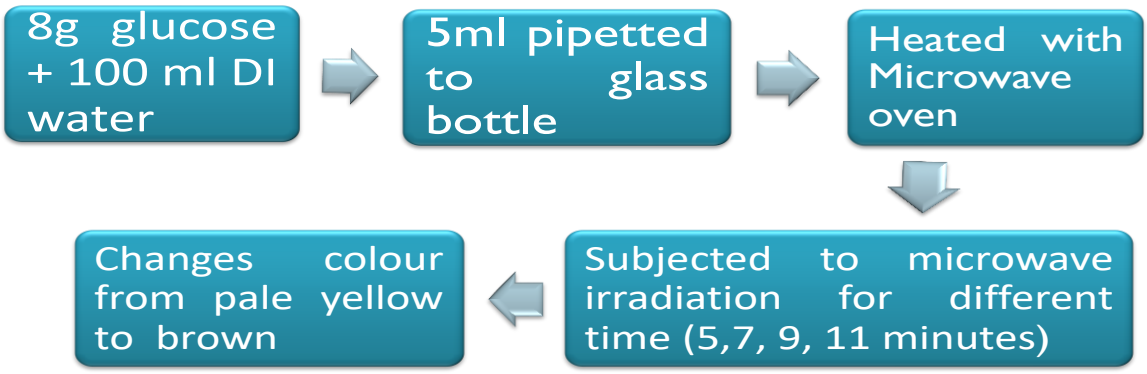

Fig. 5.3 Diagrammatical representation of CQD formation

When the solutions were kept in a UV chamber and subjected to UV radiation different solutions show different fluorescent colour. UV-Visible absorption and transmission studies were carried out using Ocean Optics Maya 2000-Pro UV compact spectrometer, white light source and necessary optical fibres and lenses. For photoluminescence study, laser sources of wavelength 540nm, 450nm and 280nm was used as excitation sources and Ocean Optics spectrophotometer was used as a detector.

Transmission electron microscopy images were taken to analyse morphological, compositional and crystallographic information about the sample. Surface area electron diffraction pattern was also taken to identify whether the sample is crystalline or not.

Even though the synthesized CQDs were highly water soluble, it cannot form into a thin film when coated on a glass plate. Even if it was heated to a high temperature for a long time, it did not form into a thin film. The CQD's were found to be sticked on the glass plate like a sticky gel. If CQDs can be converted into a thin film, it will have numerous photonic and optoelectronic applications. On mixing CQDs with certain polymers, it can be possible to coat on the substrate as a thin film. But it must be confirmed that when mixed with a polymer, its transparency and photoluminescence properties should not change. So, the choice of the polymer is an important factor. Since CQDs are water soluble we search for a water-soluble polymer and found that PVA is exactly apt for it. PVA is a non-toxic, comparatively low cost and optically transparent polymer which is easily soluble in water. So, we choose PVA as the polymer to mix CQD to form thin film.

We had synthesized CQD-PVA composite by mixing CQDs with 2wt% PVA solution. 2wt% PVA solution was prepared by mixing 0.2g PVA in 10ml distilled water and stirred for 45minutes using a magnetic stirrer at a temperature of 80^0C. Then the PVA solution were mixed with the CQDs in the ratio 3:1 by using a magnetic stirrer. The mixture was coated on a glass plate by using a spin coater with a spinning speed of 5000rpm. Then the film allowed to dry by using an oven. UV-Visible absorption and transmission studies of the prepared CQD-PVA film were carried out using Ocean Optics Maya 2000-Pro UV compact spectrometer, white light source and necessary optical fibres and lenses. Photoluminescence spectra of the CQD-PVA composite film was also obtained by exciting a laser of wavelength 450nm.

5.3 Result and Discussions

Highly photoluminescent, water soluble CQDs were prepared from 8% glucose solution by microwave heating of the solution for different time such as 5, 6, 7, 9, 11, 13 minutes. Fig. 5.4 represents the CQDs formed by microwave heating at different time. From the fig. 5.4 it is clear that the solution changed its colour from transparent to pale yellow and brown as a result of formation of CQDs. The size of the CQDs increased with increasing microwave heating time. We had repeated the experiment by changing the microwave heating time, power, source concentration and solution volume etc. and optimized synthesizing process flow and the parameters to get low cost, but high yield uniformly sized quantum dots. It was discovered that the growth of the CQDS were significantly influenced by experimental variables such as microwave power, heating time, source concentration, and solution volume etc. The synthesized CQDs had a uniform size distribution due to the simultaneous, homogeneous, fast heating provided by the microwave oven.

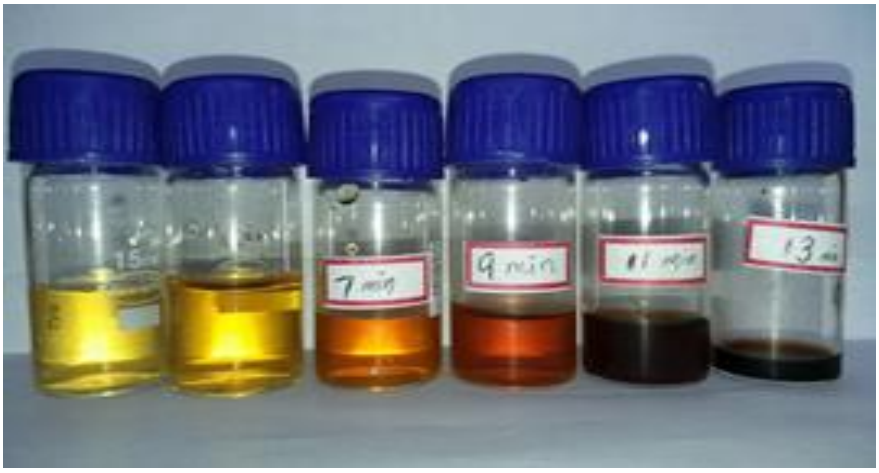

Fig. 5.4: CQDs formed by microwave heating at different time

The newly prepared CQDs under UV light is as shown in the fig. 5.5. The prepared CQDs were stable for at least six months in room temperature.

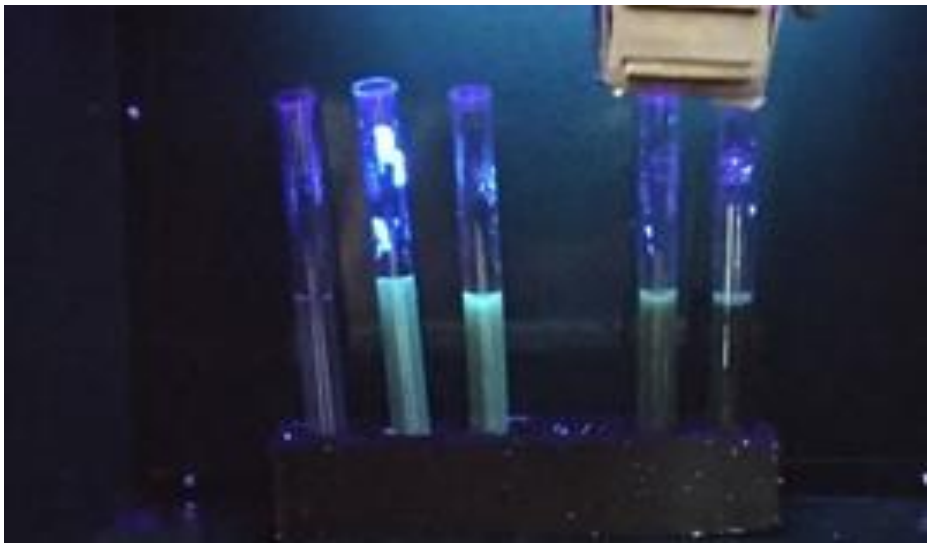

Fig. 5.5: CQDs illuminated by UV light

The photoluminescence of CQDs by two excitation wavelength 540nm and 450nm are presented in the fig. 5.6. From the photoluminescence spectra it is clear that emission wavelength of CQDs is independent of size of the CQDs. But the intensity of the emission that depends on the size of the CQDs. Also, CQDs can exhibit different emission colours when they are excited at different excitation wavelengths.

In contradictory to the other QDs, the size independent emission is a common phenomenon observed in many carbon based QDs and this unique optical properties of CQDs attributed to the self-passivated layer on the surface of CQDs. Different kinds of functional groups (C-OH, C-O-C, C-H etc.) are presented on the surface of the CQDs forming surface states. These functional groups have various energy levels which may result in a series of emissive traps. When a certain excitation wavelength illuminates CQDs, a surface state emissive trap will dominate the emission. As the excitation wavelength changes, another corresponding surface state emissive trap will become dominant. Since both the absorption and emission spectrum of the CQDs are independent of size, the emissive traps induced by the surface states of the functional groups should play an important role in the emission.

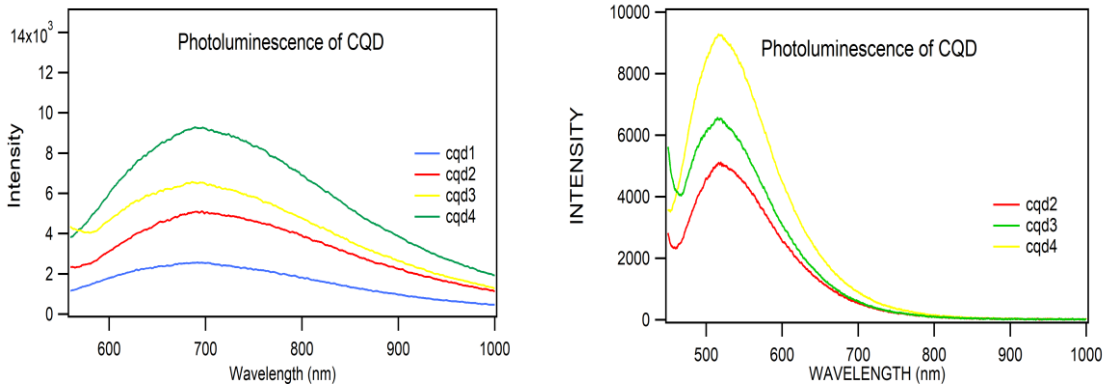

Fig. 5.6: Photoluminescence of CQDs with excitation wavelength of (i) 540 nm and (ii) 450nm

The photoluminescence of CQDs with excitation wavelength of 280nm is as shown in the fig. 5.7. Here also emission wavelength is independent of the size of the CQDs.

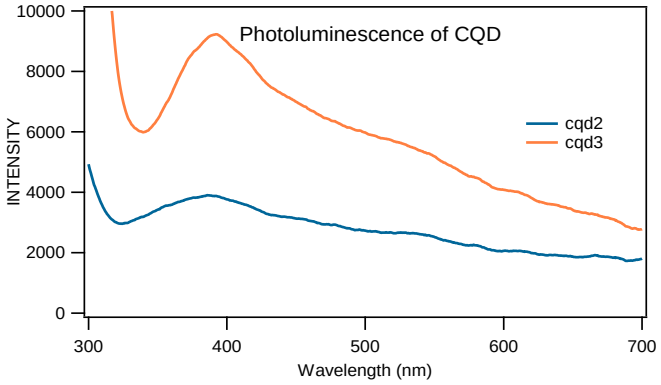

Fig. 5.7 **:** Photoluminescence of CQDs with excitation wavelength of 280nm

The absorption spectra of CQDs are as shown in the fig. 5.8. The transmission spectra of CQDs are also presented in the fig. 5.9.

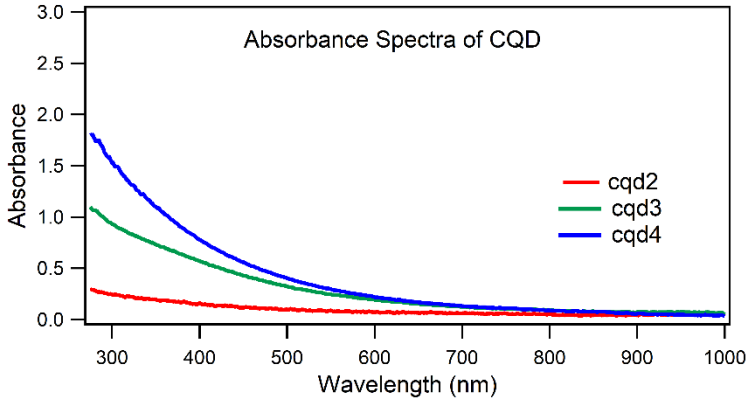

Fig. 5.8: Absorption spectra of CQD

From the transmission and absorption spectra, it is clear that CQDs show strong optical absorption in the UV region. ie. CQDs are effective photon-harvesting agents especially in short-wavelength region, due to the π-π* transition of C=C bonds. Also, the surface functional groups may also greatly contribute to the absorption at the UV-visible region.

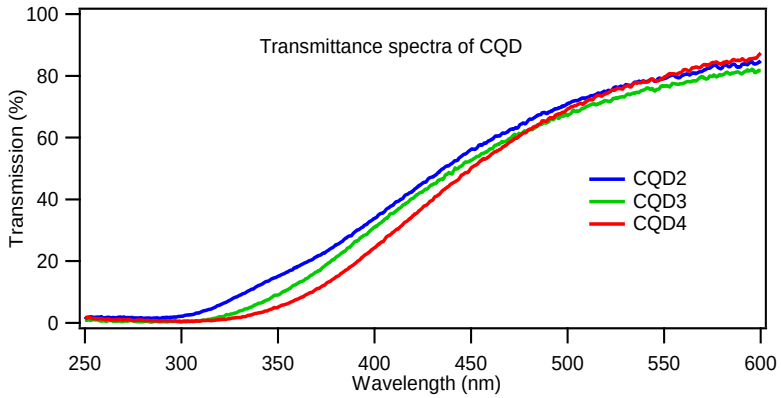

Fig. 5.9: Transmission spectra of CQD

We also attempted another method of preparing the CQDs by heating the glucose solution in an oven for 4 hours at 180^0C. 1g glucose powder was dissolved in 15ml distilled water to make the glucose solution. We obtained a brown suspension after filtering it with filter paper. The transmission spectra of the resultant CQDs are as shown in the fig. 5.10. Here the low transmission window is greater than the previously prepared CQDs. This may be due to the lack of proper filtering. If it was filtered by a track membrane there will be a better result.

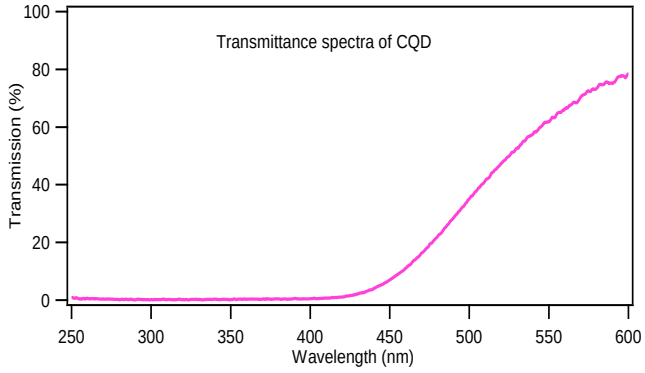

Fig. 5.10: Transmission spectra of CQDs prepared by heating in a oven

Fig. 5.11 shows the transmission electron microscopy (TEM) image of the monodispersed CQDs. From TEM images it is clear that quantum dots were formed with majority of QDs with sizes less than 10nm. So, it was realized that the synthesized quantum dots were Carbon quantum dots.

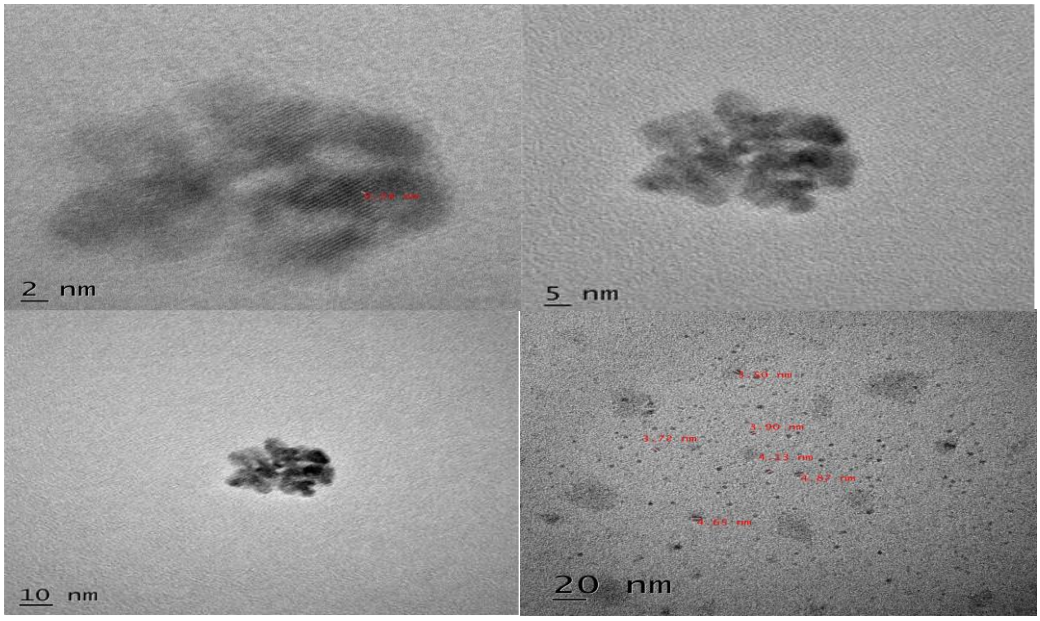

Fig. 5.11: Transmission electron microscopy image of the CQDs.

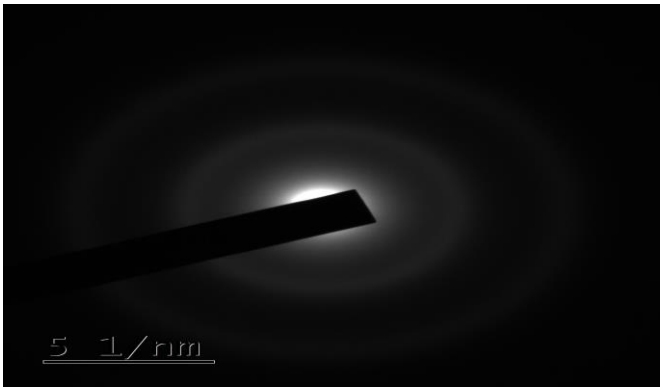

Fig. 5.12: The selected area electron diffraction (SAED) pattern of monodispersed CQDs

The selected area electron diffraction (SAED) pattern of monodispersed CQDs is as shown in the fig. 5.12. From the SAED pattern it is clear that CQDs have neither pure crystalline nor amorphous structure. But a structure intermediate between these two.

The synthesized highly luminescent carbon quantum dots were stable for at least three months at room temperature. The photoluminescent properties of the CQDs may be due to either bandgap transitions corresponding to conjugated p-domains (Aziz et al., 2019) or due to

the self passivated layer on the surface of the CQDs. (Tang et al., 2012) Also, the photoluminescent properties of the CQDs vary sharply with the size of the CQDs.

The synthesized CQDs didn't form into a thin film when coated on a glass substrate. After coating CQDs on a glass substrate and heated for a long time, the CQDs were found to be adhered to the glass substrate like a sticky gel. It was not dry even after being heated for a long time. If it is possible to make a thin film using CQDs, it will have variety of photonic and opto-electronic applications. On mixing CQDs with PVA, it can be possible to form a thin film by coating on the substrate. Since CQDs are water soluble, it can easily mix with PVA because PVA also a water-soluble polymer. PVA is non-toxic, comparatively low cost and optically transparent polymer. Also, all our works are related with PVA. So, we choose PVA as the polymer to mix CQD to form a thin film.

Transmission and absorption studies of the prepared CQD-PVA film was as shown in the fig. 5.13. The transmission and absorbance of the CQD-PVA film are in line with the CQD in solution form.

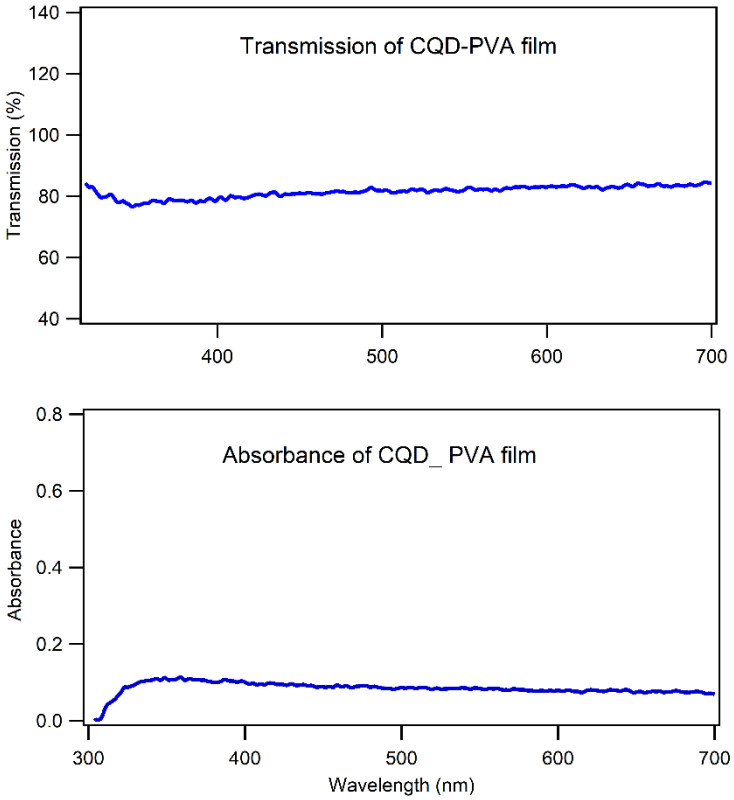

Fig. 5.13: Transmission and absorbance of CQD-PVA film

The transmission and absorbance spectra of the CQD-PVA composite when taken from a cuvette was as shown in the fig. 5.14. As compared to pure CQDs, transmission was decreased and absorption was increased. This may be due to the presence of PVA in the bulk composite form.

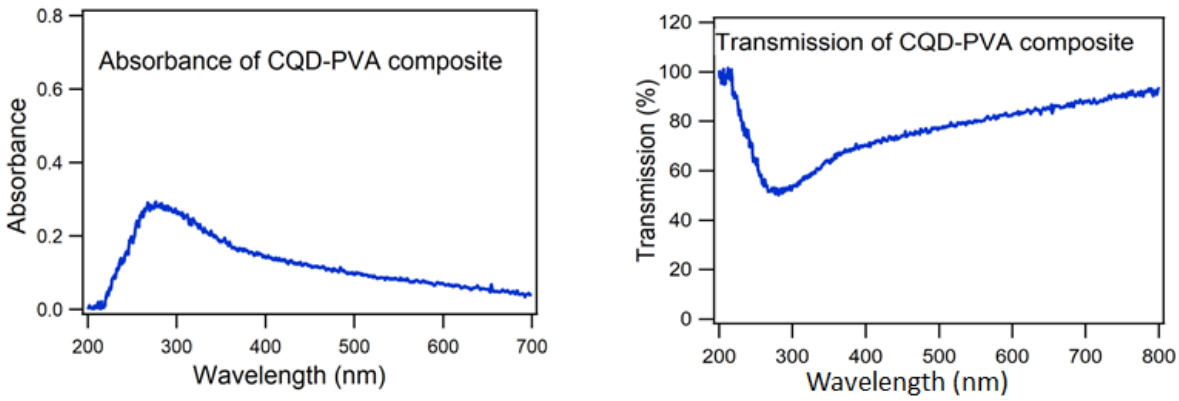

Fig. 5.14: Transmission and absorbance of CQD-PVA composite

The photoluminescence spectra of CQD-PVA nano composite film excited by a laser of 540nm is presented in the fig. 5.15. In the photoluminescence spectra the peak emission was observed at 700nm. So, this photoluminescence spectra are also consistent with the spectra of CQD in solution form.

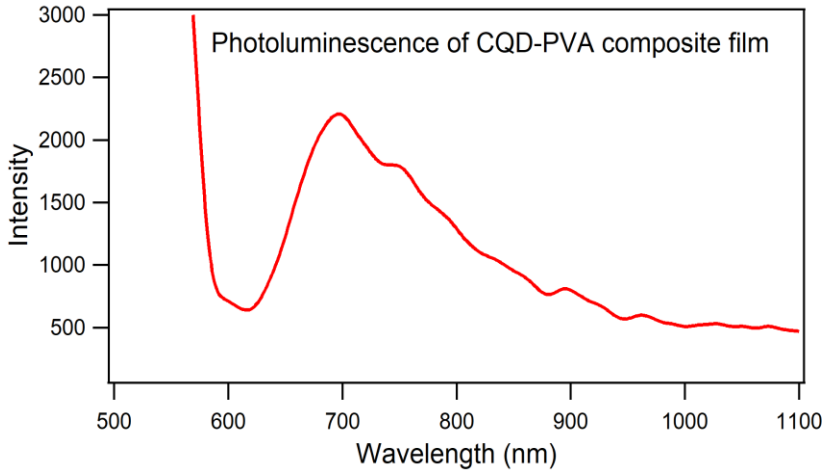

Fig. 5.15: Transmission and absorbance of CQD-PVA composite

5.4 Conclusions

In this chapter, we had synthesized highly photoluminescent, eco-friendly carbon quantum dots from naturally occurred D-Glucose by microwave assisted hydrothermal method. From the photoluminescence spectra of CQDs, with different excitation wavelength of 280nm 450nm and 540nm, it is obvious that emission wavelength of CQDs were independent of size of the CQDs. But the intensity of emission depends on the size of the CQDs. Also, CQDs can exhibit different emission colours when they were excited at different excitation wavelengths. From the absorption and transmission spectra, it is clear that CQDs show strong optical absorption in the UV region. ie. CQDs are effective photon-harvesting agents especially in short-wavelength region, due to the π-π* transition of C═C bonds. Also, the surface functional groups may also greatly contribute to the absorption at the UV-visible region. From TEM images it is clear that the synthesized quantum dots were uniformly sized. For film formation, CQDs were mixed with PVA and coated on glass substrate. The obtained CQD-PVA composite film were also emitted light around 700nm when excited by a wavelength of 540nm. The emission spectra of CQD-PVA nano composite film was also consistent with the spectra of CQD in solution form.

Chapter -6

Surface Plasmon Coupled Emission by Active Optical Components

Surface Plasmon Coupled Emission by Active Optical Components

In the previous chapter, we had described the synthesizing method of highly photoluminescent carbon quantum dots by microwave assisted hydrothermal method. Transmission, absorbance and photoluminescence studies of the synthesized CQDs had done. These quantum dots must be converted into thin films for use in photonic and opto-electronic applications. In order to form a thin film of CQDs, we had mixed CQDs with PVA and CQD-PVA nano composite thin film had done. Now in this chapter, we had studied the light matter interactions or energy transfer mechanism by incorporating an emitting material with multilayers. We performed surface plasmon coupled emission experiments with multilayers containing the active optical components and discovered the effect of PMMA on surface plasmon coupled emission tuning. Thus, the potential applications of the previously fabricated structures explored for the photonic applications.

6.1 Introduction and Motivation

During the last decade, surface plasmon resonance applied sensing devices have an important growth in photonic and biomedical applications. Surface plasmon resonance is a promising technique and now a days, surface plasmon resonance (SPR) and surface plasmon coupled emission (SPCE) are widely used in the field of biosciences and material sciences. Both the SPR and SPCE depends on the unique optical conditions that leads to the surface plasmon modes. (I. Gryczynski et al., 2004a)

SPR is the resonant oscillations of conduction electrons at the interface between metal and a dielectric material stimulated by incident light. Typical metals that support surface plasmons are silver and gold; but metals such as Cu, Sn, Cr etc have also been used. (Amendola et al., 2017) For SPR to occur the incoming radiations has to match its momentum to that of plasmon, and when it is happened, the intensity of the reflected light decreases sharply. (Jiang et al., 2018) The merging of two rapidly expanding research areas

fluorescence and plasmonic, gave rise to the surface plasmon–coupled emission (SPCE). In SPCE, the excited fluorophores interact with the surface plasmons on a thin metal film. (Lakowicz et al., 2006) The sensitivity of this approach can be substantially improved with good collecting efficiency owing to the directional emission.

SPR occurs when a monochromatic light is incident on a thin metal film through a prism of moderate refractive index such as glass. As the angle of incidence is gradually increased, a total internal reflection takes place at the prism interface. So, we expect high reflectivity for incident angles above total internal reflection. But, due to the evanescent waves, free electrons within the metal oscillate generating surface plasmons. When the angle of incidence (θ_I) matches with the SPR angle (θ_{SP}), incident light gets absorbed by the surface plasmon for a small range of angles around θ_{SP}. These kinds of absorption occur when the momentum of the incident light through the prism matches with the momentum of the surface plasmon. (I. Gryczynski et al., 2004b) The momentum matching has to occur for the in-plane component of the incident wave vector. So, p-polarized light with a perpendicular electric field can excite surface plasmons. (Holman et al., 2013)

Theoretically, SPR phenomena would not have appeared if the hemicylindrical prism had not been there. Because the wave vector of surface plasmons (k_{sp}) propagating through the interface, is often less than the wave vector of light in free space (k_0). It was necessary to match the wave vector or increase k_0 by using a material with a higher refractive index, usually a glass prism. (Lakowicz, 2004) In these circumstances a hemicylindrical glass prism was used and SPR is not achievable without a glass prism.

The wave vectors, of the incident light in-plane of the metal dielectric interface (k_x) and the surface plasmon (k_{sp}), are given by

$$k_x = \frac{2\pi}{\lambda} n_p \sin\theta_I$$

and

$$k_{sp} = \frac{2\pi}{\lambda} \sqrt{\frac{n_m^2 \, n_s^2}{n_m^2 + n_s^2}}$$

Where n_p is the refractive index of the prism and n_m and n_s are refractive index of the metal and the effective refractive index of the metal dielectric interface respectively. The condition for SPR absorption to occur is when the light wave vector equals surface plasmon wave vector (Kurihara and Suzuki, 2002) as given by

$$k_x = k_{sp} = \frac{2\pi}{\lambda} n_p \sin\theta_{sp}$$

and

$$\theta_{sp} = \sin^{-1}\left(\frac{1}{np}\sqrt{\frac{n_m^2 n_s^2}{n_m^2 + n_s^2}}\right)$$

Where θ_{SP} is surface plasmon resonance angle.

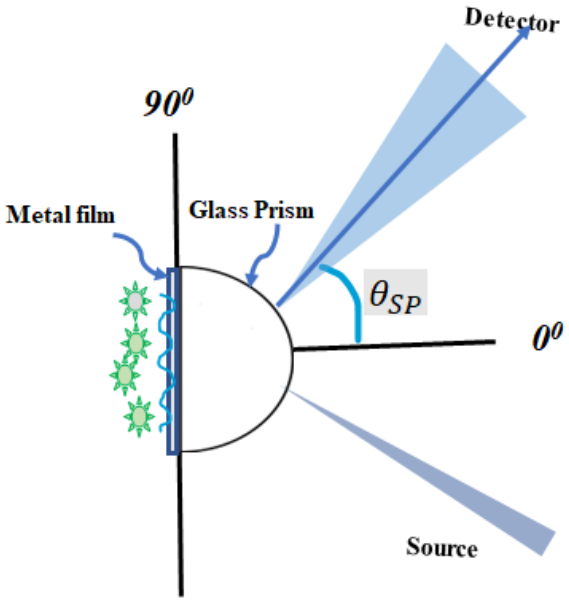

Fig. 6.1: Representation of SPR Phenomenon

The resonance condition is achieved by tuning the angle of the incident light, θ_I. The angle required for the resonance, θ_{SP}, is related to n_p, n_m and n_s. So, the minimum reflectivity angle θ_{SP} is highly sensitive to the refractive index of the medium. Adsorption and desorption on the metal surface changes the effective refractive index of the metal–dielectric interface and hence the resonance angle. Therefore, monitoring of the θ_{SP} change can be used to analyse the adsorption– desorption or association–dissociation activities that take place on the metal surface. (Damos et al., 2005) Fig. 6.1 shows geometrical representation of SPR phenomenon at the metal surface. SPR sensing method is widely used in the studies on interaction between biological molecules, detection of lipid bilayer membranes, studying the hybridization and adsorption of DNA, etc. (Phillips and Cheng, 2007)

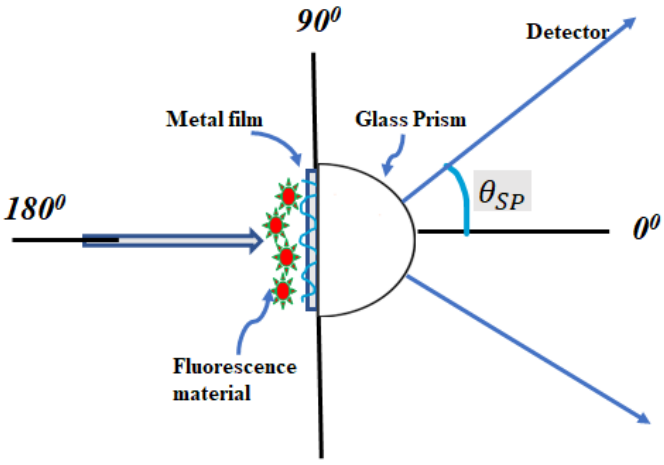

Fig. 6.2 Experimentation geometry for SPCE

The SPCE phenomenon is the consequence of the near-field interaction of fluorophores with the surface plasmons that provides a new pathway for creation of far-field radiation. (Lakowicz et al., 2008) Within the near-field distance, the fluorophores can experience the energy field, and the excited state fluorophore strongly couple with the surface plasmons,

thereby releasing energy as radiation from the prism. This is possible only when the wave-vector was matching. (Knoblauch and Geddes, 2019) The surface plasmons can radiate into the substrate at definite angles with fascinating polarization properties. (Lakowicz, 2004) The interactions of the fluorophores with the metal film result into steered emission. The resulting SPCE is highly directional and steered either back into the substrate or into the sample media, depending on the optical system. (Dutta Choudhury et al., 2015) The experimentation geometry for SPCE is presented in the fig. 6.2. These steering of the optical energy from fluorophores can be applied in many devices for fluorescence sensing. These properties can apply in a wide range of simple, inexpensive, and robust devices in biology and medicine. (Dutta Choudhury et al., 2015)

SPR and SPCE has to be consider as two entities and studied and analysed separately. The SPR provides a simple and instinctive approach to understanding SPCE. SPR methods give a qualitative idea about the presence of the molecules and is a convenient detection method, but gives poor quantitative features. On the other hand, SPCE methods focused on fluorescence enhancement, control, steering and directionality based on Reverse-Kretschmann (RK) configuration. SPCE depends on interactions of the excited fluorophore with the metal surface. The interaction may be independent of the mode of excitation; that is, it does not require evanescent wave or surface-plasmon excitation. SPR is the angle-dependent absorption of thin metal films where as SPCE is the inverse process of the SPR absorption of thin metal films. SPCE occurs over a narrow angular distribution, converting normally isotropic emission into easily collected directional emission. (Johansen et al., 2000; Lakowicz, 2004) Also, experimental studies showed that optical excitation is not essential for directional emission. SPCE can also be applied to chemiluminescent and electro-chemiluminescent species. (Solaimuthu et al., 2020) Again, directional emission has also been observed as forms of phosphorescence and two-photon excited fluorescence. (Cao et al., 2012)

One of the most popular methods in biological sciences, biotechnology, and medical diagnostics is fluorescence detection. Fluorescence has an important role in gene expression, biotechnology, sensing and medical diagnostics among other applications. The SPR technique in association with fluorescence technology can reveal several characteristics of the biological system. (Jans and Huo, 2012) By employing wavevector matching at the metal surfaces, the typical omnidirectional fluorescence can be changed into directional emission.

Now the interaction of fluorophores with metals is an active area of research. (Badugu et al., 2013)

But, studies on fluorescence control were limited to emission properties and its steering and hence a proper understanding on the correlation of SPR and SPCE is lacking. The present work demonstrates a method to couple surface plasmon resonance phenomenon to the fluorescence to tune the fluorescence emission. We had made an effort to correlate the measured Plasmon Coupled Emission Tuning with the standard SPR. This novel setup could open up a new perspective towards the understanding of detection, kinetics and dynamics of bio molecules.

In this work, we had demonstrated the surface plasmon coupled fluorescence emission tuning and directionality in metal dielectric multilayered structures in reverse Kretschman configurations. The setup contained a metal-dielectric layered structure coupled to a hemicylindrical prism in a Reverse Kretschmann (RK) configuration. By introducing a small coating of Poly Methyl Methacrylate (PMMA) polymer before and after the fluorescein material, we were able to compare the impact of PMMA layer on plasmon coupled emission tuning.

6.2 Materials and Methods:

Silver (Ag) films of thickness ~45nm were deposited on clean glass slides by thermal vapour deposition method by maintaining a vaccum of $5x10^{-5}$ mbar. The deposition rate was maintained at ~10 Å/s. Poly Vinyl Alcohol (PVA)-Fluorescin (PVAF) composite thin films were prepared by the following procedure. 2wt% solution of PVA (from Sigma Aldrich) was first prepared by dissolving appropriate quantity of PVA in distilled water and on constant stirring for 45min. Temperature was maintained at ~80 ^{0}C during stirring. Fluorescein(FL) solution was prepared by dissolving 0.5wt% of Fluorescein (from Sigma Aldrich) in isopropyl alcohol. The prepared PVA and FL solutions were then mixed at a ratio 100:1 to get PVAF solution. PVAF solution was then spin coated on top of silver film at 5000 rpm and dwelling time of 2 min to get a thickness of ~80nm. The layered structure Ag/PVAF thus obtained was named as Metal-Fluorescin (MF). 0.5wt% PMMA (purchased from Alfa Aesar) solution was prepared by dissolving 0.05g PMMA in 10ml toluene and spin coated at 5000 rpm and dwelling time of 2 min to get a thickness of 38nm. To study the influence of polymer on PCET, PMMA layer was coated as a buffer layer between Ag and PVAF with a spinning speed of 5000rpm. PMMA was also coated on top of Ag/PVAF

structure with the same spinning speed 5000rpm. The samples were named as Metal/PMMA/Fluorescin (MPF) and Metal/Fluorescin/PMMA (MFP) respectively. In fig. 6.3, the three samples are schematically represented.

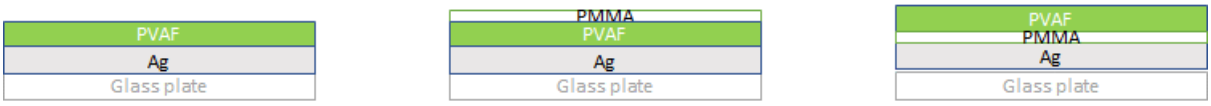

(a) (b) (c)

Fig. 6.3: Representation of the three sample (a) MF (b)MFP and (c)MPF

So, we had prepared three samples. (1) Ag/PVAF (Metal/Fluorescein- MF) – Thin films of a mixture of Polyvinyl alcohol (PVA) and flurescent material, (PVAF) were deposted on the silver film. (2)Ag/PVAF/PMMA (Metal/Fluorescein/PMMA- MFP) – Thin films of PVAF were coated on the silver film and Polymethyl Methacrylate (PMMA) were coated on the PVAF film and (3) Ag/PMMA/PVAF ((Metal/PMMA/Fluorescein- MPF)- Again thin films of two layers, first PMMA and then PVAF were coated on the silver. On multi layer fabrication with PMMA we found the effect of PMMA on surface plasmon coupled emission tuning.

Schematic of the experimental setup to study surface plasmon coupled emission tuning is presented in fig. 6.4. The sample was coupled to a hemi cylindrical prism (n=1.5) by using glycerine (index-matching liquid to maintain the optical index continuity between the prism and the glass substrate) as the coupling agent. A diode laser of wavelength λ=450nm was allowed to fall normally to the sample to excite the fluorescein molecules within the PVA matrix and the emission studies were done by Reverse Kretschmann configuration (RK). The collection optics were mounted on a rotational platform to record the emission spectra at different angles ranging from 20^0 to 90^0 with an interval of 1^0. The direction opposite to the excitation laser was taken as the reference angle (0^0). The emitted light was fed to a high sensitivity spectrometer (Ocean Optics; Model: Maya2000Pro) through optical fibres. Ocean optics Spectra Suite software was used to control and collect the emission spectra from the spectrometer.

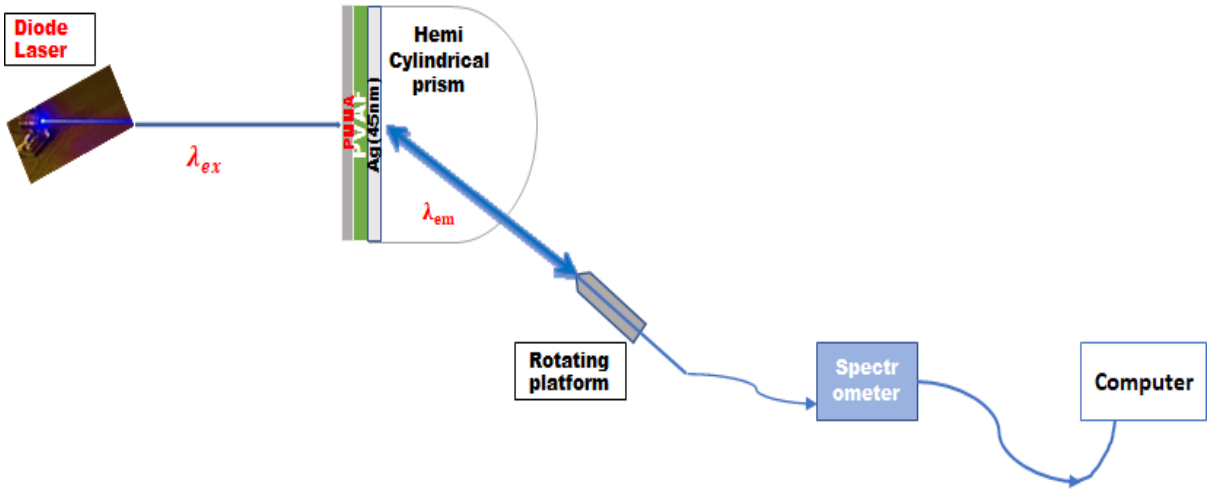

Fig. 6.4: Schematic of the experimental setup for surface plasmon coupled emission tuning

Thin films were deposited on the metal film by a spin coater (Apex instruments spinNXG-P1). The UV-Visible transmission studies were carried out using Ocean Optics Maya 2000-Pro UV compact spectrometer, white light source and necessary optical fibres and lenses. The thickness of the deposited film was estimated by comparing the transmission spectra with transfer matrix model simulations. For modelling the SPR for more than one layer, we can choose transfer matrix model simulations (TMM) or other commercial software. For the present work we have used WINSPALL software (version 3.02) to simulate SPR curves of all the three samples, MF, MFP and MPF.

Furthermore, we had spin coated a CQD-PVA nano composite film on the metal (Ag) film and the light matter interactions of the CQD-PVA nano composite film had done. For this on a glass substrate, a silver film of thickness 45nm was coated by physical vapour deposition method. Then the CQD-PVA composite was coated on the top of Ag film by a spin coater at a spinning speed of 5000rpm. The substrate with the sample attached to a hemi-cylindrical glass prim by using glycerol as the momentum matching liquid. The sample was excited by a laser source of excitation wavelength 450nm in reverse Kretschmann configuration. The CQDs absorb the excitation energy and emit wavelengths near to 700nm. The angle tuned emission spectra of the sample were recorded from 10^{o} to 70^{o} with an interval of 1^{0}. The direction normal to the substrate from the prism side was taken as the reference direction (0^{0}). All the collected spectra were then combined and plot an image with wavelength along x-axis, angle along y-axis and the emission intensity as colour map.

6.3 Results and Discussions

The transmission spectra of the Ag film, Ag/PVAF and Ag/PVAF/PMMA film were presented as fig. 6.5(a), 6.5(b) and 6.5(c) respectively. The thickness of the deposited film was estimated by fitting transmission spectra with the transfer matrix model simulations. The simulation spectra were also presented in the fig. 6.5.

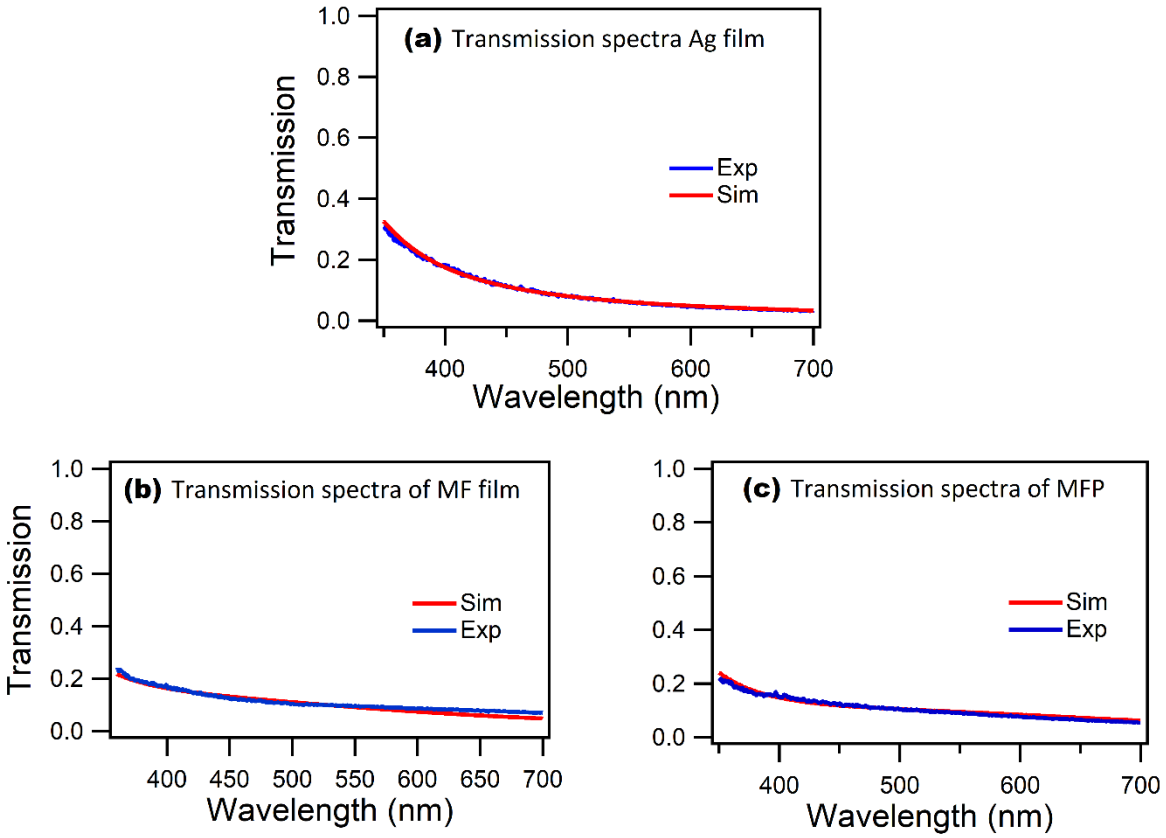

Fig. 6.5: Transmission spectra of (a)Ag film (b)Ag/PVAF (c) Ag/PVAF/PMMA

On comparing the transmission and the simulation spectra by TMM simulations, the thickness of Ag film was found to be 45nm, PVA film was found to be 80nm and PMMA film was found to be 35nm. Since we just added one or two drops of fluorescein solution to PVA (in a ratio of 1:100) while making the fluorescein mixed PVA solution, we solely focused on PVA when optimising thickness of PVAF film. Similarly, the transmission and the simulation spectra of the (a) Ag (b) Ag/PMMA(MP) and (c) Ag/PMMA/PVAF (MPF) film are presented in fig. 6.6.

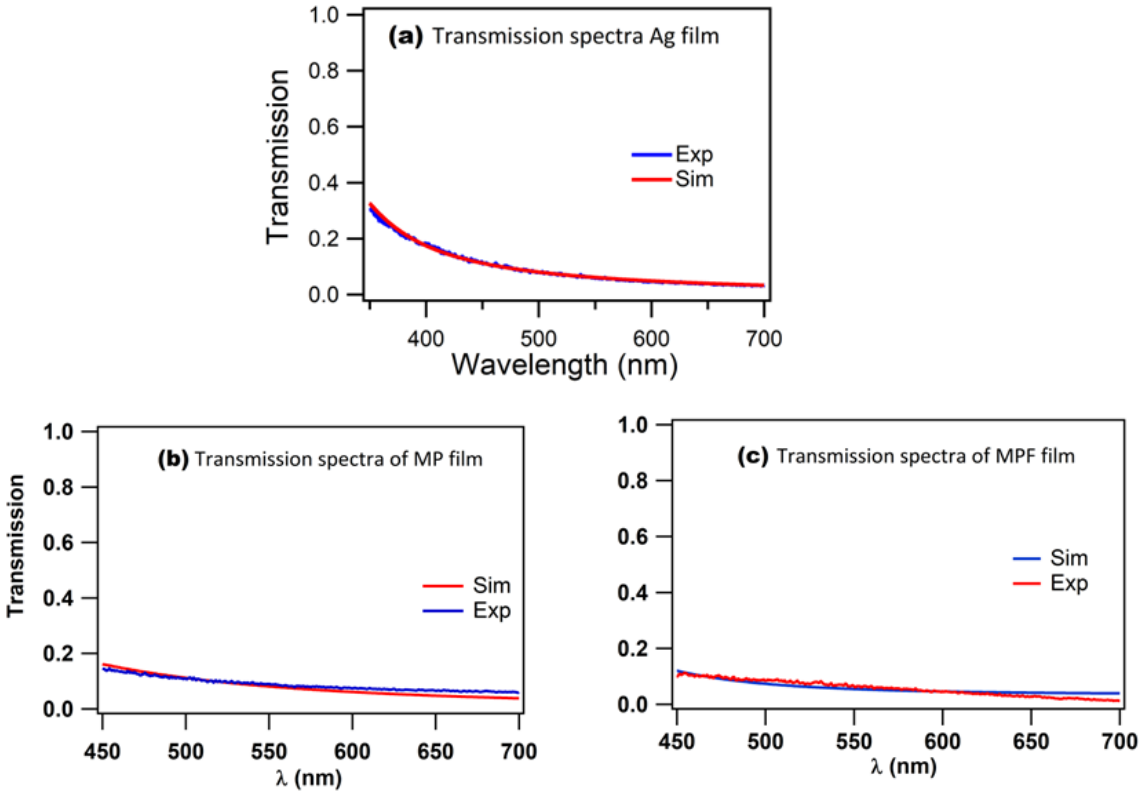

Fig. 6.6: Transmission spectra of (a)Ag film (b)Ag/PMMA(c) Ag/ PMMA/PVAF

Here also, on comparing the transmission and the simulation spectra by TMM simulations, the thickness of Ag film was found to be 45nm, PMMA film was found to be 35nm and PVA film was found to be 80nm resprctively. We had examined the surface plasmon coupled emission tuning using these multi-layered dielectric structures in reverse Kretschmann configuration and discovered the impact of PMMA film on SPCE tuning.

Now the three samples MF, MFP and MPF were excited with the excitation wavelength of λ_{ex} -450 nm in Reverse-Kretschmann configuration as shown in fig. 6.4. The fluorescein molecules absorb light energy from the laser source and emit radiations in the wavelengths between 500nm and 650nm. This is because the free spectral emission wavelength of fluorescein is from 500nm to 650nm. The emission spectra were collected in a rotational platform by the optical fibres and recorded by a high sensitivity spectrometer. The angle tuned emission spectra were recorded from 20^0 to 90^0 with an interval of 1^0. The direction normal to the substrate from the prism side was taken as the reference direction.

Ocean Optics Spectra Suit software was used to collect and control the emission spectra. For a particular sample, all the collected spectra were then combined to plot an image with wavelength along x-axis, angle along y-axis and the fluorescence intensity as colour map. Image plots of the samples MF is presented in fig. 6.7.

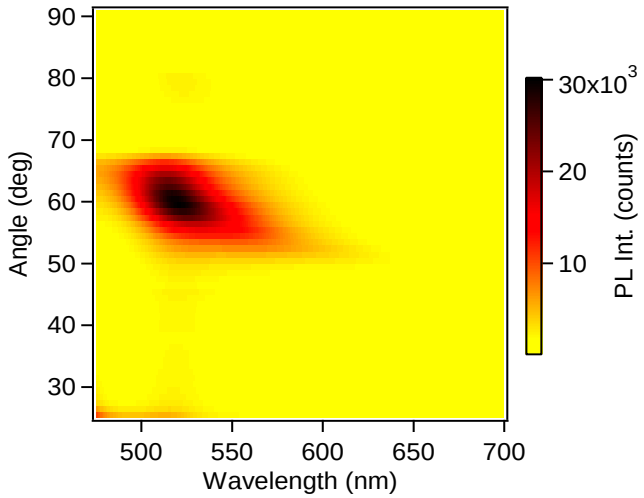

Fig. 6.7: Image plots of the sample MF

From the image plots it was clear that emission was not observed at all angles but was observed in an angular range 52^0 to 67^o. The angle tuned emission spectra that was also presented in the fig. 6.8. It is obvious from the angle tuned emission spectra that tuning observed in the emission spectra.

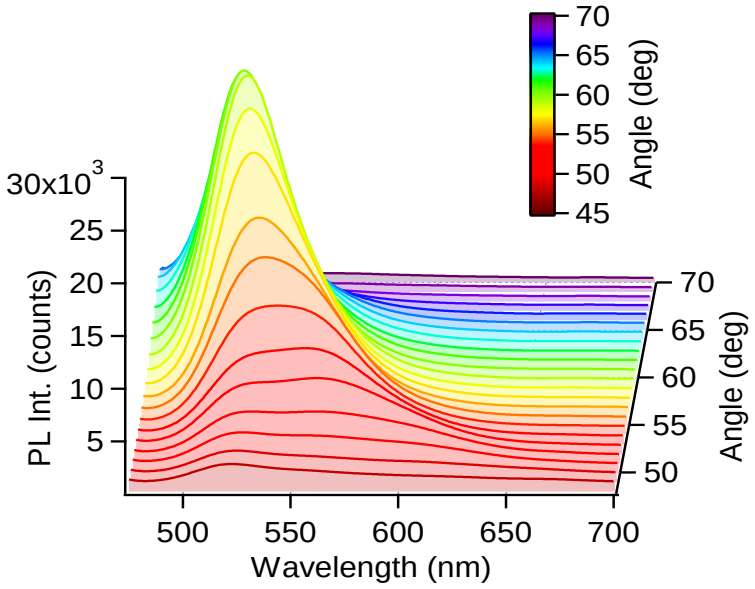

Fig. 6.8: The angle tuned emission spectra of the sample MF

Using WINSPALL software, the SPR curves were simulated for the sample Ag/PVAF multilayer system. In simulations, PVAF layer was replaced by PVA layer of equivalent thickness. i.e. Refractive index of PVA was used in the simulations. Thus, the SPR reflection curves were simulated using WINSPALL software by providing appropriate refractive indices for Ag and PVA layers. The simulation spectra for the sample Ag/PVAF were presented in the fig. 6.9. From the fig.6.9, as the angle tuned from 52^0 to 64^0 wavelength changed from 580nm to 519nm. This simulation results were exactly matched with the experimental results. Fig. 6.10 shows the experimental emission spectra exactly consistent with the simulation spectra by WINSPALL software.

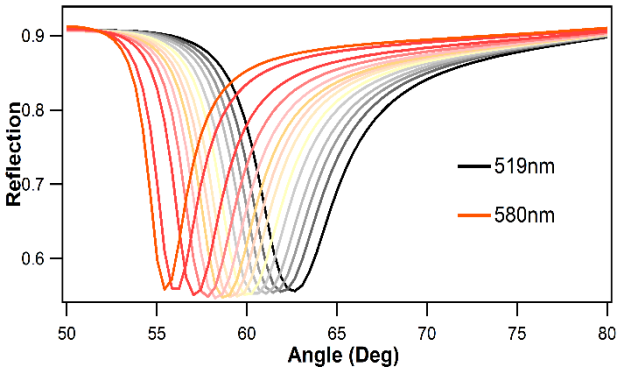

Fig. 6.9: SPR curves simulated by Winspall software for the sample MF

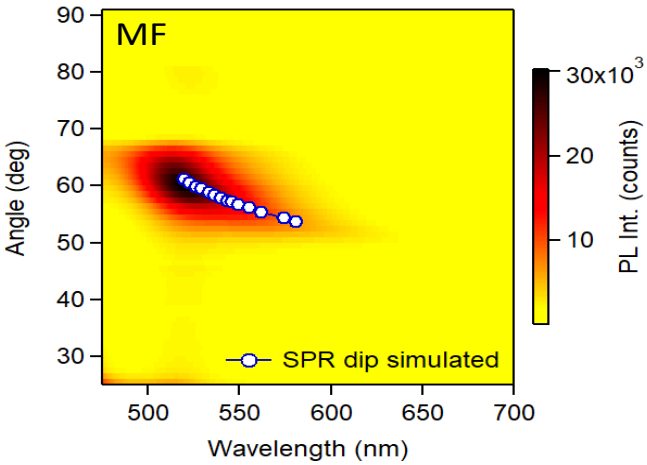

Fig. 6.10: Experimental emission spectra coincide with the SPR curves simulated by Winspall software fo the sample MF

The emission angle was consistent with the surface plasmon angle calculated by using WINSPALL software for the emission wavelength. When the incident angle (θ_I) matches with the SPR angle (θ_{SP}), incident light gets absorbed by the surface plasmons for a small range of angles around θ_{SP}. Absorption by surface plasmons at Ag/PVAF interface occurs when the momentum of the incident light through the prism matches the momentum of the surface plasmon.

The observed emission tuning could be explained from the experimental and simulation results. Within the near field distance, the excited fluorescein molecule can experience the energy field and the excited state fluorophore strongly couple with the surface plasmon and thereby releasing energy as radiation from the prism. This is possible only when the wave vector was matching. i.e., when the momentum matching conditions are satisfied, the surface plasmon will absorb these radiations and reflectivity minimum will be observed

at these angles and the emission observed in the angular range 52^0 to 64^0. If the fluorophore having emission wavelength λ, is placed near the metal film, it emit radiations through the substrate at the surface plasmon angle θ_{sp}, at the wavelength λ, due to the near-field coupling of the emission with the surface plasmon mode. i.e., The emission of the fluorophore is coupled to the reflectivity dip due to the SPR at θ_{sp}. Because the excited fluorescein molecules emit light from 500nm to 640nm, when the momentum matching conditions are satisfied, surface plasmons will absorb these radiations and a reflectivity minimum will be observed at these angles. For the sample MF, the emission was observed from 520nm to 600nm when angle varied from 52^o to 64^o. So, the tuning was due to surface plasmon coupled emission. The line profile in the emission spectra showed that the emission might be from two or more types of fluorescein molecules. The experimental results were exactly matched with the simulation results. As the angle was increased the peak emission wavelength shift towards lower wavelength region (tuned emission). The emitted light was highly directional and so, the coupling of fluorescence emission with the surface plasmons are useful to steer the direction of emission.

This plasmon coupled fluorescence tuning depends on a lot parameters such as thickness of the metal, distance between the fluorophores and the metal surface, orientation of the fluorophores and refractive index of the prism etc. The thickness of metal and the dielectric layer can be optimised according to the spectral range of the fluorophore. Depending on the thicknesses of the dielectric layer and the optical properties of the metals, the fluorescence emission can be tuned to certain wavelength. In RK configuration, as the light incident on the sample the Fluorescein molecules within PVA excited uniformly across the thickness and emit wavelengths in the range 500nm to 640 nm. But only those molecules placed at a certain distance from the metal surface and have specific orientations will coupled to the metal surface and produce plasmon coupled emission tuning. Hence, by using surface plasmon resonance-based emission we can tune the emission wavelengths.

It was discovered that when sample thickness increases, the number of surface plasmon modes also does. According to earlier reports, samples with a thickness of less than 140 nm only displayed one SPR mode. Since the PVAF layer was 80 nm thick, the sample Ag/PVAF only displayed one surface plasmon mode. Here the free spectral emission wave length of fluorescein ranges from 500nm to 640nm. To achieve a broad range of PCFE tuning, we must employ an emitting material with a broad emission range.

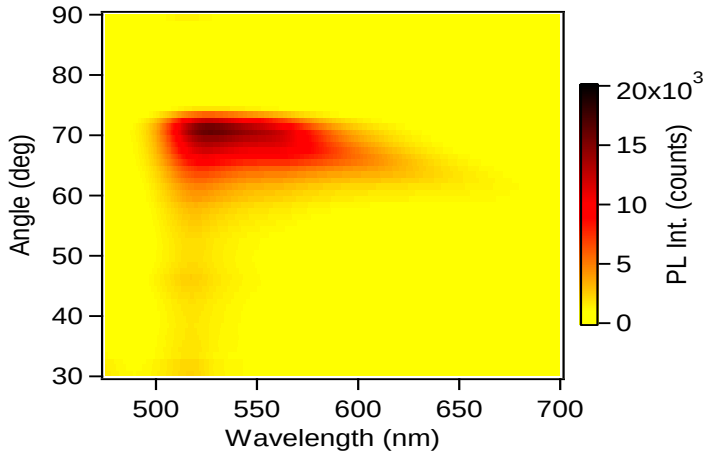

Fig. 6.11: Image plots of the sample MFP

The same phenomena -PCFE tuning and directionality- was again appeared for the second sample Ag/PVAF/PMMA. Similar to Ag/PVAF, for the sample Ag/PVAF/PMMA, the emission was tuned from 560nm to 630nm when the angle ranged from 60^0 to 72^0. Here also, when the momentum matching conditions are satisfied, the excited fluorescein molecules coupled with the surface plasmon and emission observed in the angular range 60^0 to 72^0. In addition to this tuning, at the angle 70^0 a directionality also observed. This is due to the uncoupled emission of the fluorescein molecule in the PVA matrix. So, after adding a PMMA layer above the metal- fluorescein layer, a tuning–directionality duality was observed. This is due to coupled and uncoupled emission of fluorescein molecules on the metal surface. The image plots of the sample Ag/PVAF/PMMA is presented in the fig. 6.11. Fig. 6.12 shows the angle tuned emission spectra of the sample Ag/PVAF/PMMA.

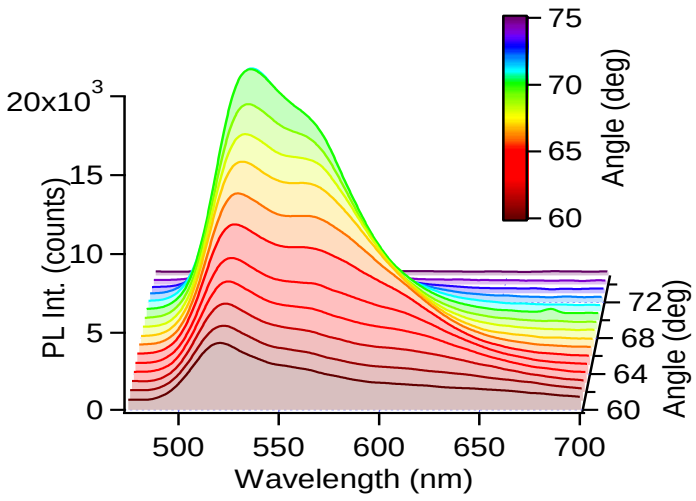

Fig. 6.12: Angled tuned emission spectra of the sample

Using WINSPALL software, the SPR curves were simulated for the sample Ag/PVAF/PMMA multilayer system. The SPR reflection curves simulated using WINSPALL software for the sample Ag/PVAF/PMMA is presented in the fig. 6.13. From the fig. 6.13, it was clear that as the angle tuned from 65^0 to 74^0, the wavelength changed from 615nm to 560nm. The observed SPR reflection dip matches well with the experimental results. Fig. 6.14 shows the experimental emission spectra exactly consistent with the simulation spectra by WINSPALL software. This surface plasmons coupled emission tuning occur only when the momentum of the incident light through the prism matches the momentum of the surface plasmon. So, this study can be applied in the sensor applications. On coating a layer of biomaterial above the Ag-Fluorescein layer, and the emission studies gives the characteristic properties of that material.

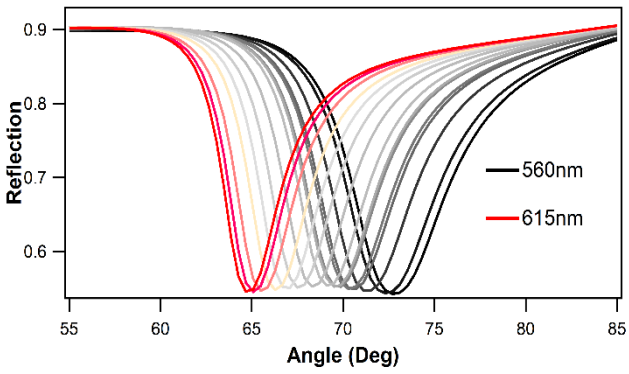

Fig. 6.13: SPR curves simulated by Winspall software for the sample MFP

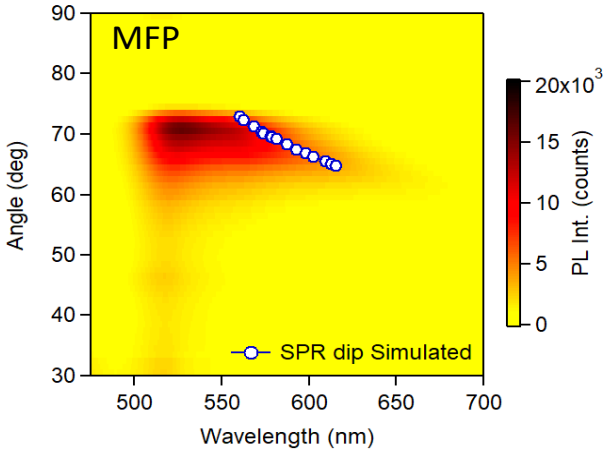

Fig. 6.14: Experimental emission spectra consistent with the SPR curves simulated by Winspall software for the sample MFP

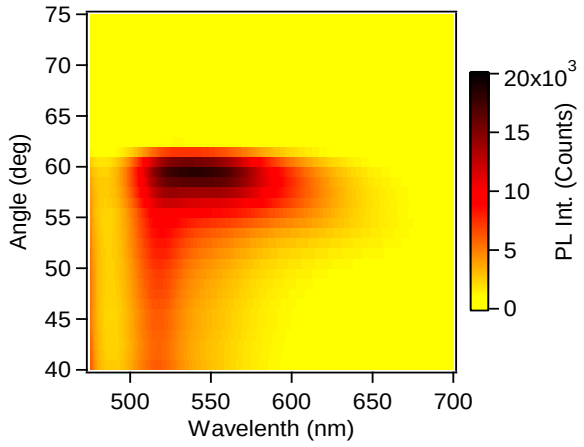

Fig. 6.15: Image plots for the sample MPF

But in the third sample Ag/PMMA/PVAF no tuning was observed. Fig. 6.15 shows the image plots and fig. 6.16 shows the angle tuned emission spectra for the sample Ag/PMMA/PVAF and from it is clear that no tuning was observed.

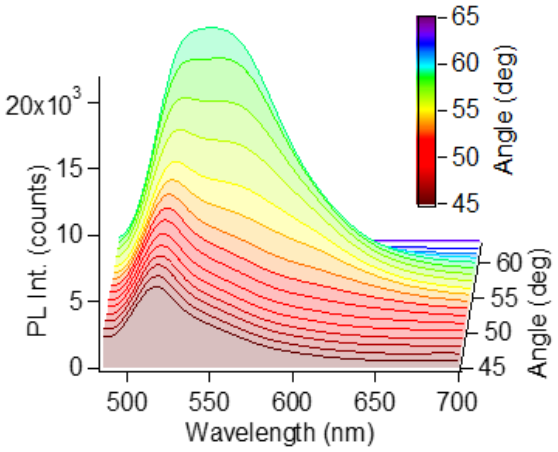

Fig. 6.16: Angle tuned emission spectra for the sample MPF

So, on coating PMMA layer of thickness 35nm between Ag and PVAF, the interaction between fluorescein molecule and the surface plasmon become weak. Thus PMMA molecule decoupling the fluorophore and surface plasmon. So, the tuning was disappeared. Even though directionality were appeared. This is due to the uncoupled emission of the fluorescein molecules. So by introducing PMMA, the near field coupling effect of the fluorescein molecule with the surface plasmon had gone and the tuning was disappeared. This experiment confirmed that tuning was due to surface plasmon coupled emission. Since in the third sample no tuning was observed, we consider only first and second sample for the simulations.

Now for the first and second sample, MF and MFP, the emission tuning were observed above 540nm. Based on the literature, the fluorescein molecule has three structures or configurations with peak emission wavelengths of 520nm, 540nm, and 560nm. So, for the two samples Ag/PVAF and Ag/PVAF/PMMA, we multi-peak fitted the emission peak with the wavelength of the fluorescein molecule with the corresponding angle. Fig. 6.17(a) and 6.17(b) represents the curve fitted samples at the angle 52^0 and 53^0 for the emission peak of fluorescein with wavelength for the sample MF. We had curve fitted at all angles from 52^0 and 64^0 for the samples MF. However, just two examples are presented here.

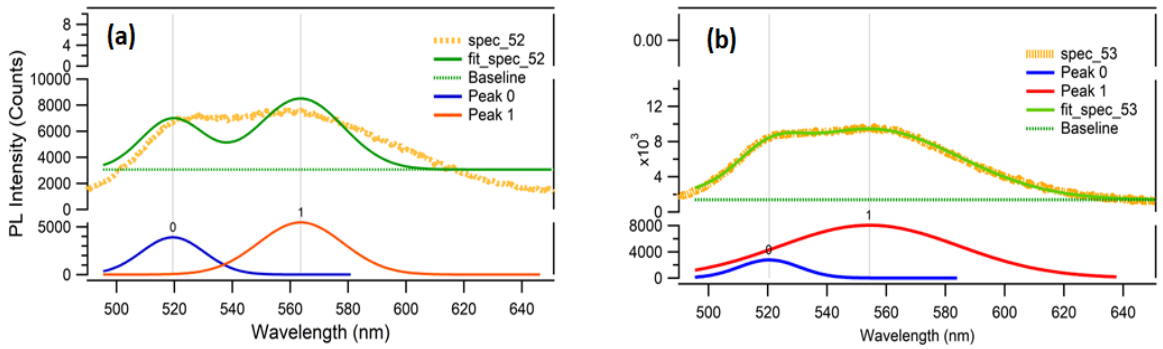

Fig. 6.17: Sample of curve fitted emission peak wavelength for the sample MF

In a similar way, we had curve fitted the emission peak from 64^0 and 72^0 for the second sample MFP also. Two plots are presented in the fig. 6.18 below.

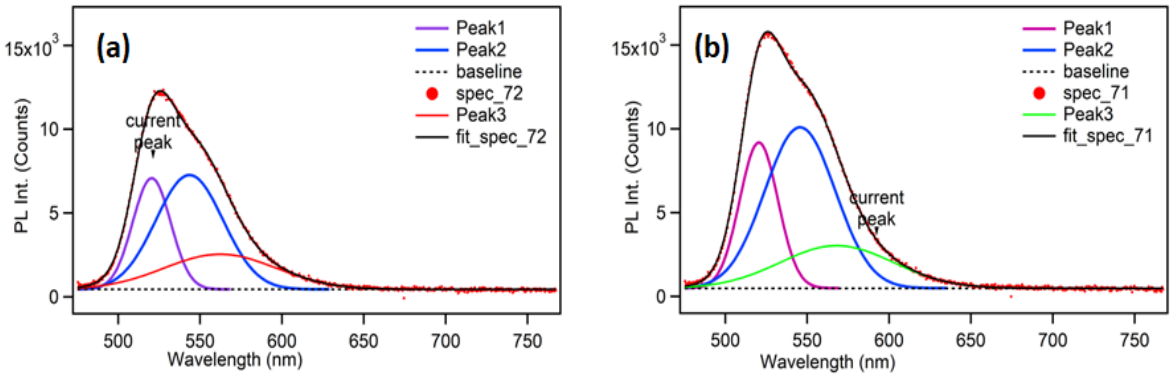

Fig. 6.18: Sample of curve fitted emission peak with wavelength for the sample MFP

In our work, for both the sample MF and MFP, the tuning was observed above 540nm. So, we considered the third component (configuration) of fluorescein molecule with peak emission wavelength 560nm for the curve fitting. Fig. 6.19 shows the peak emission wavelength fitted for the third component (structure) of fluorescein molecule for the two sample Ag/PVAF and Ag/PVAF/PMMA with the corresponding angle.

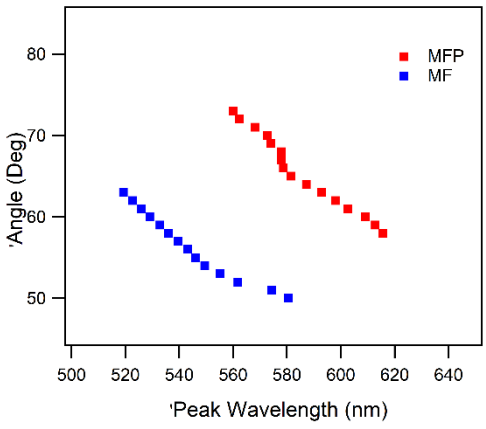

Fig. 6.19: Variation of emission peak with wavelength for the sample MF and MPF

We used WINSPALL software to simulate the peak emission curve of the fluorescein molecule for the two samples MF and MFP and the simulated curve and the experimental curves were presented in the fig. 6.20. Fig. 6.20 shows peak emission wavelength fitted for the third component of the fluorescein molecule and the SPR curves simulated using WINSPALL software for the two sample Ag/PVAF and Ag/PVAF/PMMA. From the fig. 6.20 it is clear that the experimental curve deviated from simulated curve as the peak emission wavelength increased from 540nm. This is because the fluorescein molecule has three configurations (structures) with emission wavelength 520nm, 540nm and 560nm. So, we have to consider the coupled emission wavelength of the fluorescein structures of emission wavelength 520nm, 540nm and 560nm rather than only 560nm. So, the peak emission wavelength is decided by the coupled emission wavelength of the fluorescein structures. So the peak emission wavelength does not depends on the individual fluorescein molecule and the structures. As a result, the emission wavelength of 540nm must also be considered while fitting the curve. The structure with an emission wavelength of 520nm had no impact on tuning. So, tuning was due to coupled emission effect of the fluorescein structures and does not depends on individual molecule or structures.

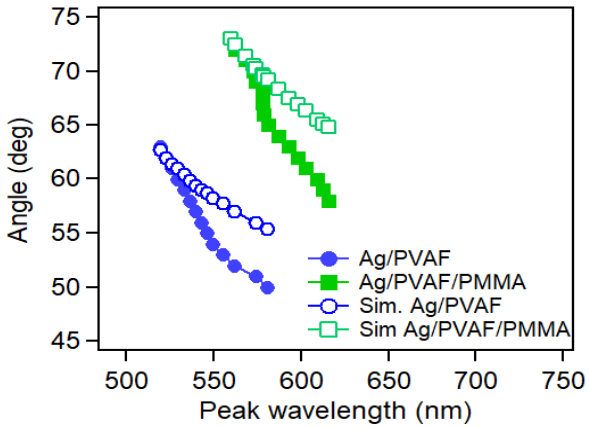

Fig. 6.20: Peak emission wavelength fitted for 560nm and Simulated curve for the sample MF and MPF

Fig. 6.21 shows the simulated SPR curves of Ag/PVAF and Ag/PVAF/PMMA. These curves were exactly consistent with the experimental curves. On coating PMMA above Ag/PVAF layer, the peak emission wavelength and emission angle changes. So, this experiment can be used in sensor applications. On coating any material above the Ag-fluorescein layer, emission studies give the characteristic properties of that material.

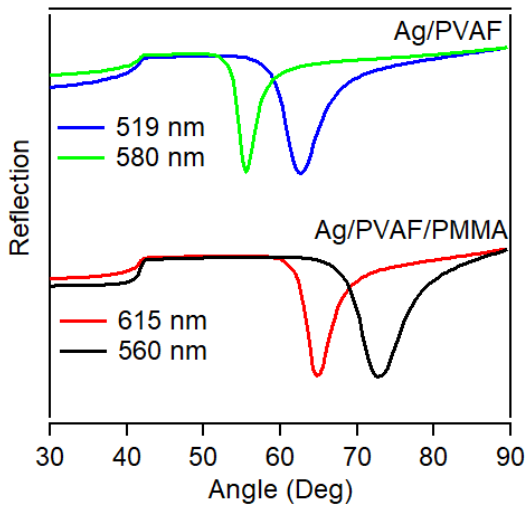

Fig. 6.21: Simulated SPR for the sample MF and MPF

Fig. 6.22 shows the polar plots for the three sample Ag/PVAF, Ag/PVAF/PMMA and Ag/PMMA/PVAF respectively. For the first sample, strong coupling between fluorescein and surface plasmon were present and hence tuning was observed. Similar to the first sample, in the second sample also, strong plasmon coupled emission tuning was observed. But in the third sample from the fig. 6.22(c), it is clear that weak coupling and hence no tuning was observed.

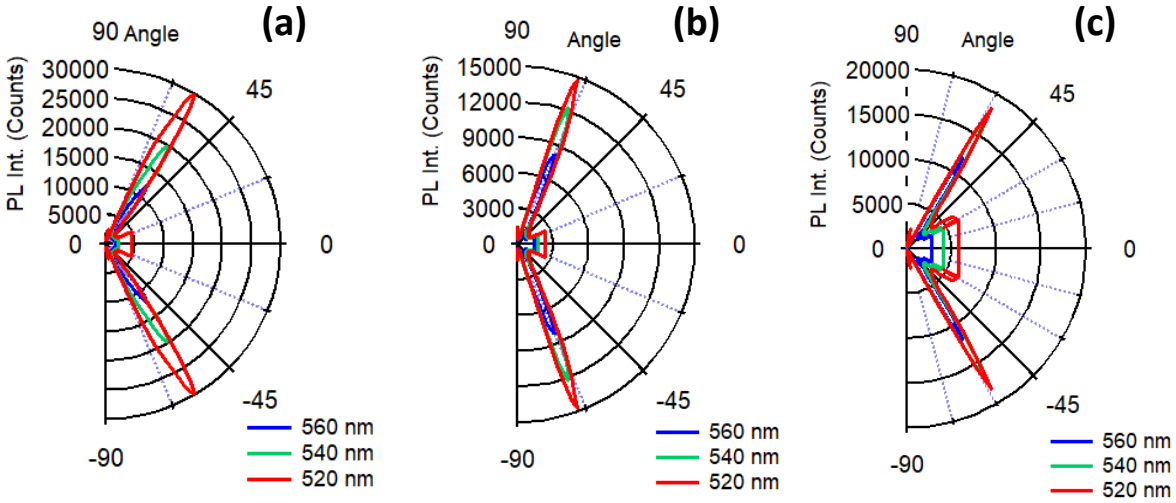

Fig. 6.22: Polar plots for the three sample (a) MF, (b) MFP and (c) MPF

Again, the angle tuned emission spectra of the prepared CQD-PVA composite film in the Reverse Kretschmann configuration was as shown in the fig. 6.23. The angle tuned emission spectra were recorded from 20^o to 70^o with an interval of 1^0. The direction normal to the substrate from the prism side was taken as the reference(0^0). All the collected spectra were then combined to plot an image with wavelength along the X axis, angle along the Y axis and the photoluminescence intensity as colour map. From the emission spectra, it is clear that emission was observed around 700nm with an excitation wavelength of 540nm. It was found that when pure CQD solution excited by laser of 540nm, the emission occurred around 700nm. So, this spectra of CQD-PVA nono composite film are very much in line with the photoluminescence spectra of CQD. Also, the emission was not observed at all angles but was observed within the angular range 40^o to 48^o. So, the emission directionality was enhanced.

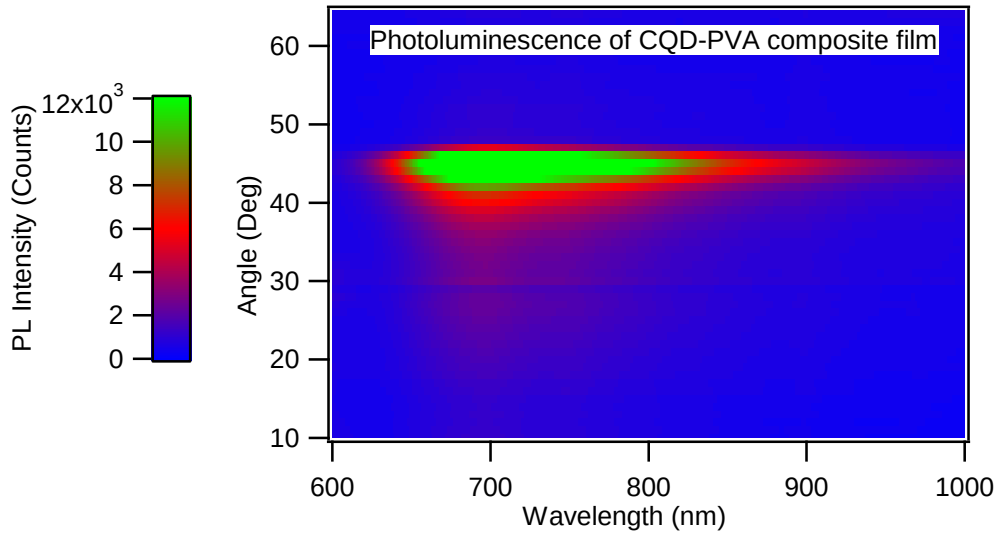

Fig. 6.23: Emission spectra of CQD-PVA nano composite

6.4 Conclusions

Plasmon coupled fluorescence tuning was observed in metal dielectric multilayered structures in reverse Kretschmann configuration. On multilayer fabrication with PMMA, we had studied the influence of PMMA on surface plasmon coupled emission tuning. The sample MF exhibited strong plasmon coupled fluorescence tuning, with emission ranging from 600nm to 520nm when the angle changed from 52^o to 64^o. The second sample MFP also showed substantial surface plasmon coupled emission tuning. As the angle varied from 60^o to 72^o wavelength changed from 630nm to 560nm In addition to this tuning, at the angle 70^o a

directionality also observed. This is due to uncoupled emission of fluorescein molecules. For the third sample MPF, the near-field coupling effect of the fluorescein molecule with the surface plasmon mode had gone and tuning was disappeared. By using multi-layered coating in SPCET we had verified that the emission tuning was due to the strong coupling of emission with the surface plasmon resonance. This coupling was independent of the fluorophore molecules but depends only on the emission wavelength range. Moreover, the coupling becomes weak on introducing a thin layer in between the metal and the fluorophore layer, concluding that, for SPCET to observe, it is not necessary to introduce a buffer layer.

Chapter -7

Conclusions

7.1 Summary and Conclusions

In this chapter, we had summarised the research works carried out in this thesis and provide a clear understanding of the work and fresh prospects for future investigation.

Regarding the big challenges of nanotechnology in our prospective living and the current trend of study in this area, we attempted the investigation on the topic "Realization of active and passive optical components and their applications using multilayered polymer/inorganic thin films ". Now a days, multilayer thin films are common elements of many opto-electronic and photonic devices. These multilayer thin films have numerous applications in many fields of science and technology including photoluminescence devices, optical coating, antibacterial activities, solar cells, light emitting diodes, sensors, lasers, medical applications, photocatalytic activity and health care etc. Attempts have been made to design and fabricate multilayer thin films and optical filters using a low-cost and easy process, with good results when compared to nanofabrication employing more advanced and expensive procedures. In addition, we investigated the possible applications of multilayer thin films in photonic and opto-electronic applications. The entire research work was presented in the previous six chapters.

In chapter 1, we had presented a comprehensive discussion about the multilayer thin films and the fabrication techniques, materials used for the fabrication and applications of multi-layer thin films. Even though different methods were adopted for the fabrication of multilayer thin films, solution chemistry technique is cost effective and the easy method. We had designed the multilayer thin films by transfer matrix model simulations and the theory was also described in the chapter. Also, we had discussed about the active and passive optical components and studied the light matter interactions of these active and passive optical components with multilayers. Motivation, objectives and the outline of the present work had also been discussed in this chapter.

In chapter 2, we discussed briefly the experimental techniques used in this study attempt. This includes the experimental techniques used for the fabrication of multilayer thin films, preparation of CQDs and the plasmon coupled fluorescence tuning experiment. The characterization techniques were also presented in this chapter. The thin film fabrication was done by a spin coater and a physical vapour deposition unit and CQDs were prepared by microwave assisted hydrothermal method. The optical characterization of the prepared sample

was done by UV- Visible spectrophotometer, white light source and necessary optical fibres and lenses. The structural characterization was done by X-ray diffractometer, FTIR spectrometer, optical microscope and transmission electron microscopy etc.

In chapter 3, we had designed different types of optical filters using transfer matrix model (TMM) simulations. So, the multi-layered thin film coatings were conveniently used to realise different types of optical filters like anti-reflection coatings, highly reflecting mirrors, high pass filters, comb filters etc. In this chapter we had discussed about these optical filters elaborately. Employing single layer, bi layer, and tri-layered optical coatings, anti-reflection (AR) coatings were demonstrated. One and two layered coatings exhibit strong transmission for a specific range of wavelengths, but three-layered coating exhibits high transmission for a broad range of wavelengths. A tri-layered optical coating with a middle layer having an optical thickness of $\lambda/2$ may be used, which can expand the width of the zero-reflectance window. We had designed distributed Bragg reflectors by arranging alternating sequence of layers of high and low refractive index materials in a periodic manner. According to simulation results, 40 periods were needed to attain reflectivity of more than 90% for an index contrast of 0.08, while 15 periods were required for an index contrast of 0.31. Reflectivity of 90% was attained for 5 periods for an index contrast of 0.64 and 0.87. So, we had realized that reflectivity increased with the refractive index contrast as well as the number of periods. Comb filters were designed by sandwiching a thick optically transparent layer between two DBRs. As the thickness of the middle layer increased, a greater number of low reflectance peaks were opened and the full width at half maximum (FWHM) of the window decreased. Multiple layers of materials with various refractive indices were layered in a periodic pattern with various optical thicknesses to create the dichroic filters. We had designed six sets of dichroic filters and both the quarter wave thicknesses and non-quarter wave thicknesses were considered while choosing the optical thicknesses of the filters. The contrast between the material's refractive indices and their optical thicknesses determine the cut-off wavelength. The cut-off wavelength shifted towards lower wavelengths and hence had a higher pass band as the refractive index contrast between high and low refractive index materials was reduced. In addition to this, the ripple in the transmitted light was minimised. The dichroic filter exhibits greater pass band and extremely low ripples in the transmission spectra when the ratio of the thicknesses of high and low refractive index material was roughly equal to 0.11.

In chapter 4, we had fabricated a flexible polymer DBR by a simple solution chemistry method. We had developed a variable refractive index, optically transparent, high index

polymer (Titania doped poly vinyl alcohol nano composite polymer) by simple solution chemistry method. Here the refractive index of the polymer can be varied by simply varying the concentration of TiO_2 in PVA. A refractive index of up to 1.80 was achieved by increasing the doping levels of TiO_2 in PVA. We had fabricated flexible polymer DBR by using this newly developed polymer titania doped PVA polymer matrix composite (TPMC) as the high index polymer and PMMA as the low refractive index polymer. The reflectivity of DBR was increased by increasing number of periods as well as refractive index contrast between the pairs. The experimental results were in agreement with transfer matrix model (TMM) simulations. TMM simulation results revealed that in order to attain reflectivity more than 90%, the number of periods or refractive index contrast between the pairs may be increased. The number of periods in a DBR with a high index contrast of 0.51 can be lowered to 5 as compared to 20 in a DBR with a low index contrast of 0.17. So, in this chapter we had proposed that fabricating the flexible polymer DBRs from highly transparent and cost-effective polymers TPMC and PMMA in a simple solution chemistry method. The refractive index contrast between the pairs can be changed by simply varying the concentration of TiO_2 in PVA. So, any desired refractive index contrast, and hence stop band, can be achieved by simply varying the concentration of TiO_2 in PVA without altering any other thin film processing and DBR fabrication parameters.

In chapter 5, we had prepared highly photoluminescent CQDs from commercial D-glucose in a simple microwave assisted hydrothermal method. The solvent was de-ionised water. The materials and methods for CQD formation were described comprehensively. The transmission and absorption studies of the CQDs were done by UV-Visible spectrophotometer, white light source, and necessary optical fibres and lenses. The transmission electron microscopy images showed that the synthesized CQDs were uniformly sized. The surface area electron diffraction pattern showed that the synthesized quantum dots were not crystalline. It was found that the experimental parameters like microwave power, heating time, source concentration as well as solution volume have a distinct effect on the growth of CQDs. We had excited the CQDs with different excitation wavelength of 280nm, 450nm and 540nm and the photoluminescence spectra of the CQDs were recorded. From the photoluminescence spectra it is obvious that emission wavelength of CQDs were independent of the size of the CQDs. But the intensity of emission depends on the size of the CQDs. Also, CQDs can exhibit different emission colours when they were excited at different excitation wavelengths. From the absorption and transmission spectra, it was clear that CQDs show strong optical absorption in

the UV region. ie. CQDs are effective photon-harvesting agents especially in short-wavelength region. The synthesized CQDs didn't form into a thin film when coated on the glass substrate. In order to form a thin film of CQDs, we had mixed CQDs with PVA and the CQD-PVA nano composite thin film had formed. The photoluminescence spectra of CQD-PVA nano composite film were also consistent with the spectra of CQD in solution form.

In chapter 6, we had studied the light matter interactions or energy transfer mechanism by incorporating an emitting material with multilayers. We had demonstrated the surface plasmon coupled emission tuning and directionality in metal dielectric multilayered structures in reverse Kretschman configurations. On incorporating active optical components with multilayers, we found the influence of PMMA on surface plasmon coupled emission tuning. The experimental methods were clearly described in this chapter. We had performed the SPCE experiments on three samples: Metal/Fluorescein, Metal/Fluorescein/PMMA and Metal/PMMA/Fluorescein. The sample MF showed strong plasmon coupled fluorescence tuning, with emission ranging from 600nm to 520nm when the angle changed from 52^o to 64^o. The second sample MFP also showed substantial surface plasmon coupled emission tuning. As the angle varied from 60^o to 72^o wavelength changed from 630nm to 560nm. In addition to this tuning, at the angle 70^o a directionality also observed. This is due to uncoupled emission of fluorescein molecules. For the third sample MPF, the near-field coupling effect of the fluorescein molecule with the surface plasmon mode had gone and tuning was disappeared. This is because, on coating PMMA between metal and fluorescein, PMMA decouples the fluorescein molecule from that of surface plasmon and hence no tuning was observed. So, it is confirmed that the tuning was due to surface plasmon coupled emission. Again we had repeated the experiment by CQD as the active optical component. Here, the emission was not observed at all angles but was observed within the angular range 40^o to 48^o. Therefore, a variety of photonic and opto-electronic applications are possible with this CQD-PVA nano composite film. Consequently, the prospective uses of the previously fabricated structures for photonic applications were investigated by combining active optical materials with multilayers.

The following subsections summarize our research findings:

7.1.1 Realization of passive optical components by simulation

We had realized the passive optical components by designing different types of optical filters like antireflection coatings, distributed Bragg reflectors, comb filters and dichroic filters by numerical simulation method.

7.1.2 Realization of passive optical components by Experimentation

We had realized passive optical components, the distributed Bragg reflectors experimentally. By using the solution chemistry approach, we had synthesized a newly developed polymer, Titania doped PVA nanocomposite (T-PVA) polymer, with variable refractive index and high optical transparency. The refractive index of 1.8 was achieved by increasing the doping levels of TiO_2 in PVA. DBRs were fabricated by T-PVA and PMMA as alternating high and low refractive index layers respectively. Any desired refractive index contrast, and hence stop band and reflectivity can be achieved by simply varying the concentration of TiO2 in PVA without altering any other thin film processing and DBR fabrication parameters.

7.1.3 Realization of active optical components by Experimentation

We had realized the active optical component, Carbon quantum dots, experimentally. Through a simple, green assisted method, highly luminescent, non-toxic CQDs were prepared from commercial D-glucose by microwave assisted hydrothermal method. The microwave oven provides simultaneous, homogeneous fast heating leads to uniform size distribution of quantum dotes. The growth of CQDs were found to be significantly influenced by the experimental parameters including microwave power, heating time, source concentration, and solution volume. In order to use this active optical components in opto-electronic and photonic applications, we had mixed CQDs with PVA and CQD-PVA nano composite thin film had formed.

7.1.4 Applications of multilayers in surface plasmon coupled emission

In our work, we had realized the active and passive optical components in a simple, green assisted method. Our main goal is to investigate how the above fabricated optical components can be used in photonic and optoelectronic applications. On incorporating these optical components with multilayers, the potential applications of the above fabricated structures explored in photonic and opto-electronic applications. Using metal dielectric multi-layered structures in reverse Kretschmann configurations, we had performed the surface plasmon coupled emission experiment on three samples: Metal/Fluorescein, Metal/Fluorescein/PMMA and Metal/PMMA/Fluorescein. On multilayer fabrication with PMMA, we had studied the influence of PMMA on SPCE tuning and found that Strong plasmon coupled emission tuning was observed in the sample MF, as well as tuning and directionality in the sample MFP. There was no tuning

observed for the third sample MPF. So, by coating a thin layer of PMMA between metal and the fluorescein molecule, the interaction between the fluorescein molecule and the surface plasmon become weak and tuning was disappeared. This experiment confirmed that the tuning was caused by surface plasmon coupled emission. This study can be used in sensor applications. On coating a thin layer of biomaterial above the metal/Fluorescein layer and emission spectra gives the characteristic properties of that material.

The efficiency and functionality of optoelectronic and photonic devices can be boosted by fabricating them in a faster, more adaptive, more performant, and less expensive manner. We used a simple, inexpensive, and eco-friendly green assisted method to prepare every sample for both the fabrication of multilayers and the preparation of CQDs. In this thesis endeavour, we had fulfilled almost all of our thesis objectives. These works will create wide possibilities in the fabrication of opto-electronic and photonic devices.

Chapter -8

Recommendations and Scope for Future study

Recommendations and Scope for future study

Although all of our research objectives were completed, the scope of the study may be greatly extended and developed if more time and resources were provided. The scope for the future study are pointed out below:

- **To fabricate other optical filters like anti reflection coating, comb filters and dichroic filters in a simple, cost effective and green assisted method:** Multilayer thin film filters can be design and fabricate to realize various optical components and hence could be utilized for wide range of practical applications. Similar to the fabrication method of distributed Bragg reflectors, we can fabricate other optical filters like anti reflection coating, comb filters and dichroic filters in a simple, cost effective and green assisted method. Because the refractive index of the newly developed TPVA polymer can vary, optical filters with any desired reflectivity, peak wavelength and stop band etc. can be achieved. So, these pairs TPVA and PMMA can be used in the fabrication of different types of optical filters and can be used in many opto-electronic and photonic devices. This study opens a new gate way for the fabrication of opto-electronic and photonic devices in a simple, eco-friendly and cost-effective way.
- **CQD-PVA film formed can be used in finger print technology and can explore its potential applications in Biometric technology:** Carbon quantum dots are intensively investigated in a range of applications due to their high fluorescence performance, economical synthesis procedure and eco-friendly nature. In our research work, the highly photoluminescent CQDs were prepared in a simple, cost-effective and green assisted method. The CQD-PVA film can be employed for finger print technology, and its prospective uses in biometric technology can be investigated. On combining CQDs in the finger print technology, strong adhesion to the fingerprint residue, improved visibility, high-resolution imaging and molecular recognition agents are all features that provides. When lighted by different illumination sources, CQD based compositions for fingerprint recovery take on distinct colours, providing background-free views and maximising the accuracy of fingerprint analysis.

- **Incorporate Carbon quantum dots in lasers using distributed Bragg reflectors as fully and partially reflecting mirrors and can be used in photonic applications:** The DBR formed using TPMC and PMMA can be used in lasers as fully and partially reflecting mirrors and the CQDs can be used as active medium in lasers.
- **On coating the flexible DBR on a flexible substrate and can be used in pressure sensors:** The flexible DBR formed using TPMC and PMMA, when coating on a flexible substrate can be used in the pressure sensors. The flexible substrate will bend during the pressure variation and the thickness of the high and low refractive index polymer will vary with the bending of flexible substrate. So, by analysing the transmission and the reflection spectra, the pressure variation can be identified.
- **SPCE studies on sensor applications:** On coating a layer of bio-material (even with minute concentration) above the Ag-fluorescein layer and the emission studies gives the characteristic properties of that material. This study can be applied in sensor applications as well as in biomedical applications especially for the cancer treatment.

References

Ahmed, A., Niazi, M.B.K., Jahan, Z., Ahmad, T., Hussain, A., Pervaiz, E., Janjua, H.A., Hussain, Z., 2020. In-vitro and in-vivo study of superabsorbent PVA/Starch/g-C3N4/Ag@TiO2 NPs hydrogel membranes for wound dressing. Eur. Polym. J. 130, 109650. https://doi.org/10.1016/j.eurpolymj.2020.109650

Akash, M.S.H., Rehman, K., 2020. Ultraviolet-Visible (UV-VIS) Spectroscopy, in: Essentials of Pharmaceutical Analysis. Springer Nature Singapore, Singapore, pp. 29–56. https://doi.org/10.1007/978-981-15-1547-7_3

Akedo, J., Nakano, S., Park, J., Baba, S., Ashida, K., 2008. The aerosol deposition method. Synth. Engl. Ed. 1, 121–130. https://doi.org/10.5571/syntheng.1.121

Akl, A.A., Kamal, H., Abdel-Hady, K., 2006. Fabrication and characterization of sputtered titanium dioxide films. Appl. Surf. Sci. 252, 8651–8656. https://doi.org/10.1016/j.apsusc.2005.12.001

Alias, M.S., Alyamani, A.Y., Ooi, B.S., Alatawi, A.A., Chong, W.K., Tangi, M., Holguin-Lerma, J.A., Stegenburgs, E., Shakfa, M.K., Ng, T.K., Albadri, A.M., 2018. High Reflectivity YDH/SiO2 Distributed Bragg Reflector for UV-C Wavelength Regime. IEEE Photonics J. 10, 1–8. https://doi.org/10.1109/JPHOT.2018.2804355

Almeida, R.M., Portal, S., 2003. Photonic band gap structures by sol–gel processing. Curr. Opin. Solid State Mater. Sci. 7, 151–157.

Amendola, V., Pilot, R., Frasconi, M., Maragò, O.M., Iatì, M.A., 2017. Surface plasmon resonance in gold nanoparticles: a review. J. Phys. Condens. Matter 29, 203002. https://doi.org/10.1088/1361-648X/aa60f3

Anaya, M., Rubino, A., Calvo, M.E., Míguez, H., 2016. Solution processed high refractive index contrast distributed Bragg reflectors. J. Mater. Chem. C 4, 4532–4537. https://doi.org/10.1039/C6TC00663A

Asha, A.B., Narain, R., 2020. Nanomaterials properties, in: Polymer Science and Nanotechnology. Elsevier, pp. 343–359. https://doi.org/10.1016/B978-0-12-816806-6.00015-7

Azam, N., Najabat Ali, M., Javaid Khan, T., 2021. Carbon Quantum Dots for Biomedical Applications: Review and Analysis. Front. Mater. 8, 700403. https://doi.org/10.3389/fmats.2021.700403

Aziz, S.B., Hassan, A.Q., Mohammed, S.J., Karim, W.O., Kadir, M.F.Z., Tajuddin, H.A., Chan, N.N.M.Y., 2019. Structural and Optical Characteristics of PVA:C-Dot Composites: Tuning the Absorption of Ultra Violet (UV) Region. Nanomaterials 9, 216. https://doi.org/10.3390/nano9020216

Badugu, R., Nowaczyk, K., Descrovi, E., Lakowicz, J.R., 2013. Radiative decay engineering 6: Fluorescence on one-dimensional photonic crystals. Anal. Biochem. 442, 83–96. https://doi.org/10.1016/j.ab.2013.07.021

Bae, E., Murakami, N., Ohno, T., 2009. Exposed crystal surface-controlled TiO2 nanorods having rutile phase from TiCl3 under hydrothermal conditions. J. Mol. Catal. Chem. 300, 72–79. https://doi.org/10.1016/j.molcata.2008.10.048

Bai, J., Zhou, B., 2014. Titanium Dioxide Nanomaterials for Sensor Applications. Chem. Rev. 114, 10131–10176. https://doi.org/10.1021/cr400625j

Balili, R.B., 2012. TRANSFER MATRIX METHOD IN NANOPHOTONICS. Int. J. Mod. Phys. Conf. Ser. 17, 159–168. https://doi.org/10.1142/S2010194512008057

Barbagiovanni, E.G., Lockwood, D.J., Simpson, P.J., Goncharova, L.V., 2014. Quantum confinement in Si and Ge nanostructures: Theory and experiment. Appl. Phys. Rev. 1, 011302. https://doi.org/10.1063/1.4835095

Barbosa-García, O., Ramos-Ortíz, G., Maldonado, J.L., Pichardo-Molina, J.L., Meneses-Nava, M.A., Landgrave, J.E.A., Cervantes-Martínez, J., 2007. UV–vis absorption spectroscopy and multivariate analysis as a method to discriminate tequila. Spectrochim. Acta. A. Mol. Biomol. Spectrosc. 66, 129–134. https://doi.org/10.1016/j.saa.2006.02.033

Barhoum, A., Pal, K., Rahier, H., Uludag, H., Kim, I.S., Bechelany, M., 2019. Nanofibers as new-generation materials: From spinning and nano-spinning fabrication techniques to emerging applications. Appl. Mater. Today 17, 1–35. https://doi.org/10.1016/j.apmt.2019.06.015

Barrios, D., Vergaz, R., Sánchez-Pena, J.M., García-Cámara, B., Granqvist, C.G., Niklasson, G.A., 2015. Simulation of the thickness dependence of the optical properties of suspended particle devices. Sol. Energy Mater. Sol. Cells 143, 613–622. https://doi.org/10.1016/j.solmat.2015.05.044

Bebb, H.B., Williams, E.W., 1972. Chapter 4 Photoluminescence I: Theory, in: Semiconductors and Semimetals. Elsevier, pp. 181–320. https://doi.org/10.1016/S0080-8784(08)62345-5

Bendavid, A., Martin, P.J., Jamting, Å., Takikawa, H., 1999. Structural and optical properties of titanium oxide thin films deposited by filtered arc deposition. Thin Solid Films 355–356, 6–11. https://doi.org/10.1016/S0040-6090(99)00436-8

Berg, T.J.T.P., 2018. Intraocular light scatter, reflections, fluorescence and absorption: what we see in the slit lamp. Ophthalmic Physiol. Opt. 38, 6–25. https://doi.org/10.1111/opo.12426

Berggren, M., Dodabalapur, A., Slusher, R.E., Bao, Z., 1997. Light amplification in organic thin films using cascade energy transfer. Nature 389, 466–469. https://doi.org/10.1038/38979

Bergström, L., 1997. Hamaker constants of inorganic materials. Adv. Colloid Interface Sci. 70, 125–169.

Besso, P., Bozzi, M., Formaggi, M., Germani, S., Pasian, M., Perregrini, L., 2005. A Novel Approach for the Design of Dichroic Mirrors for Deep Space Antennas, in: European Radar Conference, 2005. EURAD 2005. Presented at the European Radar Conference, 2005. EURAD 2005., IEEE, La Defense, Paris, France, pp. 267–270. https://doi.org/10.1109/EURAD.2005.1605611

Bigdeli, A., Ghasemi, F., Abbasi-Moayed, S., Shahrajabian, M., Fahimi-Kashani, N., Jafarinejad, S., Farahmand Nejad, M.A., Hormozi-Nezhad, M.R., 2019. Ratiometric fluorescent nanoprobes for visual detection: Design principles and recent advances - A review. Anal. Chim. Acta 1079, 30–58. https://doi.org/10.1016/j.aca.2019.06.035

Blodgett, K.B., 1935. Films Built by Depositing Successive Monomolecular Layers on a Solid Surface. J. Am. Chem. Soc. 57, 1007–1022. https://doi.org/10.1021/ja01309a011

Boone, D.H., 1986. Physical vapour deposition processes. Mater. Sci. Technol. 2, 220–224. https://doi.org/10.1179/mst.1986.2.3.220

Brudieu, B., Bris, A.L., Teisseire, J., Guillemot, F., Dantelle, G., Misra, S., Cabarrocas, P.R. i, Sorin, F., Gacoin, T., 2014. Sol-Gel Route Toward Efficient and Robust Distributed Bragg Reflectors for Light Management Applications. Adv. Opt. Mater. 2, 1105–1112. https://doi.org/10.1002/adom.201400292

Budimir, M., Marković, Z., Vajdak, J., Jovanović, S., Kubat, P., Humpoličeк, P., Mičušik, M., Danko, M., Barras, A., Milivojević, D., Špitalsky, Z., Boukherroub, R., Marković, B.T., 2021. Enhanced visible light-triggered antibacterial activity of carbon quantum dots/polyurethane nanocomposites by gamma rays induced pre-treatment. Radiat. Phys. Chem. 185, 109499. https://doi.org/10.1016/j.radphyschem.2021.109499

Bunaciu, A.A., Udriştioiu, E. gabriela, Aboul-Enein, H.Y., 2015. X-Ray Diffraction: Instrumentation and Applications. Crit. Rev. Anal. Chem. 45, 289–299. https://doi.org/10.1080/10408347.2014.949616

Burdette, S.C., Walkup, G.K., Spingler, B., Tsien, R.Y., Lippard, S.J., 2001. Fluorescent Sensors for Zn^{2+} Based on a Fluorescein Platform: Synthesis, Properties and Intracellular Distribution. J. Am. Chem. Soc. 123, 7831–7841. https://doi.org/10.1021/ja010059l

Calander, N., 2004. Theory and Simulation of Surface Plasmon-Coupled Directional Emission from Fluorophores at Planar Structures. Anal. Chem. 76, 2168–2173. https://doi.org/10.1021/ac049925d

Calvo, M.E., González-García, L., Parra-Barranco, J., Barranco, A., Jiménez-Solano, A., González-Elipe, A.R., Míguez, H., 2015. Flexible Distributed Bragg Reflectors from Nanocolumnar Templates. Adv. Opt. Mater. 3, 171–175. https://doi.org/10.1002/adom.201400338

Cao, L., Meziani, M.J., Sahu, S., Sun, Y.-P., 2013. Photoluminescence Properties of Graphene versus Other Carbon Nanomaterials. Acc. Chem. Res. 46, 171–180. https://doi.org/10.1021/ar300128j

Cao, S.-H., Cai, W.-P., Liu, Q., Li, Y.-Q., 2012. Surface Plasmon–Coupled Emission: What Can Directional Fluorescence Bring to the Analytical Sciences? Annu. Rev. Anal. Chem. 5, 317–336. https://doi.org/10.1146/annurev-anchem-062011-143208

Çetin, N.E., Korkmaz, Ş., Elmas, S., Ekem, N., Pat, S., Balbağ, M.Z., Tarhan, E., Temel, S., Özmumcu, M., 2013. The structural, optical and morphological properties of CaF2 thin films by using Thermionic Vacuum Arc (TVA). Mater. Lett. 91, 175–178. https://doi.org/10.1016/j.matlet.2012.07.086

Chávez-Valdez, A., Boccaccini, A.R., 2012. Innovations in electrophoretic deposition: Alternating current and pulsed direct current methods. Electrochimica Acta 65, 70–89. https://doi.org/10.1016/j.electacta.2012.01.015

Chen, B.B., Liu, Z.X., Deng, W.C., Zhan, L., Liu, M.L., Huang, C.Z., 2016. A large-scale synthesis of photoluminescent carbon quantum dots: a self-exothermic reaction driving the formation of the nanocrystalline core at room temperature. Green Chem. 18, 5127–5132. https://doi.org/10.1039/C6GC01820C

Chen, D., 2001. Anti-reflection (AR) coatings made by sol–gel processes: A review. Sol. Energy Mater. Sol. Cells 68, 313–336. https://doi.org/10.1016/S0927-0248(00)00365-2

Chénais, S., Forget, S., 2012. Recent advances in solid-state organic lasers. Polym. Int. 61, 390–406. https://doi.org/10.1002/pi.3173

Chércoles Asensio, R., San Andrés Moya, M., de la Roja, J.M., Gómez, M., 2009. Analytical characterization of polymers used in conservation and restoration by ATR-FTIR spectroscopy. Anal. Bioanal. Chem. 395, 2081–2096. https://doi.org/10.1007/s00216-009-3201-2

Chowdhury, M.H., Ray, K., Geddes, C.D., Lakowicz, J.R., 2008. Use of silver nanoparticles to enhance surface plasmon-coupled emission (SPCE). Chem. Phys. Lett. 452, 162–167. https://doi.org/10.1016/j.cplett.2007.12.047

Christopoulos, S., von Högersthal, G.B.H., Grundy, A.J.D., Lagoudakis, P.G., Kavokin, A.V., Baumberg, J.J., Christmann, G., Butté, R., Feltin, E., Carlin, J.-F., Grandjean, N., 2007. Room-Temperature Polariton Lasing in Semiconductor Microcavities. Phys. Rev. Lett. 98, 126405. https://doi.org/10.1103/PhysRevLett.98.126405

Chung, F.H., 1974. Quantitative interpretation of X-ray diffraction patterns of mixtures. II. Adiabatic principle of X-ray diffraction analysis of mixtures. J. Appl. Crystallogr. 7, 526–531. https://doi.org/10.1107/S0021889874010387

Cialla, D., März, A., Böhme, R., Theil, F., Weber, K., Schmitt, M., Popp, J., 2012. Surface-enhanced Raman spectroscopy (SERS): progress and trends. Anal. Bioanal. Chem. 403, 27–54. https://doi.org/10.1007/s00216-011-5631-x

Coenning, W., Caloz, F., 2017. Passive Devices, in: Venghaus, H., Grote, N. (Eds.), Fibre Optic Communication, Springer Series in Optical Sciences. Springer International Publishing, Cham, pp. 547–584. https://doi.org/10.1007/978-3-319-42367-8_11

Coppola, G., Ferraro, P., Iodice, M., De Nicola, S., 2003. Method for measuring the refractive index and the thickness of transparent plates with a lateral-shear, wavelength-scanning interferometer. Appl. Opt. 42, 3882. https://doi.org/10.1364/AO.42.003882

Corso, A.J., Pelizzo, M.G., 2019. Extreme Ultraviolet Multilayer Nanostructures and Their Application to Solar Plasma Observations: A Review. J. Nanosci. Nanotechnol. 19, 532–545. https://doi.org/10.1166/jnn.2019.16477

Cox, J.T., Hass, G., Rowntree, R.F., 1954. Two-layer anti-reflection coatings for glass in the near infra-red. Vacuum 4, 445–455. https://doi.org/10.1016/0042-207X(54)90005-6

Cuevas, M., Grunhut, V., Depine, R.A., 2016. Near field evidence of backward surface plasmon polaritons on negative index material boundaries. Phys. Lett. A 380, 4018–4021. https://doi.org/10.1016/j.physleta.2016.10.013

Cui, X., Ding, R., Wang, M., Zhang, Cong, Zhang, Ce, Zhang, J., Xu, Y., 2016. In Situ Surface Assembly Derived Ultralow Refractive Index MgF_2–SiO_2 Hybrid Film for Tri-Layer Broadband Antireflective Coating. Adv. Opt. Mater. 4, 722–730. https://doi.org/10.1002/adom.201500595

Dalton, L.R., 2000. Polymeric electro-optic materials: optimization of electro-optic activity, minimization of optical loss, and fine-tuning of device performance. Opt. Eng. 39, 589. https://doi.org/10.1117/1.602403

Dameron, A.A., Davidson, S.D., Burton, B.B., Carcia, P.F., McLean, R.S., George, S.M., 2008. Gas Diffusion Barriers on Polymers Using Multilayers Fabricated by Al_2O_3 and Rapid SiO_2 Atomic Layer Deposition. J. Phys. Chem. C 112, 4573–4580. https://doi.org/10.1021/jp076866+

Damos, F.S., Luz, R.C.S., Kubota, L.T., 2005. Determination of Thickness, Dielectric Constant of Thiol Films, and Kinetics of Adsorption Using Surface Plasmon Resonance. Langmuir 21, 602–609. https://doi.org/10.1021/la0487038

Davison, J.A., Simpson, M.J., 2006. History and development of the apodized diffractive intraocular lens. J. Cataract Refract. Surg. 32, 849–858. https://doi.org/10.1016/j.jcrs.2006.02.006

Deng, Y., Liu, H., Zheng, G.-H., 2022. Plasmon resonances of nanorods in transverse electromagnetic scattering. J. Differ. Equ. 318, 502–536. https://doi.org/10.1016/j.jde.2022.02.035

Deppe, D.G., 2003. Low-Power Vertical-Cavity Surface-Emitting Lasers and Microcavity Light-Emitting Diodes Based on Apertured-Microcavities, in: Li, H.E., Iga, K. (Eds.), Vertical-Cavity Surface-Emitting Laser Devices, Springer Series in Photonics. Springer Berlin Heidelberg, Berlin, Heidelberg, pp. 227–258. https://doi.org/10.1007/978-3-662-05263-1_7

Devi, P., Saini, S., Kim, K.-H., 2019. The advanced role of carbon quantum dots in nanomedical applications. Biosens. Bioelectron. 141, 111158. https://doi.org/10.1016/j.bios.2019.02.059

DiBenedetto, S.A., Facchetti, A., Ratner, M.A., Marks, T.J., 2009. Molecular Self-Assembled Monolayers and Multilayers for Organic and Unconventional Inorganic Thin-Film Transistor Applications. Adv. Mater. 21, 1407–1433. https://doi.org/10.1002/adma.200803267

Dong, W.J., Lo, N.-T., Jung, G.H., Ham, J., Lee, J.-L., 2016. Efficiency enhancement and angle-dependent color change in see-through organic photovoltaics using distributed Bragg reflectors. Appl. Phys. Lett. 108, 103902. https://doi.org/10.1063/1.4943654

Du, Y., Luna, L.E., Tan, W.S., Rubner, M.F., Cohen, R.E., 2010. Hollow Silica Nanoparticles in UV−Visible Antireflection Coatings for Poly(methyl methacrylate) Substrates. ACS Nano 4, 4308–4316. https://doi.org/10.1021/nn101033y

Duan, W., Liu, D., Zhang, F., 2007. Design and fabrication of an infrared dichroic filter used for multi-channel image-forming system, in: Yang, L., Chen, Y., Kley, E.-B., Li, R. (Eds.), . Presented at the 3rd International Symposium on Advanced Optical Manufacturing and Testing Technologies: Advanced Optical Manufacturing Technologies, Chengdu, China, p. 672220. https://doi.org/10.1117/12.783111

Dubey, R.S., Ganesan, V., 2017. Fabrication and characterization of TiO2/SiO2 based Bragg reflectors for light trapping applications. Results Phys. 7, 2271–2276. https://doi.org/10.1016/j.rinp.2017.06.041

Dutta Choudhury, S., Badugu, R., Lakowicz, J.R., 2015. Directing Fluorescence with Plasmonic and Photonic Structures. Acc. Chem. Res. 48, 2171–2180. https://doi.org/10.1021/acs.accounts.5b00100

Edvinsson, T., 2018. Optical quantum confinement and photocatalytic properties in two-, one- and zero-dimensional nanostructures. R. Soc. Open Sci. 5, 180387. https://doi.org/10.1098/rsos.180387

Fan, H., Zhang, M., Bhandari, B., Yang, C., 2020. Food waste as a carbon source in carbon quantum dots technology and their applications in food safety detection. Trends Food Sci. Technol. 95, 86–96. https://doi.org/10.1016/j.tifs.2019.11.008

Flores-Moreno, J.M., Torre-Ibarra, M.D. la, Hernandez-Montes, M. del S., Santoyo, F.M., 2020. DHI contemporary methodologies: A review and frontiers. Opt. Lasers Eng. 135, 106184. https://doi.org/10.1016/j.optlaseng.2020.106184

Frenkel, A.I., Hills, C.W., Nuzzo, R.G., 2001. A View from the Inside: Complexity in the Atomic Scale Ordering of Supported Metal Nanoparticles. J. Phys. Chem. B 105, 12689–12703. https://doi.org/10.1021/jp012769j

Gao, Y., Guo, N., Gauvreau, B., Rajabian, M., Skorobogata, O., Pone, E., Zabeida, O., Martinu, L., Dubois, C., Skorobogatiy, M., 2006. Consecutive solvent evaporation and co-rolling techniques for polymer multilayer hollow fiber preform fabrication. J. Mater. Res. 21, 2246–2254. https://doi.org/10.1557/jmr.2006.0271

Garlisi, C., Trepci, E., Li, X., Al Sakkaf, R., Al-Ali, K., Nogueira, R.P., Zheng, L., Azar, E., Palmisano, G., 2020. Multilayer thin film structures for multifunctional glass: Self-cleaning, antireflective and energy-saving properties. Appl. Energy 264, 114697. https://doi.org/10.1016/j.apenergy.2020.114697

Garzella, C., Comini, E., Tempesti, E., Frigeri, C., Sberveglieri, G., 2000. TiO2 thin films by a novel sol–gel processing for gas sensor applications. Sens. Actuators B Chem. 68, 189–196. https://doi.org/10.1016/S0925-4005(00)00428-7

Ghini, G., Trono, C., Giannetti, A., Puleo, G.L., Luconi, L., Amadou, J., Giambastiani, G., Baldini, F., 2013. Carbon nanotubes modified with fluorescein derivatives for pH nanosensing. Sens. Actuators B Chem. 179, 163–169. https://doi.org/10.1016/j.snb.2012.10.022

Ghosh, D., Sarkar, K., Devi, P., Kim, K.-H., Kumar, P., 2021. Current and future perspectives of carbon and graphene quantum dots: From synthesis to strategy for building optoelectronic and energy devices. Renew. Sustain. Energy Rev. 135, 110391. https://doi.org/10.1016/j.rser.2020.110391

Glebov, A.L., Mokhun, O., Rapaport, A., Vergnole, S., Smirnov, V., Glebov, L.B., 2012. Volume Bragg gratings as ultra-narrow and multiband optical filters, in: Thienpont, H., Mohr, J., Zappe, H., Nakajima, H. (Eds.), . Presented at the SPIE Photonics Europe, Brussels, Belgium, p. 84280C. https://doi.org/10.1117/12.923575

Glukhov, I.A., Dadoenkova, Y.S., Bentivegna, F.F.L., Moiseev, S.G., 2020. Deterministic aperiodic photonic crystal with a 2D array of metallic nanoparticles as polarization-sensitive dichroic filter. J. Appl. Phys. 128, 053101. https://doi.org/10.1063/5.0008652

Glynn, C., O'Dwyer, C., 2017. Solution Processable Metal Oxide Thin Film Deposition and Material Growth for Electronic and Photonic Devices. Adv. Mater. Interfaces 4, 1600610. https://doi.org/10.1002/admi.201600610

González-García, L., Lozano, G., Barranco, A., Míguez, H., González-Elipe, A.R., 2010. TiO2–SiO2 one-dimensional photonic crystals of controlled porosity by glancing angle physical vapour deposition. J. Mater. Chem. 20, 6408. https://doi.org/10.1039/c0jm00680g

GR Fowles, n.d. Introduction to modern optics.

Grieshaber, D., MacKenzie, R., Vörös, J., Reimhult, E., 2008. Electrochemical Biosensors - Sensor Principles and Architectures. Sensors 8, 1400–1458. https://doi.org/10.3390/s80314000

Gryczynski, I., Malicka, J., Gryczynski, Z., Lakowicz, J.R., 2004a. Radiative decay engineering 4. Experimental studies of surface plasmon-coupled directional emission. Anal. Biochem. 324, 170–182. https://doi.org/10.1016/j.ab.2003.09.036

Gryczynski, I., Malicka, J., Nowaczyk, K., Gryczynski, Z., Lakowicz, J.R., 2004b. Effects of Sample Thickness on the Optical Properties of Surface Plasmon-Coupled Emission. J. Phys. Chem. B 108, 12073–12083. https://doi.org/10.1021/jp0312619

Gryczynski, Z., Borejdo, J., Calander, N., Matveeva, E.G., Gryczynski, I., 2006. Minimization of detection volume by surface-plasmon-coupled emission. Anal. Biochem. 356, 125–131. https://doi.org/10.1016/j.ab.2006.05.007

Gryczynski, Z., Gryczynski, I., Matveeva, E., Malicka, J., Nowaczyk, K., Lakowicz, J.R., 2004. Surface-Plasmon–Coupled Emission: New Technology for Studying Molecular Processes, in: Methods in Cell Biology. Elsevier, pp. 73–104. https://doi.org/10.1016/S0091-679X(04)75004-9

Gupta, S.S., Kuzelka, J., Singh, P., Lewis, W.G., Manchester, M., Finn, M.G., 2005. Accelerated Bioorthogonal Conjugation: A Practical Method for the Ligation of Diverse Functional Molecules to a Polyvalent Virus Scaffold. Bioconjug. Chem. 16, 1572–1579. https://doi.org/10.1021/bc050147l

Haider, A.J., AL– Anbari, R.H., Kadhim, G.R., Salame, C.T., 2017. Exploring potential Environmental applications of TiO2 Nanoparticles. Energy Procedia 119, 332–345. https://doi.org/10.1016/j.egypro.2017.07.117

Haleem, A., Javaid, M., Singh, R.P., Suman, R., Rab, S., 2021. Biosensors applications in medical field: A brief review. Sens. Int. 2, 100100. https://doi.org/10.1016/j.sintl.2021.100100

Hallaj, T., Amjadi, M., Manzoori, J.L., Shokri, R., 2015. Chemiluminescence reaction of glucose-derived graphene quantum dots with hypochlorite, and its application to the determination of free chlorine. Microchim. Acta 182, 789–796. https://doi.org/10.1007/s00604-014-1389-0

Hammond, P.T., 2004. Form and Function in Multilayer Assembly: New Applications at the Nanoscale. Adv. Mater. 16, 1271–1293. https://doi.org/10.1002/adma.200400760

Hao, J., Zhou, L., 2008. Electromagnetic wave scatterings by anisotropic metamaterials: Generalized 4 × 4 transfer-matrix method. Phys. Rev. B 77, 094201. https://doi.org/10.1103/PhysRevB.77.094201

Hartmann, C.S., 1985. Systems Impact of Modern Rayleigh Wave Technology, in: Ash, E.A., Paige, E.G.S. (Eds.), Rayleigh-Wave Theory and Application, Springer Series on Wave Phenomena. Springer Berlin Heidelberg, Berlin, Heidelberg, pp. 238–253. https://doi.org/10.1007/978-3-642-82621-4_17

He, G.S., Tan, L.-S., Zheng, Q., Prasad, P.N., 2008. Multiphoton Absorbing Materials: Molecular Designs, Characterizations, and Applications. Chem. Rev. 108, 1245–1330. https://doi.org/10.1021/cr050054x

He, H., Shao, L., Qian, H., Zhang, X., Liang, J., Luo, B., Pan, W., Yan, L., 2017. Novel birefringence interrogation for Sagnac loop interferometer sensor with unlimited linear measurement range. Opt. Express 25, 6832. https://doi.org/10.1364/OE.25.006832

He, J., Nuzzo, R.G., Rogers, J.A., 2015. Inorganic materials and assembly techniques for flexible and stretchable electronics. Proc. IEEE 103, 619–632.

Heimann, R.B., 1996. Applications of Plasma-Sprayed Ceramic Coatings. Key Eng. Mater. 122–124, 399–442. https://doi.org/10.4028/www.scientific.net/KEM.122-124.399

Henderson, H., 1960. Interference filters. Contemp. Phys. 1, 467–478. https://doi.org/10.1080/00107516008204571

Heng, Z.W., Chong, W.C., Pang, Y.L., Koo, C.H., 2021. An overview of the recent advances of carbon quantum dots/metal oxides in the application of heterogeneous photocatalysis in photodegradation of pollutants towards visible-light and solar energy exploitation. J. Environ. Chem. Eng. 9, 105199. https://doi.org/10.1016/j.jece.2021.105199

Hess, S.C., Permatasari, F.A., Fukazawa, H., Schneider, E.M., Balgis, R., Ogi, T., Okuyama, K., Stark, W.J., 2017. Direct synthesis of carbon quantum dots in aqueous polymer solution: one-pot reaction and preparation of transparent UV-blocking films. J. Mater. Chem. A 5, 5187–5194. https://doi.org/10.1039/C7TA00397H

Hiller, J., Mendelsohn, J.D., Rubner, M.F., 2002. Reversibly erasable nanoporous anti-reflection coatings from polyelectrolyte multilayers. Nat. Mater. 1, 59–63. https://doi.org/10.1038/nmat719

Ho, P.K.H., Stephen, D., Thomas, Friend, R.H., Tessler, N., 1999. All-Polymer Optoelectronic Devices. Science 285, 233–236. https://doi.org/10.1126/science.285.5425.233

Ho, W.F., Uddin, M.A., Chan, H.P., 2009. The stability of high refractive index polymer materials for high-density planar optical circuits. Polym. Degrad. Stab. 94, 158–161. https://doi.org/10.1016/j.polymdegradstab.2008.11.011

Hobson, P.A., Wedge, S., Wasey, J.A.E., Sage, I., Barnes, W.L., 2002. Surface Plasmon Mediated Emission from Organic Light-Emitting Diodes. Adv. Mater. 14, 1393–1396. https://doi.org/10.1002/1521-4095(20021002)14:19<1393::AID-ADMA1393>3.0.CO;2-B

Hofmann, W., Chase, C., Müller, M., Yi Rao, Grasse, C., Böhm, G., Amann, M.-C., Chang-Hasnain, C.J., 2010. Long-Wavelength High-Contrast Grating Vertical-Cavity Surface-Emitting Laser. IEEE Photonics J. 2, 415–422. https://doi.org/10.1109/JPHOT.2010.2049009

Holman, Z.C., De Wolf, S., Ballif, C., 2013. Improving metal reflectors by suppressing surface plasmon polaritons: a priori calculation of the internal reflectance of a solar cell. Light Sci. Appl. 2, e106–e106. https://doi.org/10.1038/lsa.2013.62

Homola, J., 1997. On the sensitivity of surface plasmon resonance sensors with spectral interrogation. Sens. Actuators B Chem. 41, 207–211. https://doi.org/10.1016/S0925-4005(97)80297-3

Howard, C.J., Sabine, T.M., Dickson, F., 1991. Structural and thermal parameters for rutile and anatase. Acta Crystallogr. B 47, 462–468. https://doi.org/10.1107/S010876819100335X

Hu, Z., Huang, F., Cao, Y., 2017. Layer-by-Layer Assembly of Multilayer Thin Films for Organic Optoelectronic Devices. Small Methods 1, 1700264. https://doi.org/10.1002/smtd.201700264

Huang, L., Chang, P., Song, X., Peng, W., Zhang, W., Gao, F., Bo, F., Zhang, G., Xu, J., 2016. Tunable in-fiber Mach-Zehnder interferometer driven by unique acoustic transducer and its application in tunable multi-wavelength laser. Opt. Express 24, 2406. https://doi.org/10.1364/OE.24.002406

Huibers, P.D.T., Shah, D.O., 1997. Multispectral Determination of Soap Film Thickness. Langmuir 13, 5995–5998. https://doi.org/10.1021/la960738n

Inkson, B.J., 2016. Scanning electron microscopy (SEM) and transmission electron microscopy (TEM) for materials characterization, in: Materials Characterization Using Nondestructive Evaluation (NDE) Methods. Elsevier, pp. 17–43. https://doi.org/10.1016/B978-0-08-100040-3.00002-X

Ismaeel, R., Lee, T., Ding, M., Belal, M., Brambilla, G., 2013. Optical microfiber passive components: Microfiber components. Laser Photonics Rev. 7, 350–384. https://doi.org/10.1002/lpor.201200024

Israelachvili, J., Wennerström, H., 1996. Role of hydration and water structure in biological and colloidal interactions. Nature 379, 219–225. https://doi.org/10.1038/379219a0

Jambunathan, R., Singh, J., 1997. Design studies for distributed Bragg reflectors for short-cavity edge-emitting lasers. IEEE J. Quantum Electron. 33, 1180–1189. https://doi.org/10.1109/3.594882

Jans, H., Huo, Q., 2012. Gold nanoparticle-enabled biological and chemical detection and analysis. Chem Soc Rev 41, 2849–2866. https://doi.org/10.1039/C1CS15280G

Jelle, B.P., Nilsen, T.-N., 2011. Comparison of accelerated climate ageing methods of polymer building materials by attenuated total reflectance Fourier transform infrared radiation spectroscopy. Constr. Build. Mater. 25, 2122–2132. https://doi.org/10.1016/j.conbuildmat.2010.11.020

Jeong, S.-H., Kim, J.-K., Kim, B.-S., Shim, S.-H., Lee, B.-T., 2004. Characterization of SiO2 and TiO2 films prepared using rf magnetron sputtering and their application to anti-reflection coating. Vacuum 76, 507–515. https://doi.org/10.1016/j.vacuum.2004.06.003

Ji, L., Chen, Y., Yuan, Y.J., 2014. Investigation of surface plasmon resonance phenomena by finite element analysis and Fresnel calculation. Sens. Actuators B Chem. 198, 82–86. https://doi.org/10.1016/j.snb.2014.02.105

Ji, S., Hyun, B.G., Kim, K., Lee, S.Y., Kim, S.-H., Kim, J.-Y., Song, M.H., Park, J.-U., 2016. Photo-patternable and transparent films using cellulose nanofibers for stretchable origami electronics. NPG Asia Mater. 8, e299–e299. https://doi.org/10.1038/am.2016.113
Jiang, N., Zhuo, X., Wang, J., 2018. Active Plasmonics: Principles, Structures, and Applications. Chem. Rev. 118, 3054–3099. https://doi.org/10.1021/acs.chemrev.7b00252
Jin, S., Hu, Y., Gu, Z., Liu, L., Wu, H.-C., 2011. Application of Quantum Dots in Biological Imaging. J. Nanomater. 2011, 1–13. https://doi.org/10.1155/2011/834139
Jin, Wa, Wang, C., Xuan, H., Jin, Wei, 2013. Tunable comb filters and refractive index sensors based on fiber loop mirror with inline high birefringence microfiber. Opt. Lett. 38, 4277. https://doi.org/10.1364/OL.38.004277
Johansen, K., Arwin, H., Lundström, I., Liedberg, B., 2000. Imaging surface plasmon resonance sensor based on multiple wavelengths: Sensitivity considerations. Rev. Sci. Instrum. 71, 3530–3538. https://doi.org/10.1063/1.1287631
Johnson, J.E., Ketelsen, L.J.-P., Ackerman, D.A., Liming Zhang, Hybertsen, M.S., Glogovsky, K.G., Lentz, C.W., Asous, W.A., Reynolds, C.L., Geary, J.M., Kamath, K.K., Ebert, C.W., Park, M., Przybylek, G.J., Leibenguth, R.E., Broutin, S.L., Stayt, J.W., Dreyer, K.F., Peticolas, L.J., Hartman, R.L., Koch, T.L., 2001. Fully stabilized electroabsorption-modulated tunable DBR laser transmitter for long-haul optical communications. IEEE J. Sel. Top. Quantum Electron. 7, 168–177. https://doi.org/10.1109/2944.954126
Johnson, S.G., Joannopoulos, J.D., Fan, S., Villeneuve, P.R., 1998. Three-dimensional photon confinement in photonic crystals of low-dimensional periodicity. IEE Proc. - Optoelectron. 145, 384–390. https://doi.org/10.1049/ip-opt:19982467
Joo, W., Kim, H.J., Kim, J.K., 2010. Broadband Antireflection Coating Covering from Visible to Near Infrared Wavelengths by Using Multilayered Nanoporous Block Copolymer Films. Langmuir 26, 5110–5114. https://doi.org/10.1021/la9035858
Kalampaliki, A.D., Vincent, S., Mallick, S., Le, H.-N., Barnoin, G., More, Y.W., Burger, A., Dotsikas, Y., Gikas, E., Michel, B.Y., Kostakis, I.K., 2021. Synthesis, spectroscopic and computational evaluation of a xanthene-based fluorogenic derivatization reagent for the determination of primary amines. Dyes Pigments 196, 109798. https://doi.org/10.1016/j.dyepig.2021.109798
Kandasamy, G., 2019. Recent Advancements in Doped/Co-Doped Carbon Quantum Dots for Multi-Potential Applications. C 5, 24. https://doi.org/10.3390/c5020024
Kaneda, K., Ishida, S., Ishida, A., Nakamae, E., 1992. Image processing and synthesis for extended depth of field of optical microscopes. Vis. Comput. 8, 351–360. https://doi.org/10.1007/BF01897121
Karim, A., Bjorlin, S., Piprek, J., Bowers, J.E., 2000. Long-wavelength vertical-cavity lasers and amplifiers. IEEE J. Sel. Top. Quantum Electron. 6, 1244–1253.
Kasha, M., 1950. Characterization of electronic transitions in complex molecules. Discuss. Faraday Soc. 9, 14. https://doi.org/10.1039/df9500900014
Kedawat, G., Srivastava, S., Jain, V.K., Kumar, P., Kataria, V., Agrawal, Y., Gupta, B.K., Vijay, Y.K., 2013. Fabrication of Artificially Stacked Ultrathin ZnS/MgF_2 Multilayer Dielectric Optical Filters. ACS Appl. Mater. Interfaces 5, 4872–4877. https://doi.org/10.1021/am400612q
Keller, H.E., 2006. Objective Lenses for Confocal Microscopy, in: Pawley, J.B. (Ed.), Handbook Of Biological Confocal Microscopy. Springer US, Boston, MA, pp. 145–161. https://doi.org/10.1007/978-0-387-45524-2_7
Kern, W., Schuegraf, K.K., 2001. Deposition Technologies and Applications, in: Handbook of Thin Film Deposition Processes and Techniques. Elsevier, pp. 11–43. https://doi.org/10.1016/B978-081551442-8.50006-7
Khan, Karim, Tareen, A.K., Aslam, M., Sagar, R.U.R., Zhang, B., Huang, W., Mahmood, A., Mahmood, N., Khan, Kishwar, Zhang, H., Guo, Z., 2020. Recent Progress, Challenges, and Prospects in Two-Dimensional Photo-Catalyst Materials and Environmental Remediation. Nano-Micro Lett. 12, 167. https://doi.org/10.1007/s40820-020-00504-3

Khan, M.I., Bhatti, K.A., Qindeel, R., Althobaiti, H.S., Alonizan, N., 2017. Structural, electrical and optical properties of multilayer TiO2 thin films deposited by sol–gel spin coating. Results Phys. 7, 1437–1439. https://doi.org/10.1016/j.rinp.2017.03.023

Kik, P.G., Brongersma, M.L., 2007. SURFACE PLASMON NANOPHOTONICS, in: Brongersma, M.L., Kik, P.G. (Eds.), Surface Plasmon Nanophotonics, Springer Series in Optical Sciences. Springer Netherlands, Dordrecht, pp. 1–9. https://doi.org/10.1007/978-1-4020-4333-8_1

Kim, B.J., Han, D., Yoo, S., Im, S.G., 2017. Organic/inorganic multilayer thin film encapsulation via initiated chemical vapor deposition and atomic layer deposition for its application to organic solar cells. Korean J. Chem. Eng. 34, 892–897. https://doi.org/10.1007/s11814-016-0303-3

Kleine, T.S., Diaz, L.R., Konopka, K.M., Anderson, L.E., Pavlopolous, N.G., Lyons, N.P., Kim, E.T., Kim, Y., Glass, R.S., Char, K., Norwood, R.A., Pyun, J., 2018. One Dimensional Photonic Crystals Using Ultrahigh Refractive Index Chalcogenide Hybrid Inorganic/Organic Polymers. ACS Macro Lett. 7, 875–880. https://doi.org/10.1021/acsmacrolett.8b00245

Knoblauch, R., Geddes, C.D., 2019. Review of Advances in Metal-Enhanced Fluorescence, in: Geddes, C.D. (Ed.), Reviews in Plasmonics 2017, Reviews in Plasmonics. Springer International Publishing, Cham, pp. 253–283. https://doi.org/10.1007/978-3-030-18834-4_10

Köhnen, A., Riegel, N., Kremer, J.H.-W., Lademann, H., Müller, D.C., Meerholz, K., 2009. The simple way to solution-processed multilayer OLEDs–layered block-copolymer networks by living cationic polymerization. Adv. Mater. 21, 879–884.

Kontges, M., Morlier, A., Eder, G., Fleis, E., Kubicek, B., Lin, J., 2020. Review: Ultraviolet Fluorescence as Assessment Tool for Photovoltaic Modules. IEEE J. Photovolt. 10, 616–633. https://doi.org/10.1109/JPHOTOV.2019.2961781

Kostoff, R.N., Stump, J.A., Johnson, D., Murday, J.S., Lau, C.G.Y., Tolles, W.M., 2006. The structure and infrastructure of the global nanotechnology literature. J. Nanoparticle Res. 8, 301–321. https://doi.org/10.1007/s11051-005-9035-8

Kou, D., Ma, W., Zhang, S., Li, R., Zhang, Y., 2020. BTEX Vapor Detection with a Flexible MOF and Functional Polymer by Means of a Composite Photonic Crystal. ACS Appl. Mater. Interfaces 12, 11955–11964. https://doi.org/10.1021/acsami.9b22033

Koutchma, T., 2009. Advances in Ultraviolet Light Technology for Non-thermal Processing of Liquid Foods. Food Bioprocess Technol. 2, 138–155. https://doi.org/10.1007/s11947-008-0178-3

Krogman, K.C., Druffel, T., Sunkara, M.K., 2005. Anti-reflective optical coatings incorporating nanoparticles. Nanotechnology 16, S338–S343. https://doi.org/10.1088/0957-4484/16/7/005

Kumar, P.M., Badrinarayanan, S., Sastry, M., 2000. Nanocrystalline TiO2 studied by optical, FTIR and X-ray photoelectron spectroscopy: correlation to presence of surface states. Thin Solid Films 358, 122–130. https://doi.org/10.1016/S0040-6090(99)00722-1

Kurihara, K., Suzuki, K., 2002. Theoretical Understanding of an Absorption-Based Surface Plasmon Resonance Sensor Based on Kretchmann's Theory. Anal. Chem. 74, 696–701. https://doi.org/10.1021/ac010820+

Kwon, J., Jeon, Y., Lee, B., 2005. Tunable dispersion compensation with fixed center wavelength and bandwidth using a side-polished linearly chirped fiber Bragg grating. Opt. Fiber Technol. 11, 159–166. https://doi.org/10.1016/j.yofte.2004.08.002

Lakowicz, J.R., 2006. Plasmonics in Biology and Plasmon-Controlled Fluorescence. Plasmonics 1, 5–33. https://doi.org/10.1007/s11468-005-9002-3

Lakowicz, J.R., 2004. Radiative decay engineering 3. Surface plasmon-coupled directional emission. Anal. Biochem. 324, 153–169. https://doi.org/10.1016/j.ab.2003.09.039

Lakowicz, J.R., Chowdury, M.H., Ray, K., Zhang, J., Fu, Y., Badugu, R., Sabanayagam, C.R., Nowaczyk, K., Szmacinski, H., Aslan, K., Geddes, C.D., 2006. Plasmon-controlled fluorescence: a new detection technology, in: Vo-Dinh, T., Lakowicz, J.R., Gryczynski, Z. (Eds.), . Presented at the Biomedical Optics 2006, San Jose, CA, p. 609909. https://doi.org/10.1117/12.673106

Lakowicz, J.R., Ray, K., Chowdhury, M., Szmacinski, H., Fu, Y., Zhang, J., Nowaczyk, K., 2008. Plasmon-controlled fluorescence: a new paradigm in fluorescence spectroscopy. The Analyst 133, 1308. https://doi.org/10.1039/b802918k

Lee, L.-H., Chen, W.-C., 2001. High-Refractive-Index Thin Films Prepared from Trialkoxysilane-Capped Poly(methyl methacrylate)−Titania Materials. Chem. Mater. 13, 1137–1142. https://doi.org/10.1021/cm000937z

Li, H., Kang, Z., Liu, Y., Lee, S.-T., 2012. Carbon nanodots: synthesis, properties and applications. J. Mater. Chem. 22, 24230. https://doi.org/10.1039/c2jm34690g

Li, M., Chen, T., Gooding, J.J., Liu, J., 2019. Review of Carbon and Graphene Quantum Dots for Sensing. ACS Sens. 4, 1732–1748. https://doi.org/10.1021/acssensors.9b00514

Li, Y., Quan, M., Tian, J., Yao, Y., 2015. Tunable multiwavelength erbium-doped fiber laser based on nonlinear optical loop mirror and birefringence fiber filter. Appl. Phys. B 119, 363–370. https://doi.org/10.1007/s00340-015-6084-2

Liese, T., Radisch, V., Krebs, H.-U., 2010. Fabrication of multilayer Laue lenses by a combination of pulsed laser deposition and focused ion beam. Rev. Sci. Instrum. 81, 073710. https://doi.org/10.1063/1.3462985

Lim, H., Liu, Y., Kim, H.Y., Son, D.I., 2018. Facile synthesis and characterization of carbon quantum dots and photovoltaic applications. Thin Solid Films 660, 672–677. https://doi.org/10.1016/j.tsf.2018.04.019

Lim, S.Y., Law, C.S., Markovic, M., Marsal, L.F., Voelcker, N.H., Abell, A.D., Santos, A., 2019. Rational Management of Photons for Enhanced Photocatalysis in Structurally-Colored Nanoporous Anodic Alumina Photonic Crystals. ACS Appl. Energy Mater. 2, 1169–1184. https://doi.org/10.1021/acsaem.8b01721

Lim, S.Y., Shen, W., Gao, Z., 2015. Carbon quantum dots and their applications. Chem. Soc. Rev. 44, 362–381. https://doi.org/10.1039/C4CS00269E

Lisichkin, G.V., Olenin, A.Yu., 2020. Synthesis of surface-modified quantum dots. Russ. Chem. Bull. 69, 1819–1828. https://doi.org/10.1007/s11172-020-2968-3

Liu, B.-T., Tang, S.-J., Yu, Y.-Y., Lin, S.-H., 2011. High-refractive-index polymer/inorganic hybrid films containing high TiO2 contents. Colloids Surf. Physicochem. Eng. Asp. 377, 138–143. https://doi.org/10.1016/j.colsurfa.2010.12.046

Liu, C., Zhang, Q., Wang, D., Zhao, G., Cai, X., Li, L., Ding, H., Zhang, K., Wang, H., Kong, D., Yin, L., Liu, L., Zou, G., Zhao, L., Sheng, X., 2018. High Performance, Biocompatible Dielectric Thin-Film Optical Filters Integrated with Flexible Substrates and Microscale Optoelectronic Devices. Adv. Opt. Mater. 6, 1800146. https://doi.org/10.1002/adom.201800146

Liu, J., Li, R., Yang, B., 2020. Carbon Dots: A New Type of Carbon-Based Nanomaterial with Wide Applications. ACS Cent. Sci. 6, 2179–2195. https://doi.org/10.1021/acscentsci.0c01306

Liu, J., Ueda, M., 2009. High refractive index polymers: fundamental research and practical applications. J. Mater. Chem. 19, 8907. https://doi.org/10.1039/b909690f

Liu, S., Wang, Y., Liao, C., Wang, G., Li, Z., Wang, Q., Zhou, J., Yang, K., Zhong, X., Zhao, J., Tang, J., 2014. High-sensitivity strain sensor based on in-fiber improved Fabry–Perot interferometer. Opt. Lett. 39, 2121. https://doi.org/10.1364/OL.39.002121

Liu, Y., Kang, N., Ke, X., Wang, D., Ren, L., Wang, H., 2016. A fluorescent nanoprobe based on metal-enhanced fluorescence combined with Förster resonance energy transfer for the trace detection of nitrite ions. RSC Adv. 6, 27395–27403. https://doi.org/10.1039/C5RA27622E

Löbl, P., Huppertz, M., Mergel, D., 1994. Nucleation and growth in TiO2 films prepared by sputtering and evaporation. Thin Solid Films 251, 72–79. https://doi.org/10.1016/0040-6090(94)90843-5

Lova, P., 2018. Selective Polymer Distributed Bragg Reflector Vapor Sensors. Polymers 10, 1161. https://doi.org/10.3390/polym10101161

Lova, P., Manfredi, G., Boarino, L., Comite, A., Laus, M., Patrini, M., Marabelli, F., Soci, C., Comoretto, D., 2015. Polymer Distributed Bragg Reflectors for Vapor Sensing. ACS Photonics 2, 537–543. https://doi.org/10.1021/ph500461w

Lova, P., Manfredi, G., Comoretto, D., 2018. Advances in functional solution processed planar 1D photonic crystals. Adv. Opt. Mater. 6, 1800730.

Lu, C.-H., Muenzel, S., Fleischer, J.W., 2013. High-Resolution Light-Field Microscopy, in: Imaging and Applied Optics. Presented at the Computational Optical Sensing and Imaging, OSA, Arlington, Virginia, p. CTh3B.2. https://doi.org/10.1364/COSI.2013.CTh3B.2

Lu, S., Xiao, F., Guo, Z., Wang, L., Li, H., Liao, B., 2016. Numerical simulation of multilayered multiple metal cast rolls in compound casting process. Appl. Therm. Eng. 93, 518–528. https://doi.org/10.1016/j.applthermaleng.2015.09.114

Luk'yanchuk, B.S., Paniagua-Domínguez, R., Minin, I., Minin, O., Wang, Z., 2017. Refractive index less than two: photonic nanojets yesterday, today and tomorrow. Opt. Mater. Express 7, 1820–1847.

Madsen, C.K., Lenz, G., 1998. Optical all-pass filters for phase response design with applications for dispersion compensation. IEEE Photonics Technol. Lett. 10, 994–996. https://doi.org/10.1109/68.681295

Martinet, C., Paillard, V., Gagnaire, A., Joseph, J., 1997. Deposition of SiO2 and TiO2 thin films by plasma enhanced chemical vapor deposition for antireflection coating. J. Non-Cryst. Solids 216, 77–82. https://doi.org/10.1016/S0022-3093(97)00175-0

Mehta, A., Mishra, A., Basu, S., Shetti, N.P., Reddy, K.R., Saleh, T.A., Aminabhavi, T.M., 2019. Band gap tuning and surface modification of carbon dots for sustainable environmental remediation and photocatalytic hydrogen production – A review. J. Environ. Manage. 250, 109486. https://doi.org/10.1016/j.jenvman.2019.109486

Mendelsohn, J.D., Barrett, C.J., Chan, V.V., Pal, A.J., Mayes, A.M., Rubner, M.F., 2000. Fabrication of Microporous Thin Films from Polyelectrolyte Multilayers. Langmuir 16, 5017–5023. https://doi.org/10.1021/la000075g

Meng, Z., Keten, S., 2018. Unraveling the Effect of Material Properties and Geometrical Factors on Ballistic Penetration Energy of Nanoscale Thin Films. J. Appl. Mech. 85, 121004. https://doi.org/10.1115/1.4041041

Mitzi, D.B., 2001. Thin-Film Deposition of Organic−Inorganic Hybrid Materials. Chem. Mater. 13, 3283–3298. https://doi.org/10.1021/cm0101677

Moridi, A., Hassani-Gangaraj, S.M., Guagliano, M., Dao, M., 2014. Cold spray coating: review of material systems and future perspectives. Surf. Eng. 30, 369–395. https://doi.org/10.1179/1743294414Y.0000000270

Morissette, S.L., Lewis, J.A., Cesarano, J., Dimos, D.B., Baer, T., 2004. Solid Freeform Fabrication of Aqueous Alumina-Poly(vinyl alcohol) Gelcasting Suspensions. J. Am. Ceram. Soc. 83, 2409–2416. https://doi.org/10.1111/j.1151-2916.2000.tb01569.x

Muallem, M., Palatnik, A., Nessim, G.D., Tischler, Y.R., 2015. Room Temperature Fabrication of Dielectric Bragg Reflectors Composed of a CaF_2/ZnS Multilayered Coating. ACS Appl. Mater. Interfaces 7, 474–481. https://doi.org/10.1021/am506531p

Murthy, K.V.R., Virk, H.S., 2013. Luminescence Phenomena: An Introduction. Defect Diffus. Forum 347, 1–34. https://doi.org/10.4028/www.scientific.net/DDF.347.1

Nakayama-Ratchford, N., Bangsaruntip, S., Sun, X., Welsher, K., Dai, H., 2007. Noncovalent Functionalization of Carbon Nanotubes by Fluorescein−Polyethylene Glycol: Supramolecular Conjugates with pH-Dependent Absorbance and Fluorescence. J. Am. Chem. Soc. 129, 2448–2449. https://doi.org/10.1021/ja068684j

Naraoka, R., Okawa, H., Hashimoto, K., Kajikawa, K., 2005. Surface plasmon resonance enhanced second-harmonic generation in Kretschmann configuration. Opt. Commun. 248, 249–256. https://doi.org/10.1016/j.optcom.2004.11.094

Nisticò, R., Scalarone, D., Magnacca, G., 2017. Sol-gel chemistry, templating and spin-coating deposition: A combined approach to control in a simple way the porosity of inorganic thin films/coatings. Microporous Mesoporous Mater. 248, 18–29. https://doi.org/10.1016/j.micromeso.2017.04.017
Noomnarm, U., Clegg, R.M., 2009. Fluorescence lifetimes: fundamentals and interpretations. Photosynth. Res. 101, 181–194. https://doi.org/10.1007/s11120-009-9457-8
Oghbaei, M., Mirzaee, O., 2010. Microwave versus conventional sintering: A review of fundamentals, advantages and applications. J. Alloys Compd. 494, 175–189. https://doi.org/10.1016/j.jallcom.2010.01.068
Park, J.P., Lee, J.-J., Kim, S.-W., 2016. Highly luminescent InP/GaP/ZnS QDs emitting in the entire color range via a heating up process. Sci. Rep. 6, 30094. https://doi.org/10.1038/srep30094
Pérez-Ocón, F., Pozo, A.M., Serrano, J.M., Rabaza, O., 2022. Sensors for Continuous Measuring of Sucrose Solutions Using Surface Plasmon Resonance. Appl. Sci. 12, 1350. https://doi.org/10.3390/app12031350
Persson, M.-L., Roos, A., Wall, M., 2006. Influence of window size on the energy balance of low energy houses. Energy Build. 38, 181–188. https://doi.org/10.1016/j.enbuild.2005.05.006
Petersen, E.J., Pinto, R.A., Shi, X., Huang, Q., 2012. Impact of size and sorption on degradation of trichloroethylene and polychlorinated biphenyls by nano-scale zerovalent iron. J. Hazard. Mater. 243, 73–79. https://doi.org/10.1016/j.jhazmat.2012.09.070
Petrila, L.-M., Bucatariu, F., Mihai, M., Teodosiu, C., 2021. Polyelectrolyte Multilayers: An Overview on Fabrication, Properties, and Biomedical and Environmental Applications. Materials 14, 4152. https://doi.org/10.3390/ma14154152
Phillips, K.S., Cheng, Q., 2007. Recent advances in surface plasmon resonance based techniques for bioanalysis. Anal. Bioanal. Chem. 387, 1831–1840. https://doi.org/10.1007/s00216-006-1052-7
Piyasena, P., Dussault, C., Koutchma, T., Ramaswamy, H.S., Awuah, G.B., 2003. Radio Frequency Heating of Foods: Principles, Applications and Related Properties—A Review. Crit. Rev. Food Sci. Nutr. 43, 587–606. https://doi.org/10.1080/10408690390251129
Powell, A., Minson, P., Trapaga, G., Pal, U., 2001. Mathematical modeling of vapor-plume focusing in electron-beam evaporation. Metall. Mater. Trans. A 32, 1959–1966. https://doi.org/10.1007/s11661-001-0008-y
Prontera, C.T., Pugliese, M., Giannuzzi, R., Carallo, S., Esposito, M., Gigli, G., Maiorano, V., 2021. Flexible distributed Bragg reflectors as optical outcouplers for OLEDs based on a polymeric anode. J. Inf. Disp. 22, 39–47. https://doi.org/10.1080/15980316.2020.1825537
Pruessner, M.W., Stievater, T.H., Khurgin, J.B., Rabinovich, W.S., 2011. Integrated waveguide-DBR microcavity opto-mechanical system. Opt. Express 19, 21904–21918.
Qiao, P., Yang, W., Chang-Hasnain, C.J., 2018. Recent advances in high-contrast metastructures, metasurfaces, and photonic crystals. Adv. Opt. Photonics 10, 180. https://doi.org/10.1364/AOP.10.000180
Quaranta, G., Basset, G., Martin, O.J.F., Gallinet, B., 2018. Recent Advances in Resonant Waveguide Gratings. Laser Photonics Rev. 12, 1800017. https://doi.org/10.1002/lpor.201800017
Rack, P.D., Holloway, P.H., 1998. The structure, device physics, and material properties of thin film electroluminescent displays. Mater. Sci. Eng. R Rep. 21, 171–219. https://doi.org/10.1016/S0927-796X(97)00010-7
Raether, H., 1988. Surface plasmons on smooth surfaces, in: Surface Plasmons on Smooth and Rough Surfaces and on Gratings, Springer Tracts in Modern Physics. Springer Berlin Heidelberg, Berlin, Heidelberg, pp. 4–39. https://doi.org/10.1007/BFb0048319
Rani, U.A., Ng, L.Y., Ng, C.Y., Mahmoudi, E., 2020. A review of carbon quantum dots and their applications in wastewater treatment. Adv. Colloid Interface Sci. 278, 102124. https://doi.org/10.1016/j.cis.2020.102124

Reddick, R.C., Warmack, R.J., Ferrell, T.L., 1989. New form of scanning optical microscopy. Phys. Rev. B 39, 767–770. https://doi.org/10.1103/PhysRevB.39.767
Reichelt, K., Jiang, X., 1990. The preparation of thin films by physical vapour deposition methods. Thin Solid Films 191, 91–126. https://doi.org/10.1016/0040-6090(90)90277-K
Resende, P.M., Sanz, R., Caballero-Calero, O., Martín-González, M., 2018. Cost-Effective, Flexible, Hydrophobic, and Tunable Structural Color Polymeric Bragg Reflector Metastructures. Adv. Opt. Mater. 6, 1800408.
Reyes-Coronado, D., Rodríguez-Gattorno, G., Espinosa-Pesqueira, M.E., Cab, C., de Coss, R., Oskam, G., 2008. Phase-pure TiO_2 nanoparticles: anatase, brookite and rutile. Nanotechnology 19, 145605. https://doi.org/10.1088/0957-4484/19/14/145605
Rigosi, A.F., Hill, H.M., Li, Y., Chernikov, A., Heinz, T.F., 2015. Probing Interlayer Interactions in Transition Metal Dichalcogenide Heterostructures by Optical Spectroscopy: MoS_2 /WS_2 and $MoSe_2$ /WSe_2. Nano Lett. 15, 5033–5038. https://doi.org/10.1021/acs.nanolett.5b01055
Ritchie, A.W., Cox, H.J., Gonabadi, H.I., Bull, S.J., Badyal, J.P.S., 2021. Tunable High Refractive Index Polymer Hybrid and Polymer–Inorganic Nanocomposite Coatings. ACS Appl. Mater. Interfaces 13, 33477–33484.
Rurack, K., Spieles, M., 2011. Fluorescence Quantum Yields of a Series of Red and Near-Infrared Dyes Emitting at 600−1000 nm. Anal. Chem. 83, 1232–1242. https://doi.org/10.1021/ac101329h
Samantara, A.K., Acharya, C., Satpathy, D., Panda, C.R., Bhaskara, P.K., Sasmal, A., 2018. Functionalized graphene, in: Fullerens, Graphenes and Nanotubes. Elsevier, pp. 545–584. https://doi.org/10.1016/B978-0-12-813691-1.00013-0
Sanchez, C., Belleville, P., Popall, M., Nicole, L., 2011. Applications of advanced hybrid organic–inorganic nanomaterials: from laboratory to market. Chem. Soc. Rev. 40, 696. https://doi.org/10.1039/c0cs00136h
Scher, J.A., Elward, J.M., Chakraborty, A., 2016. Shape Matters: Effect of 1D, 2D, and 3D Isovolumetric Quantum Confinement in Semiconductor Nanoparticles. J. Phys. Chem. C 120, 24999–25009. https://doi.org/10.1021/acs.jpcc.6b06728
Schou, J., 2009. Physical aspects of the pulsed laser deposition technique: The stoichiometric transfer of material from target to film. Appl. Surf. Sci. 255, 5191–5198. https://doi.org/10.1016/j.apsusc.2008.10.101
Schubert, M.F., Xi, J.-Q., Kim, J.K., Schubert, E.F., 2007. Distributed Bragg reflector consisting of high- and low-refractive-index thin film layers made of the same material. Appl. Phys. Lett. 90, 141115. https://doi.org/10.1063/1.2720269
Schulze, D.W., Slaughter, J.M., Falco, C.M., 1988. Molecular Beam Epitaxy For Multilayer Fabrication, in: Christensen, F.E. (Ed.), . Presented at the 32nd Annual Technical Symposium, San Diego, CA, United States, p. 75. https://doi.org/10.1117/12.948772
Scriven, L.E., 1988. Physics and Applications of DIP Coating and Spin Coating. MRS Proc. 121, 717. https://doi.org/10.1557/PROC-121-717
Sednev, M.V., Wurm, C.A., Belov, V.N., Hell, S.W., 2013. Carborhodol: A New Hybrid Fluorophore Obtained by Combination of Fluorescein and Carbopyronine Dye Cores. Bioconjug. Chem. 24, 690–700. https://doi.org/10.1021/bc3006732
Sethiya, A., Agarwal, D.K., Agarwal, S., 2020. Current trends in drug delivery system of curcumin and its therapeutic applications. Mini Rev. Med. Chem. 20, 1190–1232.
Shahidi, S., Moazzenchi, B., Ghoranneviss, M., 2015. A review-application of physical vapor deposition (PVD) and related methods in the textile industry. Eur. Phys. J. Appl. Phys. 71, 31302. https://doi.org/10.1051/epjap/2015140439
Shahrubudin, N., Lee, T.C., Ramlan, R., 2019. An Overview on 3D Printing Technology: Technological, Materials, and Applications. Procedia Manuf. 35, 1286–1296. https://doi.org/10.1016/j.promfg.2019.06.089

Shapiro, H.M., 2001. Chapter 5 Optical measurements in cytometry: Light scattering, extinction, absorption, and fluorescence, in: Methods in Cell Biology. Elsevier, pp. 107–129. https://doi.org/10.1016/S0091-679X(01)63009-7
Shekar, B.C., Sathish, S., Sengoden, R., 2013. Spin Coated Nano Scale PMMA Films for Organic Thin Film Transistors. Phys. Procedia 49, 145–157. https://doi.org/10.1016/j.phpro.2013.10.021
Shetty B, G., Crasta, V., Kumar N B, R., K, R., Bairy, R., Shankaragouda Patil, P., 2019. Promising PVA/TiO2, CuO filled nanocomposites for electrical and third order nonlinear optical applications. Opt. Mater. 95, 109218. https://doi.org/10.1016/j.optmat.2019.109218
Shumaker-Parry, J.S., Campbell, C.T., 2004. Quantitative Methods for Spatially Resolved Adsorption/Desorption Measurements in Real Time by Surface Plasmon Resonance Microscopy. Anal. Chem. 76, 907–917. https://doi.org/10.1021/ac034962a
Shuni Chu, Burrus, C., 1984. Multirate filter designs using comb filters. IEEE Trans. Circuits Syst. 31, 913–924. https://doi.org/10.1109/TCS.1984.1085447
Siddique, R.H., Vignolini, S., Bartels, C., Wacker, I., Hölscher, H., 2016. Colour formation on the wings of the butterfly Hypolimnas salmacis by scale stacking. Sci. Rep. 6, 36204. https://doi.org/10.1038/srep36204
Singh, I., Arora, R., Dhiman, H., Pahwa, R., 2018. Carbon Quantum Dots: Synthesis, Characterization and Biomedical Applications. Turk. J. Pharm. Sci. 15, 219–230. https://doi.org/10.4274/tjps.63497
Singh, S., Kanetkar, V.R., Sridhar, G., Muthuswamy, V., Raja, K., 2003. Solid-state polymeric dye lasers. J. Lumin. 101, 285–291. https://doi.org/10.1016/S0022-2313(02)00571-9
Sjöback, R., Nygren, J., Kubista, M., 1995. Absorption and fluorescence properties of fluorescein. Spectrochim. Acta. A. Mol. Biomol. Spectrosc. 51, L7–L21. https://doi.org/10.1016/0584-8539(95)01421-P
Smirnov, J.R.C., Calvo, M.E., Míguez, H., 2013. Selective UV Reflecting Mirrors Based on Nanoparticle Multilayers. Adv. Funct. Mater. 23, 2805–2811. https://doi.org/10.1002/adfm.201202587
Solaimuthu, A., Vijayan, A.N., Murali, P., Korrapati, P.S., 2020. Nano-biosensors and their relevance in tissue engineering. Curr. Opin. Biomed. Eng. 13, 84–93. https://doi.org/10.1016/j.cobme.2019.12.005
Song, X., Zhai, J., Wang, Y., Jiang, L., 2005. Fabrication of Superhydrophobic Surfaces by Self-Assembly and Their Water-Adhesion Properties. J. Phys. Chem. B 109, 4048–4052. https://doi.org/10.1021/jp045152l
Sridharan, D., Waks, E., 2011. All-Optical Switch Using Quantum-Dot Saturable Absorbers in a DBR Microcavity. IEEE J. Quantum Electron. 47, 31–39. https://doi.org/10.1109/JQE.2010.2070487
Stucky, G.D., Mac Dougall, J.E., 1990. Quantum Confinement and Host/Guest Chemistry: Probing a New Dimension. Science 247, 669–678. https://doi.org/10.1126/science.247.4943.669
Stueber, M., Holleck, H., Leiste, H., Seemann, K., Ulrich, S., Ziebert, C., 2009. Concepts for the design of advanced nanoscale PVD multilayer protective thin films. J. Alloys Compd. 483, 321–333. https://doi.org/10.1016/j.jallcom.2008.08.133
Sun, W., Tan, A.W.-Y., Wu, K., Yin, S., Yang, X., Marinescu, I., Liu, E., 2020. Post-Process Treatments on Supersonic Cold Sprayed Coatings: A Review. Coatings 10, 123. https://doi.org/10.3390/coatings10020123
Tada, H., Mann, S., Miaoulis, I., Wong, P., 1999. Effects of a butterfly scale microstructure on the iridescent color observed at different angles. Opt. Express 5, 87. https://doi.org/10.1364/OE.5.000087
Takeuchi, H., Sakata, H., 2008. Single mode lasing in polymeric distributed-feedback structure formed on inorganic distributed Bragg reflector. Laser Phys. Lett. 5, 41–44. https://doi.org/10.1002/lapl.200710092

Tan, X., Tu, Y., Deng, C., Czarnowski, A. von, Yan, W., Ye, M., Yi, Y., 2018. Enhancement of light trapping for ultrathin crystalline silicon solar cells. Opt. Commun. 426, 584–588. https://doi.org/10.1016/j.optcom.2018.06.003

Tan, X.-M., Chen, H.-J., Cui, H., Lv, Y.-K., Zhao, G.-K., Luo, Z.-C., Luo, A.-P., Xu, W.-C., 2017. Tunable and switchable dual-waveband ultrafast fiber laser with 100 GHz repetition-rate. Opt. Express 25, 16291. https://doi.org/10.1364/OE.25.016291

Tang, L., Ji, R., Cao, X., Lin, J., Jiang, H., Li, X., Teng, K.S., Luk, C.M., Zeng, S., Hao, J., Lau, S.P., 2012. Deep Ultraviolet Photoluminescence of Water-Soluble Self-Passivated Graphene Quantum Dots. ACS Nano 6, 5102–5110. https://doi.org/10.1021/nn300760g

Tinone, M.C.K., Haga, T., Kinoshita, H., 1996. Multilayer sputter deposition stress control. J. Electron Spectrosc. Relat. Phenom. 80, 461–464. https://doi.org/10.1016/0368-2048(96)03016-2

Toby, B.H., Egami, T., 1992. Accuracy of pair distribution function analysis applied to crystalline and non-crystalline materials. Acta Crystallogr. A 48, 336–346. https://doi.org/10.1107/S0108767391011327

Tyona, M.D., 2013. A theoritical study on spin coating technique. Adv. Mater. Res. 2, 195–208. https://doi.org/10.12989/AMR.2013.2.4.195

Venckatesh, R., Balachandaran, K., Sivaraj, R., 2012. Synthesis and characterization of nano TiO2-SiO2: PVA composite - a novel route. Int. Nano Lett. 2, 15. https://doi.org/10.1186/2228-5326-2-15

Walheim, S., Schäffer, E., Mlynek, J., Steiner, U., 1999. Nanophase-Separated Polymer Films as High-Performance Antireflection Coatings. Science 283, 520–522. https://doi.org/10.1126/science.283.5401.520

Wang, J., Zhang, Y., Yu, Y., Ye, F., Feng, Z., Huang, Z., Liu, X., Zhou, X., 2019. Spectrally flat white light emission based on red-yellow-green-blue dye-loaded metal-organic frameworks. Opt. Mater. 89, 209–213. https://doi.org/10.1016/j.optmat.2019.01.019

Wang, R., Lu, K.-Q., Tang, Z.-R., Xu, Y.-J., 2017. Recent progress in carbon quantum dots: synthesis, properties and applications in photocatalysis. J. Mater. Chem. A 5, 3717–3734. https://doi.org/10.1039/C6TA08660H

Weng, Y., Chen, G., Zhou, X., Yan, Q., Guo, T., Zhang, Y., 2019. Design and fabrication of bi-functional TiO_2 /Al_2O_3 nanolaminates with selected light extraction and reliable moisture vapor barrier performance. Nanotechnology 30, 085702. https://doi.org/10.1088/1361-6528/aaf4e1

Whittaker, A.G., Mingos, D.M.P., 1994. The Application of Microwave Heating to Chemical Syntheses. J. Microw. Power Electromagn. Energy 29, 195–219. https://doi.org/10.1080/08327823.1994.11688249

Wi, S., Kim, H., Chen, M., Nam, H., Guo, L.J., Meyhofer, E., Liang, X., 2014. Enhancement of Photovoltaic Response in Multilayer MoS_2 Induced by Plasma Doping. ACS Nano 8, 5270–5281. https://doi.org/10.1021/nn5013429

Widjonarko, N., 2016. Introduction to Advanced X-ray Diffraction Techniques for Polymeric Thin Films. Coatings 6, 54. https://doi.org/10.3390/coatings6040054

Wongcharoen, T., Rahman, B.M.A., Grattan, K.T.V., 1996. Accurate characterization of optical filters with two-dimensional confinement. J. Light. Technol. 14, 2596–2603. https://doi.org/10.1109/50.548160

Wu, Q., Zhou, M., Gong, Y., Li, Q., Yang, M., Yang, Q., Zhang, Z., 2018. Three-dimensional bandgap-tuned Ag_2S quantum dots/reduced graphene oxide composites with enhanced adsorption and photocatalysis under visible light. Catal. Sci. Technol. 8, 5225–5235. https://doi.org/10.1039/C8CY01522H

Wu, Y., Yang, J., Wang, S., Ling, Z., Zhang, H., Wei, B., 2019. High-Performance White Organic Light-Emitting Diodes Using Distributed Bragg Reflector by Atomic Layer Deposition. Appl. Sci. 9, 1415. https://doi.org/10.3390/app9071415

Wu, Z., Lee, D., Rubner, M.F., Cohen, R.E., 2007. Structural Color in Porous, Superhydrophilic, and Self-Cleaning SiO2/TiO2 Bragg Stacks. Small 3, 1445–1451. https://doi.org/10.1002/smll.200700084

Wu, Z.L., Liu, Z.X., Yuan, Y.H., 2017. Carbon dots: materials, synthesis, properties and approaches to long-wavelength and multicolor emission. J. Mater. Chem. B 5, 3794–3809. https://doi.org/10.1039/C7TB00363C

Xiao, M., Shawkey, M.D., Dhinojwala, A., 2020. Bioinspired Melanin-Based Optically Active Materials. Adv. Opt. Mater. 8, 2000932. https://doi.org/10.1002/adom.202000932

Xiao, S., Wang, T., Liu, T., Zhou, C., Jiang, X., Zhang, J., 2020. Active metamaterials and metadevices: a review. J. Phys. Appl. Phys. 53, 503002. https://doi.org/10.1088/1361-6463/abaced

Xu, A., Wang, G., Li, Y., Dong, H., Yang, S., He, P., Ding, G., 2020. Carbon-Based Quantum Dots with Solid-State Photoluminescent: Mechanism, Implementation, and Application. Small 16, 2004621. https://doi.org/10.1002/smll.202004621

Yan, Y., Kuang, W., Shi, L., Ye, X., Yang, Y., Xie, X., Shi, Q., Tan, S., 2019. Carbon quantum dot-decorated TiO2 for fast and sustainable antibacterial properties under visible-light. J. Alloys Compd. 777, 234–243. https://doi.org/10.1016/j.jallcom.2018.10.191

Yang, W., Li, X., Fei, L., Liu, W., Liu, X., Xu, H., Liu, Y., 2022. A review on sustainable synthetic approaches toward photoluminescent quantum dots. Green Chem. 24, 675–700. https://doi.org/10.1039/D1GC02964A

Yang, X., Bandyopadhyay, S., Shao, L.-Y., Xiao, D., Gu, G., Song, Z., 2019. Side-Polished DBR Fiber Laser with Enhanced Sensitivity for Axial Force and Refractive Index Measurement. IEEE Photonics J. 11, 1–10. https://doi.org/10.1109/JPHOT.2019.2919392

Yao, J., Yang, M., Duan, Y., 2014. Chemistry, Biology, and Medicine of Fluorescent Nanomaterials and Related Systems: New Insights into Biosensing, Bioimaging, Genomics, Diagnostics, and Therapy. Chem. Rev. 114, 6130–6178. https://doi.org/10.1021/cr200359p

Yao, Y., Tao, J., Zou, J., Zhang, B., Li, T., Dai, J., Zhu, M., Wang, S., Fu, K.K., Henderson, D., Hitz, E., Peng, J., Hu, L., 2016. Light management in plastic–paper hybrid substrate towards high-performance optoelectronics. Energy Environ. Sci. 9, 2278–2285. https://doi.org/10.1039/C6EE01011C

Ye, L., Li, Y., Xia, B., Zhang, Y., Jiang, B., 2016. Template-free sol–gel preparation of nanoporous ORMOSIL films with adjustable refractive index. Mater. Lett. 176, 5–8. https://doi.org/10.1016/j.matlet.2016.03.006

Ye Zhou, Huang, M.C.Y., Chase, C., Karagodsky, V., Moewe, M., Pesala, B., Sedgwick, F.G., Chang-Hasnain, C.J., 2009. High-Index-Contrast Grating (HCG) and Its Applications in Optoelectronic Devices. IEEE J. Sel. Top. Quantum Electron. 15, 1485–1499. https://doi.org/10.1109/JSTQE.2009.2021145

Yildiz, A., Lisesivdin, S.B., Kasap, M., Mardare, D., 2008. Electrical properties of TiO2 thin films. J. Non-Cryst. Solids 354, 4944–4947. https://doi.org/10.1016/j.jnoncrysol.2008.07.009

Yimsiri, P., Mackley, M.R., 2006. Spin and dip coating of light-emitting polymer solutions: Matching experiment with modelling. Chem. Eng. Sci. 61, 3496–3505. https://doi.org/10.1016/j.ces.2005.12.018

Yu, E.T., van de Lagemaat, J., 2011. Photon management for photovoltaics. MRS Bull. 36, 424–428. https://doi.org/10.1557/mrs.2011.109

Yuan, Y., Giri, G., Ayzner, A.L., Zoombelt, A.P., Mannsfeld, S.C.B., Chen, J., Nordlund, D., Toney, M.F., Huang, J., Bao, Z., 2014. Ultra-high mobility transparent organic thin film transistors grown by an off-centre spin-coating method. Nat. Commun. 5, 3005. https://doi.org/10.1038/ncomms4005

Yuk, J.S., McDonagh, C., MacCraith, B.D., 2010. Demonstration of a surface plasmon-coupled emission (SPCE)-based immunoassay in the absence of a spacer layer. Anal. Bioanal. Chem. 398, 1947–1954. https://doi.org/10.1007/s00216-010-4026-8

Zhang, F., Feng, X., Zhang, Y., Yan, L., Yang, Y., Liu, X., 2016. Photoluminescent carbon quantum dots as a directly film-forming phosphor towards white LEDs. Nanoscale 8, 8618–8632. https://doi.org/10.1039/C5NR08838K
Zhang, H., Chen, G., Bahnemann, D.W., 2009. Photoelectrocatalytic materials for environmental applications. J. Mater. Chem. 19, 5089. https://doi.org/10.1039/b821991e
Zhang, J.Z., 1997. Ultrafast Studies of Electron Dynamics in Semiconductor and Metal Colloidal Nanoparticles: Effects of Size and Surface. Acc. Chem. Res. 30, 423–429. https://doi.org/10.1021/ar960178j
Zhang, X.-F., Zhang, J., Liu, L., 2014. Fluorescence Properties of Twenty Fluorescein Derivatives: Lifetime, Quantum Yield, Absorption and Emission Spectra. J. Fluoresc. 24, 819–826. https://doi.org/10.1007/s10895-014-1356-5
Zhang, Y., Lim, C.-K., Dai, Z., Yu, G., Haus, J.W., Zhang, H., Prasad, P.N., 2019. Photonics and optoelectronics using nano-structured hybrid perovskite media and their optical cavities. Phys. Rep. 795, 1–51. https://doi.org/10.1016/j.physrep.2019.01.005
Zhang, Z., Zheng, T., Li, X., Xu, J., Zeng, H., 2016. Progress of Carbon Quantum Dots in Photocatalysis Applications. Part. Part. Syst. Charact. 33, 457–472. https://doi.org/10.1002/ppsc.201500243
Zhang, Z., Zheng, T., Xu, J., Zeng, H., Zhang, N., 2017. Carbon Quantum Dots/Bi_2WO_6 Composites for Efficient Photocatalytic Pollutant Degradation and Hydrogen Evolution. Nano 12, 1750082. https://doi.org/10.1142/S1793292017500825
Zheng, J., Zhang, C., Dickson, R.M., 2004. Highly Fluorescent, Water-Soluble, Size-Tunable Gold Quantum Dots. Phys. Rev. Lett. 93, 077402. https://doi.org/10.1103/PhysRevLett.93.077402
Zheng, L., Teng, F., Ye, X., Zheng, H., Fang, X., 2020. Photo/Electrochemical Applications of Metal Sulfide/TiO_2 Heterostructures. Adv. Energy Mater. 10, 1902355. https://doi.org/10.1002/aenm.201902355
Zheng, Z.Z., Liu, M., Guo, S.Z., Wu, J.B., Lu, D.S., Li, G., Liu, S.S., Wang, X.Q., Kaplan, D.L., 2015. Incorporation of quantum dots into silk biomaterials for fluorescence imaging. J. Mater. Chem. B 3, 6509–6519. https://doi.org/10.1039/C5TB00326A
Zhu, M.-Q., Jin, H.-D., Bi, P.-Q., Zong, F.-J., Ma, J., Hao, X.-T., 2016. Performance improvement of TiO_2 /Ag/TiO_2 multilayer transparent conducting electrode films for application on photodetectors. J. Phys. Appl. Phys. 49, 115108. https://doi.org/10.1088/0022-3727/49/11/115108
Zhu, S., Yu, A.W., Hawley, D., Roy, R., 1986. Frustrated total internal reflection: A demonstration and review. Am. J. Phys. 54, 601–607. https://doi.org/10.1119/1.14514
Zimmermann, J., Zeug, A., Röder, B., 2003. A generalization of the Jablonski diagram to account for polarization and anisotropy effects in time-resolved experiments. Phys Chem Chem Phys 5, 2964–2969. https://doi.org/10.1039/B303138A